ELECTROCHEMICAL AND ELECTRON-MICROSCOPICAL STUDIES OF ANODICALLY CORRODED SILVER-GOLD ALLOYS

BY

D. CARTER

A Thesis submitted for the degree of Doctor of Philosophy of the University of Warwick

Department of Physics
University of Warwick.

September 1985

This Thesis is dedicated to my wife, Gill

CONTENTS

ACKNOWLEDGEMENTS

I wish to thank my supervisor, Professor A. J. Forty, for his interest and involvement during this study. I am also grateful to Mr T Naylor for the construction of the electrochemical cell and to Mr A Lovejoy for the construction of the potentiostat. I am indebted to the Science Research Council for the granting of a studentship during the period of full-time study.

Finally, and most of all, I would like to thank my wife, Gill, for her unlimited patience and support during the course of this work.

DECLARATION

This dissertation is submitted to the University of Warwick in support of my application for admission to the degree of Doctor of Philosophy. It contains an account of my own work performed at the Department of Physics of the University of Warwick, full-time from October 1978 to September 1980, and part-time from October 1980 to September 1985, under the supervision of Professor A. J. Forty. No part of it has been used previously in a degree thesis submitted to this or any other University. The work described in this thesis is the result of my own independent research except where acknowledged in the text.

September 1985

D. Carter

ABSTRACT

The aims of the project are to investigate the electrochemical parting of silver from silver-gold. Direct measurements by X-ray analysis of corroded specimens show that silver cannot be parted from alloys with initial concentrations of under 55at% silver, it can be incompletely parted from alloys with between 55at% and 80at% silver, and it can be fully parted from alloys which are over 80at% silver.

The alloys are used to produce well-defined and characteristic voltammograms, and the lowest potential at which silver can be dissolved from them is shown to be composition-dependent, higher potentials being required to part silver from the less silver-rich alloys. Cyclic voltammograms, together with coulometric measurements, and X-ray analyses of specimen compositions before and after electrochemical treatments provide evidence that the dissolution of silver from these alloys is accompanied by the formation of a new phase, possibly a gold oxide. Since, at the potentials of under 1400mV used for this work, this new phase is not formed on pure gold, it is inferred that the dissolution of silver is associated with the formation a chemical and/or a physical environment in which the new phase can form. This phase has a maximum thickness for alloys with an initial silver concentration of about 64at%.

A specialised electrochemical cell, designed and built for this work, is used for the electrochemical treatment of thin, electron-transparent specimens of gold and silver-gold. Following corrosion the specimens are examined with transmission electron microscopy. The development of corrosion micromorphologies is seen not to be strongly composition-dependent, commencing in all silver-rich silver-gold alloys by the formation of isolated pits with diameters of about 50Å. After longer periods of corrosion, channels about 50Å wide cover the surface of the intragranular regions; when more charge is passed, even these previously apparently uncorroded regions close to grain boundaries and holes through the alloy become covered with networks of channels. The electrochemical observations presented lead to the idea that gold atoms are redistributed from the centres of developing pits and channels by the formation and decomposition of the new phase during the dissolution of silver.

CHAPTER 1

INTRODUCTION

1.1 General Approach

This thesis is concerned with the selective dissolution of silver from silver-gold alloys. The approach has been to apply electron microscope X-ray analysis and electrochemical methods to study this phenomenon. A major aspect of this is the electrochemical characterisation of silverr-gold alloys from which the selective dissolution of silver can take place. The electrochemical characterisation, together with X-ray microanalysis, provides information not only about the processes occurring at a metal/electrolyte interface (such as metal dissolution and oxygen evolution) but also about surface films which are formed on the alloys.

The use of electron microscopy approach is dependent upon the design and use of an electrochemical cell capable of handling alloy specimens sufficiently thin for subsequent electron microscopical examination without the need of any thinning. Such a technique allows new information to be sought on the development of an anodically produced corrosion micromorphology, particularly in the early stages.

1.2 Corrosion of Metals

The naturally occurring ores of most metallic elements are found in an oxidised (or combined) condition. The extraction and refining of metal ores consists of a reduction process; two commonly known examples of this process include the reduction of iron ore (Fe_2O_3 with SiO_2) in the blast furnace, where the reduction is carried out with hot CO, and the electrolytic reduction of aluminium from bauxite in the Hall cell. Once metals have been refined, however, they then have a thermodynamic tendency to revert to a combined state, and they become susceptible to the processes of oxidation and corrosion.

Corrosion phenomena are complex, and the emphasis of any study will vary with the particular system. There are three factors which play a part in corrosion processes. The first factor is the metal itself, and consideration needs to be given to the detailed atomic structure and composition, and the nature and frequency of microscopic and macroscopic inhomogeneities. The second factor is the environment, its chemical nature, the concentration of reactive species and impurities, pressure, temperature and (for studies such as of boiler-pipe corrosion which involve flowing electrolytes) its velocity and impingement. The relationship between the metal and the environment provides the third factor. Considerations of the metal/environment interface involve the kinetics of metal oxidation and dissolution, kinetics of reduction of species in solution, the nature and location of corrosion products, the

types of films which grow on the metal surface and the dissolution behaviour of these films.

Clearly, the more complex and interdependent are the corrosion reactions of a system, the more difficult it is to elucidate the separate mechanisms involved. The approach adopted for this present work is to choose a well-defined and well-characterised metal/electrolyte system, where the electrolyte is not chemically aggressive, and in which there is no passivating surface deposit or film formed during corrosion. In such a system it should be possible to relate the microstructure of the metal, its composition determined before and after anodic treatments and the electrochemical observations to the corrosion behaviour of the metal.

The corrosion of a metal is strongly influenced by its microstructure. Shreir (1976) lists the factors that are thought to be important, and they are given in table 1.2.1

Table 1.2.1. Heterogeneities in Metals

1. Atomic
a) Sites within a given surface layer ('normal' sites; these vary according to the particular crystal plane.
b) Sites at edges of partially complete layers.
c) Point defects in the surface layer: vacancies (molecules missing in the surface layer), kink sites (molecules missing at edge of layer), molecules adsorbed on top of complete layer.
d) Disordered molecules at point of emergence of dislocations (screw or edge) in metal surface.
2. Microscopic
a) Grain boundaries- usually, but not invariably, more reactive than grain interior.
b) Phases - metallic (single metals, solid solutions, intermetallic compounds), non-metallic, metal compounds, impurities, etc.
- heterogeneities due to thermal or mechanical

causes.

3. Macroscopic

a) Grain boundaries.
b) Discontinuities on metal surface- cut edges, scratches, discontinuities in oxide films (or other chemical films) or in applied metallic or non-metallic coatings.
c) Bimetallic couples of dissimilar metals.
d) Geometrical factors-general design, crevices, contact with non-metallic materials, etc.

The use of silver-gold alloys eliminates multiphase effects, since this alloy occurs as a single phase at all compositions. The influence of other microstructural features such as grain boundaries can be reduced by paying particular attention to the method of fabricating alloy specimens. Microstructural imperfections play a major part in corrosion processes, since they not only provide localised anodic sites which may promote pitting (anodic sites are usually much smaller than cathodic regions, so metal ions are dissolved or combined over limited regions), but bulk diffusion of ionic species occurs preferentially along grain boundaries. The method of vapour deposition employed limits macroscopic imperfections, so that only microscopic and atomic heterogeneities remain.

The forms of corrosion may be summarised into five broad groups (Shreir, 1976). First, the corrosion may be uniform, occurring over all areas of the metal at a similar rate. This is the case for many oxidation, tarnishing and passivation reactions. Second, the corrosion may be localised, when some areas corrode at higher rates than others, due to heterogeneities in the metal, the environment or the geometry of the system. Localised corrosion leads to crevice corrosion, intergranular corrosion and bimetallic corrosion.

The third type of corrosion - pitting - is an extreme case of localised corrosion. Selective dissolution, which is the process with which we are concerned in this work, is the fourth type of corrosion. It occurs when one component of an alloy (usually the most active component) is selectively removed from the alloy, so that the alloy becomes enriched in its more noble element. Finally, there is that form of corrosion which occurs by conjoint action, where localised attack takes place due to synergetic action of a mechanical fracture and corrosion; examples of this include erosion-corrosion, and stress-corrosion cracking.

Corrosion products are formed in all corrosion systems, whether the corrosion is 'dry', occurring in a gas or vapour, or 'wet', where the corrosion takes place in an aqueous environment. The nature of the corrosion product plays a fundamental part in the rate and extent of all corrosion phenomena. The corrosion product may be thin, continuous and adherent, in which case the product itself may inhibit the formation of any further corrosion product. This important phenomenon is known as passivity, and the passivation of many metals has wide commercial significance. One example is the atmospheric oxidation of aluminium. Although aluminium is chemically active, when exposed to the atmosphere it becomes protected by a thin, adherent, continuous film of aluminium oxide

Thin films such as tarnish layers on metals provide protection against further corrosion. No such corrosion protection

occurs when a scale is formed. Unlike tarnishes, scales may be many thousands of monomolecular layers thick. Scales are often poorly adherent and are discontinuous. Electrolyte penetration through the discontinuities in the scale enables further corrosion of the metal to take place, and the tendency of many scales to become detached from the surface also enables corrosion to continue.

Whether the corrosion product is a tarnish or a scale, the corrosion process will be significantly influenced by the interaction of the corrosion product with the environment. In the case of aqueous corrosion, as used in this work, phases formed at the metal/solution interphase may be solid compounds or they may be solvated ions. If the corrosion products are solid compounds then some degree of passivation might take place, dependent upon the coherence and adherence of the film, its rate of formation and its solubility. Alternatively, the corrosion phase formed at the interphase might be hydrated ions, in which case corrosion will proceed by the ionisation of metal atoms as long as the solubility product of the dissolved species is not exceeded. The rate of dissolution will be influenced and in some cases controlled by ionic transport away from the metal/solution interphase by drift, diffusion, natural or forced convection.

1.3 Selective Dissolution

There are many applications for pure metals, such as copper used in the electrical industry, but these are far outweighed by the applications of alloys. Commercially used alloys include the brasses (copper and zinc), solder (lead and tin) and stainless steel (mainly iron and nickel). Most alloys consist of more than two species; indeed, stainless steels may commonly be made of eight or ten different metals in various proportions. Jewellery, aluminium alloys and the coinage metals are alloys which are also composed of more than two metals.

When an alloy is subjected to a corrosive or chemically aggressive environment it does not usually behave as if it were composed of a single 'alloy' species. Although the component metals of the alloy do interact and modify each others behaviour, they also respond individually to the environment. The greater the electrochemical potential difference between each metal, the greater will be the difference in their activities in the corrosive environment, and the situation can be reached where the less noble of the metals will be very active, whereas the more noble component or components will be relatively inert. Under these circumstances the alloy undergoes selective dissolution, where the less noble (and hence more active) metal is dissolved from the alloy, leaving a residue enriched with the more noble element.

There are various processes which might be involved in selective dissolution. These include the processes of ionisation and perhaps redeposition which occur in all corrosion reactions and volume and surface structural rearrangements. Until now studies of selective dissolution have involved mainly investigations of the mechanisms by which atoms of the dissolving species are removed from the bulk alloy.

In discussing the various transport processes that might be involved in selective dissolution it is useful to consider the surface microstructure of a crystal. Surfaces of a crystal which has been grown slowly from its vapour or on a surface prepared by cleavage are often stepped, with the steps themselves being imperfect. Atomic defects which are not visible in a microscopic image will also be present: these defects are vacant sites and surface adatoms. This is the terrace-kink-ledge model of a crystal surface developed by Burton, Cabrera and Frank (1951), shown in figure 1.3.1. The least firmly bound of the surface atoms are those on kink sites (K), hence dissolution will be expected to occur preferentially from these sites. If the dissolving crystal consists of just one atomic species (in other words, if A atoms and B atoms on the figure are the same element) then the removal of atoms from kink sites by dissolution or vaporisation will expose more atoms of the same type to positions on kink sites, so a succession of atoms may be removed.

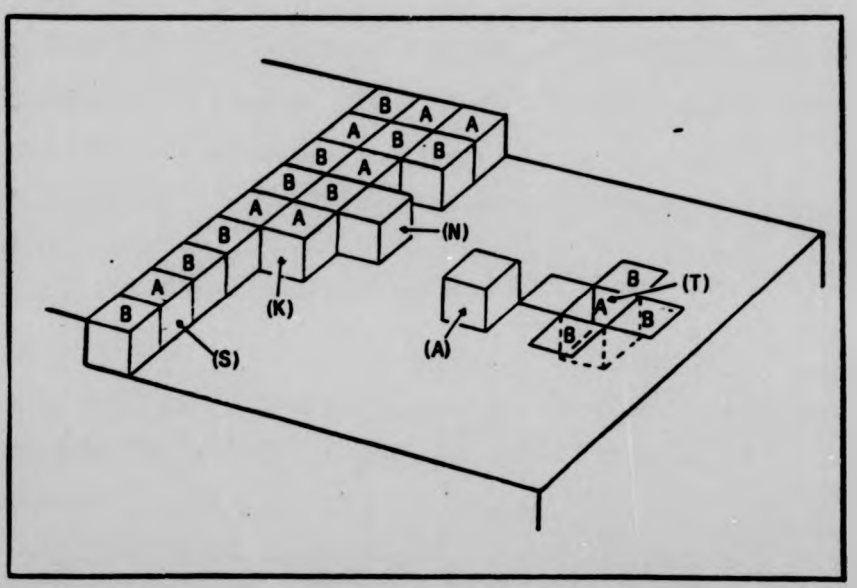

Figure 1.3.1 An idealised terrace/ledge/kink model of a crystal surface, composed of soluble A atoms and noble B atoms. K is a kink site on a surface ledge; N is a detached atom on a ledge; (A) is an adsorbed atom and T is a terrace site.

If this simple explanation of the dissolution mechanism is now applied to a binary alloy AB where the components A and B are in random solid solution and where the selective dissolution of the less noble element A can occur, a rapid coverage of the surface by B atoms is predicted. With such an alloy, at sufficiently low potentials, the current will be provided by the less noble A atoms, but the current will soon become diminished as the available A atoms on kink sites are removed: the removal of A atoms from kink sites leaves increasing numbers of the noble B atoms on kink sites. Further dissolution will only proceed by the removal of A atoms from non-kink sites on steps (S) or terraces (T), but atoms on these sites are more firmly bound, so a greater activation energy or overpotential is required. Eventually, the alloy would be expected to become 'passivated' when all surface sites are occupied by noble B atoms and, should no other mechanism be involved, a 'passive' surface layer would be expected to form very rapidly. This would happen, for example, when the A atoms had been removed from the four atomic surface layers in an alloy where the ratio of the baser A to the nobler B atoms was 3:1. In practice this does not occur. Not only may de-alloying extend far beyond these first few atomic layers but, in the case of silver-gold alloys, it is generally known (and supported by data presented in this thesis: chapter 4) that alloys where the ratio of silver:gold is 3:1 (or greater) do not undergo passivation, and such alloys may become completely dealloyed.

For selective dissolution to continue beyond the first few atomic layers of the alloy, notwithstanding the accumulation of the noble atoms at the surface, more complex mechanisms than those considered in the terrace-ledge-kink model of crystal dissolution must be involved in the dissolution process. These additional mechanisms must involve the migration of surface atoms, so that the reaction does not become passivated by the build up of the noble metal to cover the surface. Additionally, the continued dissolution of the less noble metal from the underlying alloy requires a mass transport mechanism to bring these deeper atoms to the surface.

There are various forms of mass transport which may provide the mechanism to expose further atoms of the less noble species to the surface during the corrosion reaction. For example, Pickering and Wagner (1967) propose that volume diffusion from the underlying alloy will repopulate the surface with A atoms, and thereby maintain the dissolution process. This model requires a high diffusion flux of atoms; the grain boundary diffusion coefficients for metals at room temperature which have been obtained by extrapolating back from experimentally obtained values at high temperatures (Czanderna and Summermatter, 1976) provide values for the diffusion coefficient D of 2×10^{-18} $cm^2 sec^{-1}$. This value for the diffusion coefficient, which is close to that for bulk lattice diffusion, would suggest that about 1000 seconds would be required for the diffusion of one of the less noble A atoms across the thickness occupied by a mere ten B atoms. This is

far too small to provide significant surface replenishment of the dissolving species. Kirsch, Poate and Eibschutz (1976), however, determine the room temperature grain-boundary diffusion coefficient of silver in polycrystalline gold (and vice-versa) to be some 10^{-14} cm^2sec^{-1} . This value produces the considerably shorter time of one second for the same diffusion distance, and the order of magnitude of diffusion currents calculated by this value corresponds with those produced electrochemically for work presented in this thesis.

Large diffusion coefficients, such as those determined by Kirsch, Poate and Eibschutz, can only be contemplated if the diffusion processes are more complex than lattice defects alone. It is thought that this rapid diffusion might be assisted by an inward flow of lattice vacancies and divacancies generated at the surface by selective dissolution at terrace sites. Although some of these will be trapped at vacancy sinks at dislocations and grain boundaries, the remainder will be available to enhance the diffusion of the noble metal inwards from the corrosion front, and to enhance the diffusion of atoms of the less noble metal from the bulk alloy to the corrosion front. Pickering and Wagner provide support for this with measurements of partial dissolution currents and changes of potential of copper-gold alloys. Pickering (1968) in addition used X-ray diffraction measurements of the surface layers on brass (copper-zinc) to support the volume diffusion model.

Having considered possible transport mechanisms in the alloy we should now consider what might be taking place at the surface. There are two modes of dissolution of single-phase binary alloys AB, where A denotes the baser and B the nobler element. In the first case, both elements may be ionised simultaneously, though the rates of ionisation may differ. This is the likely dissolution mode where there is little difference in the ionisation potentials of the separate metals in the ionising environment, or if the dissolution takes place at a high enough potential. If the nobler of the metals is redeposited at cathodic sites, then localised cells would tend to be produced; such cells would work against continuing redeposition.

An alternative mechanism, shown by the dealloying of noble metal alloys, is that of the selective dissolution of the less noble element, and this mode of dissolution occurs when there is a large difference in the electrode potential of each metal in the alloy. Pickering and Wagner (1967) consider that it is this latter mechanism which occurs when brasses and noble metal alloys dissolve, leaving a spongy residue of the nobler of the two metals. A refinement of this concept is that, following the selective dissolution of the more reactive metal, surface mobility of the remaining noble metal atoms causes them to form aggregates. This will expose fresh alloy to the environment, and will cause the accumulation of monolayers of the noble metal to form a three-dimensional structure which will eventually spread to cover the alloy surface; that such structures have been identified will be

discussed further in the following section. Surface phases such as oxides may also be involved in the reordering of the noble metal.

When an alloy undergoes selective dissolution of one or more of its component elements, the process might lead to complete dealloying. If this occurs then clearly the various mechanisms of mass transport within the bulk of the alloy, at the surface of the alloy and in the electrolyte adjacent to the alloy, cooperatively permit the replenishment from the bulk and removal from the surface of the dissolving species. For other alloy compositions and electrochemical conditions not all (or indeed none) of the dissolving species can be removed from the alloy; when this occurs the alloy is termed partially or completely passivated. The study of selective dissolution is concerned with elucidating those mechanisms which contribute to the continuing dealloying which takes place in some alloy/electrolyte systems, and which lead to the partial or complete passivation which occurs in other alloy/electrolyte systems.

1.4 Some Previous Studies of Selective Dissolution

Interest in the phenomenon of selective dissolution was initiated historically by the need to separate or 'part' the baser metals from noble metal alloys, notably Cu-Au and Ag-Au, in order to recover the purified noble metal. It has been known for a long time that parting only takes place when the concentration of the less noble element is sufficiently high.

If, for example, it is required to purify an alloy which consists of gold with a small amount of silver, the alloy is first melted down with silver to make a new alloy which is relatively rich in silver. This new alloy can now be fully parted to recover the pure gold.

There is a composition for many alloys which determines whether parting can occur. This composition is known as the parting limit; if the noble metal is present in a higher concentration than the parting limit then the baser metal is not dissolved at all, and the alloy has a nobility similar to that of the noble metal itself. The nature of the parting limit was demonstrated over 50 years ago by Tammann and Brauns (1931) who studied annealed silver-gold alloys in hot sulphuric acid. They found that alloys are not attacked when the alloy contains 50% or more gold, but that some attack occurs when the alloy is 49% or less gold. They established this value of 50% as the parting limit for silver-gold alloys. Tammann and Brauns examined other alloy systems and determined parting limits for them also. Following this work, Bakish and Robertson (1956) exposed Cu-Au single crystal alloys to ferric chloride solution, and found that the alloy was reduced to a sponge which retained the essential macroscopic arrangement of the alloy before chemical attack. Since the alloys were single crystals, it follows that there could be no preferential dissolution at grain boundaries caused by grain boundary segregation.

Pickering and Wagner (1967) and Pickering (1968) used electrochemical techniques linked with diffraction methods to examine the preferential dissolution of copper from copper-gold alloys. They showed that a new corrosion phase is produced during anodic dissolution of the alloy: this phase has a variable composition which is intermediate between pure gold and alloy. Measurements of lattice parameters for various copper-rich alloys after dissolution show that final alloy compositions are more gold-rich than were the original (uncorroded) alloys, before electrochemical attack. The nature of the dealloying process leading to gold-rich phases was examined further by Pickering with a rotating ring-disc electrode. The alloy under test was the central disc of the assembly, and it was subjected to anodic dissolution at a predetermined current I_d whilst the resulting potential E_d was measured. The conclusion drawn was that the ionisation-redeposition mechanism did not occur during the selective dissolution of copper. Swann and Duff (1970) observed corrosion tunnels in copper-gold and other alloys, and point out that, although the gross ionisation redeposition mechanism discounted by Pickering does not occur, some gold ionisation could take place, with the gold being redeposited on the tunnel walls.

X-ray measurements on a range of brasses (Pickering, 1970) provide further evidence for the bulk diffusion mechanism of selective dissolution. It was observed that neither the ionisation-redeposition nor the surface diffusion mechanism appear capable of producing new alloy containing appreciable

amounts of the less noble metal. He proposed that anodic dissolution which occurs via the interdiffusion of the components is consistent with the formation of new alloy phases during the preferential dissolution of zinc from zinc-rich copper-zinc alloys. This interdiffusion could be assisted by a high concentration of mono- and di-vacancies generated at the alloy surface, but even this fails to account for the rapid growth of corrosion tunnels in copper-gold alloys (up to 300 atom distances per second).

The micromorphology produced by the selective dissolution of silver from silver-gold alloys has been reported by Forty and Durkin (1980), using transmission microscopy to examine a range of chemically corroded thin-film specimens. They observe no corrosion morphology in alloys with under 50% or over 90% silver, but a series of electron micrographs of alloys whose compositions lie within these limits shows the development of island-channel-pit morphologies following exposure to nitric acid (35% to 100%). The details of corrosion morphology depend upon initial alloy composition and upon acid strength, but as corrosion proceeds the islands (which are gold-rich) spread, whilst the channels between them shrink but deepen. The pit morphology is explained as the result of partial coalescence of the islands. The model Forty and Durkin employ in their paper is that of corrosion disordering-reordering. The selective dissolution of silver creates a disordered surface, with a large concentration of surface adatoms or vacancies. This then reorders by rapid surface diffusion into the island and channel structures; the

aggregation of gold adatoms into islands continuously depassivates the surface by exposing fresh alloy to the acid, so selective dissolution of silver can continue.

Forty (1981) refines the corrosion disordering-reordering model with evidence that the corrosion disordering occurs in a near surface zone approximately 5 nm thick, and that following selective dissolution, oxidation of the residual gold takes place, to be followed by decomposition of the oxide back to gold. This oxide phase is identified by detailed analysis of electron diffraction patterns which have extra diffraction spots tentatively identified as arising from Au_2O_3. The oxide formed under these corrosion conditions should be metastable, forming during the rapid dissolution of silver at the corrosion front, but tending to decompose when the silver dissolution is complete. Whilst silver is dissolving the dynamic balance is established:

Selective Dissolution ⇝ Gold Oxidation ⇿ Decomposition

In a further paper, Durkin and Forty (1982) provide additional evidence for the identification of an overlayer formed by the corrosion of silver-gold alloys. They conclude that the corrosion phase is probably gold (I) oxide, having a simple cubic crystal structure and a lattice parameter a_o = 4.91Å. They suggest that the selective dissolution of silver from silver-gold in nitric acid produces an aqueous environment enriched in NO_2 and NO_2^- which can partially oxidise the residual gold atoms and take them into solution adjacent to

the alloy. These are then regarded as super mobile adatoms which can give rise to rapid diffusive growth of gold islands on the surface of the corroding alloy. The oxide phase forms when a build-up of NO_2 might occur over the whole surface of the alloy which is gold-rich except inside the pits; this would lower the oxidation potential for gold, so the oxide phase can form. Durkin and Forty suggest that other binary alloys might also be subjected to coupled phenomena of this kind and, if so, coupled reactions could play and important part in the parting of alloys, in oxidation, and in stress corrosion cracking.

It is worthwhile concluding this section with some discussion of stress corrosion cracking, a phenomenon in which selective dissolution is thought to have a major role. The combined action of a stress and exposure to a corrosive environment often causes greater deterioration in mechanical properties than could be accounted for by the separate addition of stress and corrosion. This combined effect is known as stress corrosion cracking, and a number of studies of selective dissolution have been carried out in order to improve understanding of stress corrosion cracking.

The initial stages of stress corrosion cracking have been identified (Harwood, 1956) as arising from conditions of large-area cathodic regions and small-area anodic regions on the metal surface. These conditions are created when the surface has compositional or microstructural differences, such as precipitates at grain boundaries, and multiphase alloys;

the alloy. These are then regarded as super mobile adatoms which can give rise to rapid diffusive growth of gold islands on the surface of the corroding alloy. The oxide phase forms when a build-up of NO_2 might occur over the whole surface of the alloy which is gold-rich except inside the pits; this would lower the oxidation potential for gold, so the oxide phase can form. Durkin and Forty suggest that other binary alloys might also be subjected to coupled phenomena of this kind and, if so, coupled reactions could play and important part in the parting of alloys, in oxidation, and in stress corrosion cracking.

It is worthwhile concluding this section with some discussion of stress corrosion cracking, a phenomenon in which selective dissolution is thought to have a major role. The combined action of a stress and exposure to a corrosive environment often causes greater deterioration in mechanical properties than could be accounted for by the separate addition of stress and corrosion. This combined effect is known as stress corrosion cracking, and a number of studies of selective dissolution have been carried out in order to improve understanding of stress corrosion cracking.

The initial stages of stress corrosion cracking have been identified (Harwood, 1956) as arising from conditions of large-area cathodic regions and small-area anodic regions on the metal surface. These conditions are created when the surface has compositional or microstructural differences, such as precipitates at grain boundaries, and multiphase alloys;

segregation at highly disordered grain boundaries also produces local anodic areas, as does local stress at grain boundaries. Other mechanical factors which may cause localised anodic regions include local rupture of a protective surface film due to strain, and plastic deformation of the metal.

Stress corrosion cracking normally occurs only in alloys. The environments in which stress corrosion occurs are often ones in which preferential dissolution of one of the alloy components also occurs. Graf and Budke (1955) noted that homogeneous alloys have the greatest susceptibility to stress corrosion cracking when the concentration of the more noble element is below the parting limit (around 50%). In, for example, silver-gold, the susceptibility for stress corrosion cracking is a maximum at a concentration of about 25% gold.

Brass is an alloy which can undergo stress corrosion cracking. In the case of alpha-brass in ammonium electrolytes, it is thought (Edeleanu and Forty, 1960) that dezincification causes embrittlement of the metal around the tip of a crack. The material which remains is thought to be a copper-enriched porous residue along which a crack may propagate until it is arrested by (for instance) a slip band. Early micromorphological studies of copper-zinc alloys by means of electron microscopy (Pickering and Swann, 1963) revealed that a tunnelling corrosion structure develops in aggressive environments which preferentially dissolve the less noble metal. Similar corrosion structures were observed in other

alloys for which selective dissolution may occur: copper-gold, copper-aluminium and zinc-aluminium.

1.5 Some Previous Electrochemical Studies of Silver, Gold and Silver-Gold Alloys

For uniformity, the potentials quoted here have been presented on the 'saturated calomel electrode' (SCE) scale, unless otherwise indicated. The zero on the hydrogen scale is at -241 mV on the SCE scale (Latimer, 1952), so to convert these values to the hydrogen scale, 241mV is added.

(a) Silver

Research into the electrochemistry of silver has primarily been for the purpose of determining and characterising anodically formed surface species. In 1908, for example, Luther and Pokorny plated silver onto platinum and anodically polarised this at small constant current in 1M NaOH solution, plotting potential/time curves. The potential climbed, but was observed to pause and hold steady for a measured time; two such potential arrests were observed. By calculating the quantity of electricity passed and relating this to the mass of silver originally plated, they identified these arrests as arising from the formation first of Ag_2O and then of Ag_2O_2. These potentials were :

$$Ag/Ag_2O : +0.40V$$

$$Ag_2O/Ag_2O_2 : +0.61V$$

both figures on the normal hydrogen scale (NHE)

Hickling and Taylor (1946) investigated the oxidation of silver in alkaline solutions using an oscilloscope to record the current response. This method allowed them to resolve the transient behaviour of the electrodes, and three main stages in the polarisation were observed. The first process was the formation of an electrolyte double layer; this was followed by the formation of Ag_2O in a film whose thickness depended upon the experimental conditions; and finally they found the formation of a higher oxide which decomposed to Ag_2O_2. With progressively decreasing alkalinity of the electrolyte, however, they found that the anodic polarisation remained fundamentally the same as in NaOH, but with increasing formation of Ag_2O. For solutions having a pH of 9 or less the silver anode did not passivate, and the anodic process was merely that of silver dissolution. There is therefore very little interest in the anodic behaviour of silver in acid solutions.

Cahan, Ockerman, Amlie and Ruetschi (1960), presented anodisation curves of sheet silver electrodes in 30% KOH. The technique they used was to modulate a steady potential with a square-wave a.c. ripple. The a.c. current response was controlled by the nature of the surface, and this work has many points of correspondence with that of Luther and of Hickling. After anodisation at various constant currents, they could produce a plateau at about +0.10V corresponding to Ag/Ag_2O. The Ag_2O films produced in these conditions were non-uniform in thickness, with a maximum thickness of about 100 monolayers. Cahan et al. attribute the drop in resistance

of their specimens following anodisations of some 250s to be the formation of higher oxides; higher oxides are known generally to be of lower resistance than lower oxides. Interestingly, they also presented evidence for the existence of a conductive, unstable oxide of silver with an oxidation state higher than AgO, in agreement with the earlier observations of Hickling and Taylor (1946). Because of the transitory nature of this film, identification of this oxide by means of X-ray diffraction techniques was not found to be possible.

In contact with potassium chloride, silver establishes a constant and reproducible potential, making the silver/silver chloride electrode useful as a reference electrode. A potential of +47mV is established for:

Ag/solid AgCl, in N/10 KCl

The standard electrode potential for silver at 25°C is (Latimer, 1952):

$$Ag \rightleftharpoons Ag^{+} + e \; ; \; +0.7991V \; (NHE)$$

Silver is generally known to have a charge transfer efficiency of unity: that is, virtually all of the charge can be accounted for by an equivalent mass deposited or dissolved monovalent silver. The combined processes of deposition and dissolution are used in silver refineries for the transfer of crude silver at anodes to refined silver deposited on cathodes (Evans, 1960). The high efficiency of this process means that the costs of silver refining are to some extent kept low. The electrolyte for this process is silver nitrate. This, like other metal nitrate salts, has a very high solubility, so

would not be capable of forming passivating surface layers on dissolving silver electrodes.

(b) Gold

Gold is the most noble of metals. In the absence of complexing agents such as cyanide and chloride ions, gold is not susceptible to bulk dissolution, although there is some evidence (Cadle and Bruckenstein, 1974; see later) that a small amount of surface dissolution can take place. Investigations into the surface processes which occur on gold electrodes are essentially investigations into the formation and reduction of anodic oxides.

There is in general poor agreement amongst the early published papers. Using moderate current densities, Armstrong, Himsworth and Butler (1933) followed the change of potential with time in 0.1M H_2SO_4, and distinguished two stages in the polarisation behaviour: a rapid linear change which they attributed to double layer charging, then a gradual rise of potential starting at +1.03V. This they considered to be the formation of Au_2O_3, initially as a monomolecular layer. A few years later, Deborin and Erschler (1940) described their findings for gold anodised at very low currents in 0.5M H_2SO_4; with long polarisation times in both acid and alkaline solutions they located a stage commencing at +0.5V (+0.65V in 1M KOH) which they attributed to the adsorption of oxygen. The total quantity adsorbed corresponded to less than would be required for monolayer coverage.

An electrolyte favoured by many researchers investigating the formation and decomposition of anodic oxides on gold is perchloric acid, since it is regarded as being a non-complexing, non-absorbing and effectively buffered medium. With 99.9+% gold foil in deoxygenated 1N $HClO_4$, Laitinen and Chao (1961) produced potential-time curves during galvanostatic (constant current) conditions. The initial current was anodic, and produced a rapidly rising potential which was explained as due to double-layer charging, followed by a second region where potential rose more slowly: this was considered to be initially due to surface oxidation which was followed, at higher potentials (over 1.70V), by the formation of some bulk oxide. The reduction voltage-time curve, produced when the current was reversed to a small but constant value, fell rapidly to a clear and very reproducible potential arrest at about 1.05V. This is the arrest potential which all specimens which they tested reached under open-circuit conditions following potentiostatic anodisation, irrespective of the potential at which the specimen had been previously maintained. Laitinen and Chao conclude that this potential is produced by the formation of Au_2O_3, a conclusion supported by many more recent workers. Unlike the results produced by later and more sophisticated techniques, however, Laitinen and Chao considered that only one surface species is formed, since they observed only one potential arrest.

Schmid and O'Brien (1964), using differential capacity measurements on polycrystalline gold in normal-perchloric acid, also found a potential arrest in potential/capacity

curves close to 1.0V which they too judged to be Au_2O_3. They suggested that this oxide probably formed in patches on the surface, and they found an additional potential arrest at about 0.65V representing, in their view, surface adsorbed Au-OH or Au-O. Brummer and Makrides (1964) used gold in perchloric acid, and located what appears to be the same potential arrest as Schmid and O'Brien, using either low cathodic currents (down to 10^{-5}amp/cm^2) or alternatively open-circuit conditions, and the potential of this arrest plateau was 950 to 1050mV. This was explained as not just arising from Au_2O_3, as before, but was thought to arise from an impurity couple as well as an oxide. They found that the higher the anodisation potential, the greater is the amount of oxide formed on the surface; the total charge passed at an anodisation potential of 1.20V was equivalent to approximately 1 monolayer of surface oxide, i.e., some 450μC/cm^2. When the potential falls from the plateau it falls through a 'kink' which, although Brummer and Makrides do not discuss in detail, could well be the same minor potential arrest which Schmid and O'Brien assign to the desorption of adsorbed Au-OH or Au-O.

In yet another paper on this topic (Ogura, Haruyama and Nagasaki (1971)), this arrest was assigned to the reduction of Au_2O_3,. These workers anodised gold in acid of pH 1.55 (which is the same as the pH of 0.1M HNO_3 used in work for this thesis). Significantly, the potential arrest in the open-circuit potential-time curve was measured to be 950mV for gold previously anodised at fixed potentials of 1050 to 1650mV, and the greater the anodisation potential, the longer

was the potential arrest maintained. Ogura et al, in common with Brummer (1964) and Schmid (1964), found that the oxidation potentials and the reduction potentials of the oxides shift approximately 60mV towards less positive potentials for each unit increase in pH. This is taken to indicate control by reactions involving a proton/electron ratio of unity, which is consistent with the formation and reduction of Au_2O_3 by the reaction:

$$2Au + 3H_2O + 6e \rightleftharpoons Au_2O_3 + 6H^+$$

One of the most recent papers on the formation and reduction of anodic oxide films on gold is that of Oesch and Janata (1983). Their work is in general agreement with previous studies and, since the additional information presented is thought to have a particular bearing on some of the results presented in this thesis, it will be discussed in more detail than hitherto.

The system used was a conventional three-electrode electrochemical cell which was potentiostatically controlled in the normal manner (see sections 3.2 and 3.3); charge was integrated graphically with an accuracy quoted as better than 3%. Using high purity (99.999%) polycrystalline wire and analytical grade reagents, Oesch and Janata selected potentiodynamic (i.e., ramped voltage) techniques to produce anodic oxides which they then proceeded to identify by the subsequent reduction peaks; the voltage scan rate was 100mV s^{-1} (for comparison, the scan rate used in work for this thesis was 50mV s^{-1}). Most of their work was carried out in

deoxygenated, phosphate-buffered neutral electrolytes at room temperature (25°C). Potentials quoted here use the more accurate relativity of +240mV on the hydrogen scale as the zero on the saturated calomel scale.

Oesch and Janata observed peaks in the anodic current for gold in buffered neutral solutions. These peaks commenced at about 0.65V and had been passed through at 1.10V. An immediate reversal of the scan at 1.10V caused the reduction peak to commence at about 0.7V. Both peaks shifted to more noble potentials in more acid solutions, but with different pH dependency: the potential of the anodic peak shifted by -50 mV/pH, but the potential of the cathodic (reduction) peak shifted -73mV/pH. In solutions of pH 1.5 one would therefore expect the anodic peak to commence at a little above 0.95V, being passed through by 1.37V. The oxide ("oxide I") responsible for the peaks is identified as anhydrous Au_2O_3, which can grow to a limiting value of only a few monomolecular layers.

When the anodisation potential was allowed to ramp to higher values (within the region of oxygen evolution) the reduction peaks were found to be much more complex, with a total of three reduction peaks. The first to be reduced (at the higher potential) is the Au_2O_3 already discussed whilst the third ("oxide III"), which is reduced at potentials some 200 to 300mV less noble than oxide I, is identified as a porous bulk oxide, Au(OH) (or hydrated Au_2O_3) which can grow to a thickness of over 100 monolayers. Measurements of charge

density indicate monolayer coverage ($0.45mCcm^{-2}$) of oxide I at 1.10V. Oxide II, formed when oxide I has reached a thickness of 2 monolayers, is suggested by Oesch and Janata to be a surface oxide which is intermediate between oxides I and III.

(c) Silver-Gold Alloys

There has been no recently published work on the electrochemistry of silver-gold alloys. Papers published in 1958 and 1960 (Tischer and Gerisher, 1958; Gerisher, 1960) provide the only authoritative base of much current knowledge on the subject. In their work Tischer and Gerisher investigated the lowest potential at which significant current could be produced at an alloy electrode, and related this to the lowest potential at which a surface layer was thought to form. They found that alloys containing over 75at% silver dissolved as if they were pure silver; the gold content did not affect the dissolution of silver. For more gold-rich specimens the dissolution of silver was hindered, and the suggestion was made that gold oxides become protective with alloys containing under 75% silver. The conclusion made was that for the gold-rich alloys the more noble metal forms a passive covering layer at a definite potential which is independent of alloy composition; the protective behaviour of this layer increases with increasing gold content until, near 50% gold, the alloys have an anodic behaviour which is virtually indistinguishable from pure gold.

They found a clear relationship between alloy composition and the potential required to produce a particular current.

Alloys whose compositions were between pure silver and Au60Ag (60% silver, 40% gold), for example, were found to have a practically linear relationship between alloy composition and the potential required to produce a current of 0.4mA/cm^2, in molar perchloric acid. The potential required for pure silver was some 350mV, rising steadily to about 1100mV to produce the same current in Au60Ag, but to produce this current in Au55Ag needed the considerably increased potential of 1550mV - and this is the potential which they measured to produce that current in all other ratios (55% silver and less). With tenfold reduction in current density the relationship was similar, although the potential required to produce that current was less (about 200mV lower); similarly with tenfold increase in current density slightly higher potentials were required (about 100mV higher). In all cases, the behaviour was as has been described for a current density of 0.4mA/cm^2. Their results led to the conclusion that the dissolution of the alloy is made possible by the removal of less noble atoms from relatively stable positions in crystal planes, through some form of 'hole nucleation' which presumably referred to surface vacancy formation. Passivation occurs when, due to the increasing gold content, the critical potential for dissolution by this hole nucleation mechanism is greater than the potential of surface passivation by the formation of an oxide layer.

1.6 Aims of This Work

Many factors influence the corrosion behaviour of metals (summarised in table 1.2.1) and the design of any series of investigations must be such that the system is as well characterised as possible. Because of the complexity of corrosion phenomena, it is not always possible to meet these conflicting requirements, and the experiment must be designed to control the variables as closely as possible.

The type of corrosion with which we are concerned in this thesis is that of selective dissolution, where the less noble element is dissolved from the alloy and as a result the alloy becomes progressively enriched with the more noble element. It has already been noted in section 1.3 that dissolution of the less noble element from a homogeneous solid solution would lead rapidly to a surface completely covered with an insoluble component. This coverage would have the effect of halting the corrosion process, unless there are mechanisms for replenishing the surface with the dissolving species. Various mechanisms have been proposed to account for the extensive dealloying which can take place for certain alloy compositions in a number of electrochemical conditions.

Some previous studies of selective dissolution have been discussed in section 1.4, as have a selection of papers on the electrochemistry of silver, gold, and of silver-gold alloys. In particular, the selective dissolution of silver from thin single-crystal films of silver-gold has been reported as

1.6 Aims of This Work

Many factors influence the corrosion behaviour of metals (summarised in table 1.2.1) and the design of any series of investigations must be such that the system is as well characterised as possible. Because of the complexity of corrosion phenomena, it is not always possible to meet these conflicting requirements, and the experiment must be designed to control the variables as closely as possible.

The type of corrosion with which we are concerned in this thesis is that of selective dissolution, where the less noble element is dissolved from the alloy and as a result the alloy becomes progressively enriched with the more noble element. It has already been noted in section 1.3 that dissolution of the less noble element from a homogeneous solid solution would lead rapidly to a surface completely covered with an insoluble component. This coverage would have the effect of halting the corrosion process, unless there are mechanisms for replenishing the surface with the dissolving species. Various mechanisms have been proposed to account for the extensive dealloying which can take place for certain alloy compositions in a number of electrochemical conditions.

Some previous studies of selective dissolution have been discussed in section 1.4, as have a selection of papers on the electrochemistry of silver, gold, and of silver-gold alloys. In particular, the selective dissolution of silver from thin single-crystal films of silver-gold has been reported as

producing a clear and distinctive micromorphology (Forty and Durkin,1980; Forty, 1981; Durkin and Forty, 1982). Very little quantitative work has been done on selective dissolution of silver from silver-gold alloys, consequently it is difficult to relate the micromorphological work with data derived from electrochemical studies. The present work is aimed to determine the electrochemical behaviour of these alloys, and to relate this in a quantitative way both to the selective dissolution of silver and to the development of a corrosion micromorphology.

CHAPTER 2

SPECIMEN PREPARATION

2.1 Introduction

The aim of this work is to use electrochemical techniques combined with X-ray microanalysis and direct microscopical observations to study the behaviour of silver-gold alloys under conditions in which they undergo selective dissolution. Specimens which meet the requirements of the combined approach of electrochemistry and X-ray microanalysis are not appropriate for transmission electron microscopy, so two methods of specimen preparation are required.

It is necessary to prepare alloys of various compositions for both of these experimental approaches. There is a further requirement that specimens should have the minimum of both surface contamination and structural faults arising from the method of preparation. Electropolishing, mechanical polishing and ion-beam thinning of bulk alloys are unsuitable for this work since they produce specimens with, respectively, a surface oxide film, a highly disordered surface, and a composition which is unknown due to preferential sputtering of one component. Whilst solidification from the melt can be used to prepare a range of gold-silver alloys, specimens prepared in this way may suffer from considerable segregation of the gold and silver during cooling. Vapour deposition has

been adopted as the preferred method of producing good quality alloy films of known compositions.

The growth and structure of evaporated metal films has been studied by Bassett and Pashley (1959), with further papers on the subject published by Pashley (1959) and Pashley and Stowell (1963). They prepared films of gold, platinum, palladium and rhodium by evaporation onto freshly cleaved muscovite mica. The evaporation techniques described by these workers have been modified for this work to produce silver-gold alloy specimens for both of the experimental approaches described here.

Direct observations require the use of transmission electron microscopy for the best resolution of microstructural features. Specimens for this purpose must therefore be thin enough to be electron transparent; this means that it must be possible to detach the thin alloy specimens for examination from the electron-opaque mica supporting substrate. Conversely, it must be possible to handle these fragile films without damaging them within an electrochemical cell, and this is only possible if the films are mounted on a firm support.

For electrochemical work and for compositional microanalyses of electrochemically corroded specimens, where the analyses are undertaken in the scanning electron microscope (Chapter 4), the presence of the substrate is acceptable. The specimens need to be uniform in composition. They are therefore made by vapour deposition but, to avoid damage,

specimens for the electrochemical work remain supported on the mica substrate. To maintain the comparability between the two approaches these alloy specimens have similarly-sized test areas to specimens prepared for transmission electron microscopy, and are of similar thickness.

2.2 Description of Specimen Fabrication Equipment

The apparatus for preparing specimens is based on a conventional vapour deposition unit (N.G.N. twelve-inch diameter coating unit). This is evacuated to pressures of 10^{-4} Pa or better by means of an oil diffusion pump backed by a rotary pump. Pressures within this system are measured with Penning gauges.

The internal arrangement of the vacuum chamber is shown in figure 2.2.1. Within the vacuum chamber are two independent sources which are placed 15cm above the substrate; each source is supplied by a low-voltage 60A power supply. A tungsten wire basket is used to evaporate silver, and a 'V'-shaped filament of tungsten wire is used to evaporate gold. To reduce the effect of radiant heating from the filaments (which would raise the temperature of the films during their preparation) a shield is sited under the sources with a small (8mm diameter) hole under each source through which the evaporated material passes. There is a further shield between the gold source and the silver source to prevent any cross-contamination

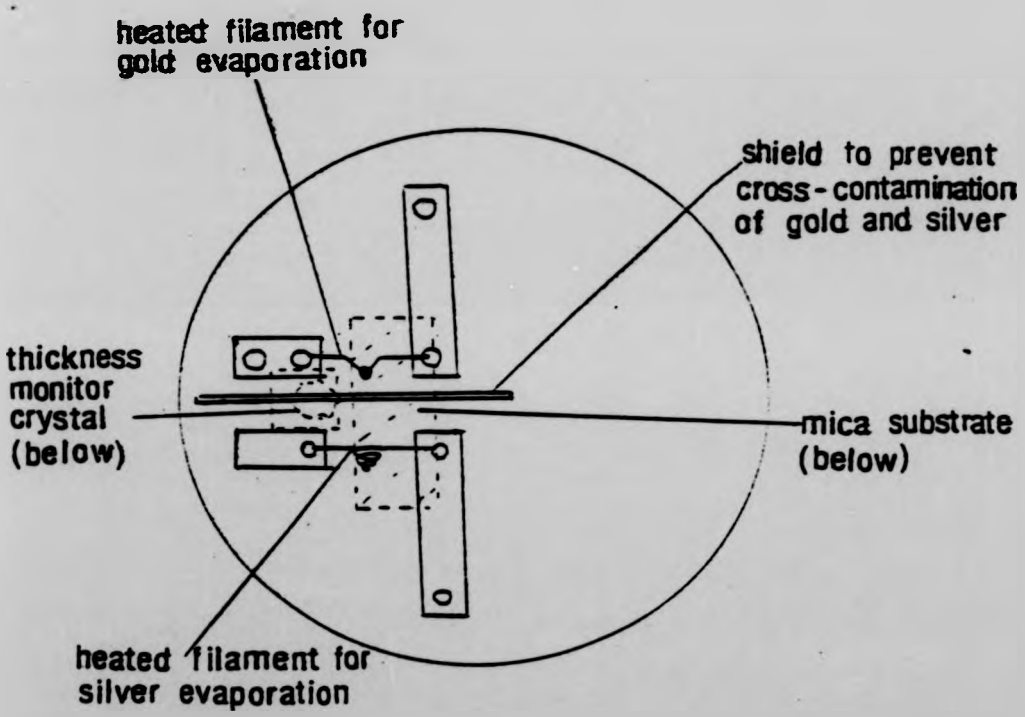

Figure 2.2.1 The arrangements of the filaments within the vacuum chamber. The mica substrate and the thickness monitor crystal are below the sources; the gold and silver vapours pass down through holes in a shield (not shown) to minimise radiant heating of the substrate.

Vapour from the filaments is deposited through the holes in the shield onto the substrates which are rectangles of freshly-cleaved mica, or which are thin films of previously prepared gold films which have been mounted on gold grids. The substrates themselves are placed on a hotplate to hold them at the required temperature. The hotplate, shown in figure 2.2.2, simply consists of two 240V, 15W heating elements of the type used in low-power soldering irons. The elements are embedded between two blocks of stainless steel. A Pt/Pt10%Rh thermocouple is attached to the upper surface of the hotplate. The thermocouple wires are fibreglass sleeved, and connected via a lead-through to an external gauge so that the substrate temperature can be continuously monitored.

The substrate temperature is controlled by altering the supply voltage to the heating elements with a mains transformer ('variac'). Specimen thickness is measured with a standard film thickness monitor (Edwards FTM 2D); the sampling crystal is adjacent to and at the same level as the substrates.

A manually operated shutter is used to shield the monitor head and the substrates from the evaporating sources. This is controlled outside the vacuum chamber, and can be rotated so that it shields only the substrates but exposes the monitor head to the sources, so allowing stable evaporation rates to be achieved before commencing the specimen preparation itself.

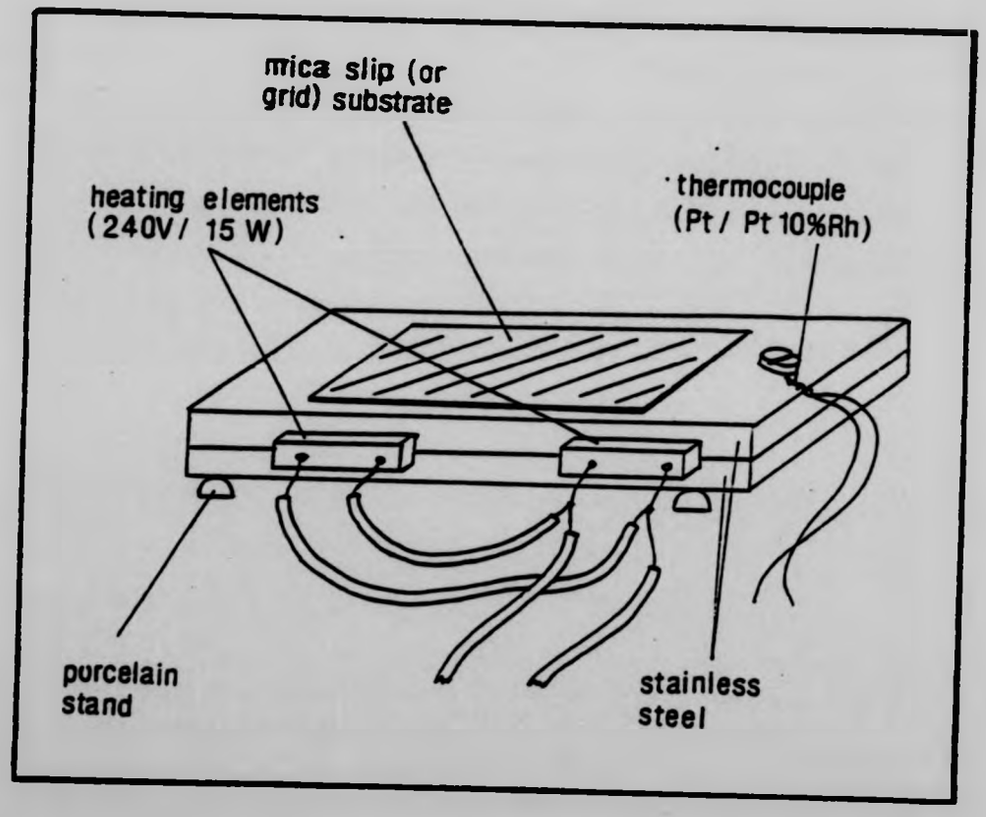

Figure 2.2.2 The substrate heater used for controlling the substrate temperature during specimen preparation.

2.3 Specimen Preparation for SEM

The specimens for electrochemistry/scanning electron microscopy (SEM) are deposited directly onto freshly cleaved mica to produce a batch of similar specimens, each of which consists of a single alloy layer of uniform composition. The substrate is held at a temperature of 285°C, since this temperature is found to produce good single crystal films of silver, with a minimum of double position twinning, with large crystal sizes (the structure of these films is discussed in section 2.6).

The shape of the specimens is determined by a stainless steel mask which rests on top of the mica (figure 2.3.1). Eighteen similar specimens are produced in one deposition. Each specimen is paddle-shaped with, as shown in figure 2.3.2, a 3mm diameter test area running into a 1mm wide strip.

The composition of these alloys is determined by the relative deposition rates of the gold and silver; first the silver is evaporated (with the shutter covering the substrates but exposing the monitor crystal) until a steady rate is reached, then, without altering the silver evaporation rate, the gold is evaporated at the rate required to produce the desired alloy composition. The combined rate is between 3 and 6 Å s^{-1}. For example, in order to produce an alloy Au67Ag (67% silver, 33% gold) the initial silver deposition rate might be stabilised at 4 Å s^{-1} and the gold brought in to produce a combined rate of 6 Å s^{-1}. The shutter is then removed and the

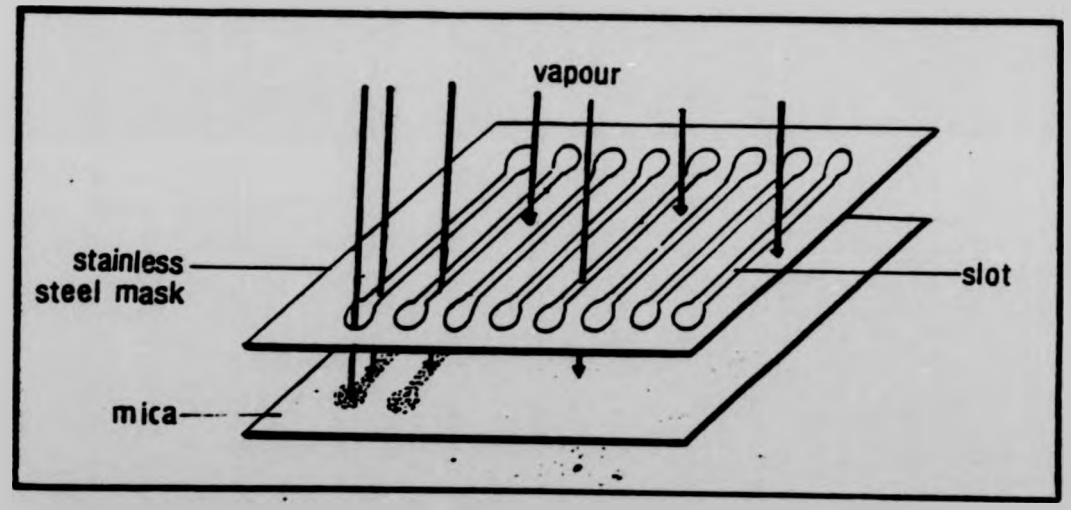

Figure 2.3.1 Deposition of pairs of 'paddle'-shaped specimens through slots cut in a stainless-steel mask, which rests on the heated mica substrate.

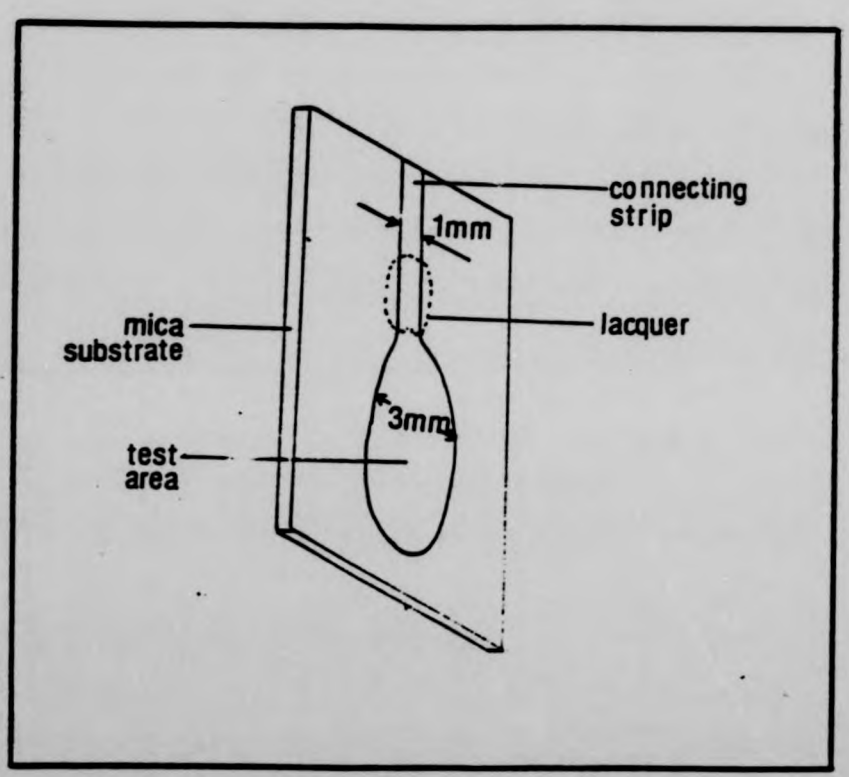

Figure 2.3.2 A 'paddle'-shaped specimens mounted on mica. The lacquer which is applied to the base of the connecting strip ensures that only the test area is exposed to the electrolyte.

metals are codeposited onto the mica.

When the desired specimen thickness has been reached, the shutter is returned to the position where it covers the substrate but does not cover the quartz crystal of the thickness monitor. The current to the gold source is switched off and the silver evaporation rate is measured. The mean silver deposition rate is taken as the average of the measured rates before and after the deposition onto the mica; the gold deposition rate is the difference between the mean silver rate and the total rate during co-deposition

Finally, all sources and the substrate heater are switched off and the specimens are allowed to cool within the vacuum chamber. When the substrate temperature has fallen to under 100°C the vacuum is broken and the specimens removed.

2.4 Specimen Preparation for TEM

Specimens intended for transmission microscopy are made by a two-stage deposition process. The first stage is to produce a thin gold film which will be the substrate for the second stage. The second stage is the deposition of an alloy onto the gold film.

The deposition conditions are as described in sections 2.3 for the production of 'paddle'-shaped specimens. The first step in the alloy preparation is the deposition of a single crystal film of silver approximately 1200 Å thick onto the whole

surface (no mask being used in this case) of a slip of freshly cleaved mica substrate at 285°C at a pressure of 10^{-4} Pa or less. The deposition rate of between 5 and 10 Å s^{-1} produces good single crystals with a minimum of holes and a mirror-smooth (111) surface. A second layer, this time 200 to 250 Å of gold, is now deposited onto the silver; this gold film is also a good single crystal in a (111) orientation epitaxial with the silver film.

After deposition and cooling, the specimen is removed from the chamber and cut into 3mm squares. Each square is floated on a bath of 35% nitric acid with the evaporated films uppermost so that the silver substrate is slowly dissolved and the mica eventually becomes detached, leaving the gold film floating on the surface. Each square is removed from the acid by drawing it carefully onto a glass slide, and it is re-floated onto distilled water. This is repeated onto a second change of distilled water to wash off traces of nitric acid.

For the second stage of specimen preparation the squares are mounted on the 3mm diameter gold grids which are commercially available to support thin films during transmission electron microscopy. Care is taken that each square completely covers the surface of its grid so that the specimens have similar areas. The grids are allowed to dry on filter paper before being replaced in the vacuum chamber for the deposition of the required alloy in the manner detailed in section 2.3 for paddle-shaped mica-mounted alloys. The two-stage process for the production of grid-mounted specimens is shown in figure

2.4.1.

The choice of material for the grids is important. The most commonly used material is copper, since copper grids are inexpensive and rigid, but copper would be electrochemically active at the potentials which these grid-mounted specimens are subjected to during the electrochemical treatments. The copper of the grids would dissolve in and contaminate the electrolyte, and an electrical couple would also be set up between the copper and the alloy metals. An alternative, which avoids all of these problems, is carbon-coated nylon grids, but these would not be able to withstand the necessary heating during the alloy deposition step of specimen preparation. Gold grids reduce the problem of contamination, but they do have two serious limitations. The first is that they are very soft and easily crumpled, so have to be handled with great care during the electrochemical stages. The second limitation is that X-ray analyses of the gold:silver ratios can yield inaccurate results for these specimens since characteristic X-rays of gold might be produced (and counted) by electrons striking the gold grid bars as well as from electrons striking the alloy.

An alternative method of specimen preparation is the production of a composite specimen consisting first of a layer of silver, then a layer of gold and finally a layer of alloy. After removal from the vacuum chamber, this composite could then be cut into 3mm squares and floated on nitric acid to dissolve the silver, the gold acting as a barrier between acid

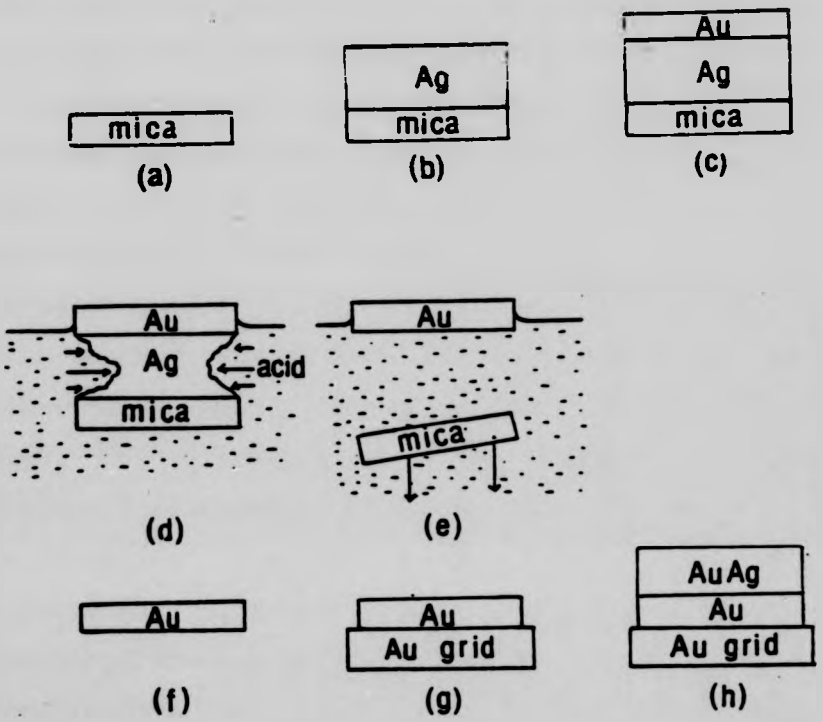

Figure 2.4.1 Stages in the preparation of alloy specimens on electron microscope grids, for electrochemistry and subsequent microscopy. (a) a slip of freshly-cleaved mica is placed in the evaporator, where (b) about 1000Å of Ag are laid, followed (c) by 200 to 250 Å of Au. When cool, the specimen is removed from the evaporator and (d) floated on 50% HNO_3 to dissolve the silver, leaving (e) the gold film floating on the surface. After being washed in two changes of distilled water, the film (f) is mounted (g) on a gold grid and replaced in the evaporator, and (h) the alloy is finally deposited onto this gold substrate.

and alloy during the stripping process. Such specimens could then be mounted on carbon-coated nylon grids which would meet the needs of both electrochemistry and X-ray microanalysis. Unfortunately, when specimens are made in this way it is found that a degree of corrosion of the alloy does take place during the stripping of the alloy from the mica, particularly in the vicinity of holes left by incomplete coalescence of adjacent crystals during deposition. Such localised corrosion has been used to advantage by Durkin (1982) in his examination of corrosion of these alloys by nitric acid, but is undesirable here where the nature and extent of electrochemically produced corrosion micromorphologies are being investigated. Transmission microscopy of specimens which have been produced in two separate deposition stages shows that, prior to electrochemical treatment, they have none of the micromorphological features (see chapter 5) associated with corrosive attack.

Although the grid-mounted specimens share the same test-area as the paddle-shaped specimens described in the previous section, there is a difference in their structures. The former consist of alloy on a gold substrate whereas the latter are alloy on a mica substrate with no intervening gold layer. This minor difference is not thought to degrade the comparability of the two specimen types.

2.5. Structure of Deposited Films

Unambiguous conclusions concerning the nature of the corrosion morphology and the conditions which produce that morphology can only be reached if the changes brought about by corrosion can be distinguished from any pre-existing morphology. Grid-mounted films have been examined by transmission electron microscopy and X-ray microanalysis both before and after electrochemical treatment. The nature and extent of the corrosive attack can therefore be distinguished from pre-existing structural faults which arise during the specimen preparation, and the development of the corrosion micromorphology can be correlated with electrochemical and microanalytical data.

Films of silver grown on freshly cleaved mica show double-position twinning. This is because there are two crystallographic orientations of these island nuclei:

$$(111)_{Ag}\ [1\bar{1}0]_{Ag} \text{ parallel to } (001)_{mica}\ [0\bar{1}0]_{mica}$$

or

$$(111)_{Ag}\ [\bar{1}10]_{Ag} \text{ parallel to } (001)_{mica}\ [010]_{mica}$$

The merging of adjacent islands of different crystallographic orientations gives rise to a structural misfit called a double positioning boundary. When deposited at between 250 and 300°C these twin domains are relatively large.

The coalescence of islands and the formation of double positioning boundaries are associated with small holes, 50 to

100nm in diameter. These holes have been shown (Durkin, 1982) to be formed during the deposition of metal, and are thought to arise from the imperfect coalescence of island nuclei, probably due to impurities and imperfections in the mica substrate. They frequently occur at the intersections of boundaries, and if the conditions of sample preparation are not optimised (for example, too low or too high a temperature, or a contaminant present in the vacuum chamber) the density of holes is likely to be such that the specimen cannot be used.

Gold deposited onto a good silver surface (that is to say, a smooth surface with large crystal sizes, a minimum of holes and other defects) will follow the crystalline epitaxy of the silver, so it is possible to make good gold films. Alloy deposited on this gold film will be epitaxial with the gold. Figure 2.5.1(a) shows a transmission micrograph of a good composite film, alloy on gold, made in the two-stage process described in the previous section. For comparison, a similar specimen is shown, made in a single step: 2.5.1(b). The former specimen was made by floating off a gold film, mounting it on a grid and depositing the alloy, and examination of the regions surrounding holes reveals no discernible structure. The latter specimen shows the corrosion structure produced around holes when the four-layer structure (alloy on gold on silver on mica) is made in one step, then the alloy-on-gold is stripped from the mica with the gold acting as a barrier for the alloy. For the reasons given in section 2.4, specimens with such a pre-existing corrosion morphology are not used here.

(a)

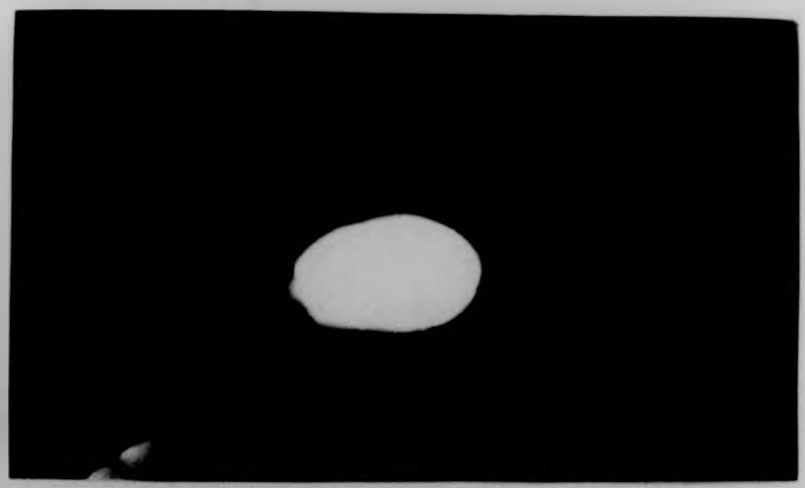

0.1μ

(b)

Figure 2.5.1 (a) An alloy prepared for electrochemical treatment in the two-stage process (see text), showing The lack of corrosion structure around holes in the specimen; (b) a similar specimen, made in a single evaporation step, showing corrosion structure developed around holes.

Photograph (b) has been kindly provided by Professor A. J. Forty, University of Warwick.

(a)

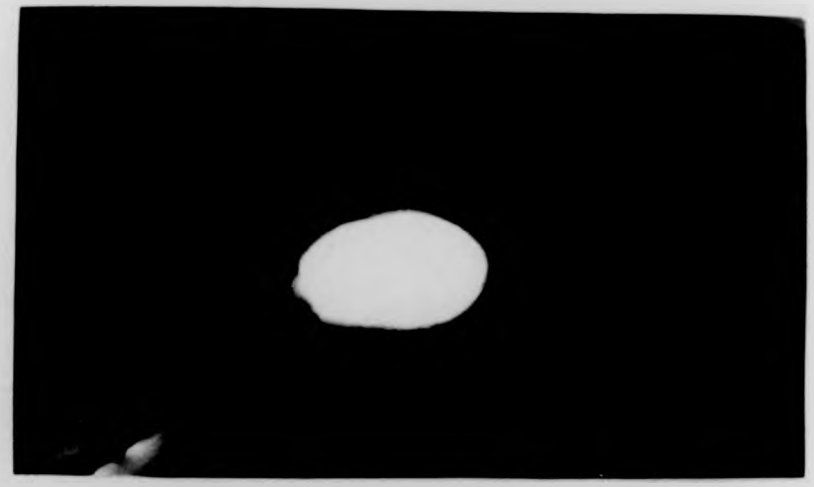

0.1μ

(b)

Figure 2.5.1 (a) An alloy prepared for electrochemical treatment in the two-stage process (see text), showing The lack of corrosion structure around holes in the specimen; (b) a similar specimen, made in a single evaporation step, showing corrosion structure developed around holes.

Photograph (b) has been kindly provided by Professor A. J. Forty, University of Warwick.

Although the surface mobility of silver on mica at elevated temperatures enables it to form good single crystal films, the same is not true of gold on mica. The paddle-shaped specimens are deposited directly onto a mica substrate, so only the pure silver specimens, and possibly the very silver-rich specimens, will have the same nature as the grid-mounted specimens. As the ratio of silver:gold is reduced, it is thought that these specimens become increasingly polycrystalline, though still with a preferred (111) surface orientation.

Segregation of silver to free surfaces and grain boundaries has been shown to take place in polycrystalline silver-gold foils (Fain and Macdonald, 1974). Durkin (1982) observed that electron microprobe analysis using E.D.X. attachments to the TEM and SEM reveal a degree of silver enrichment around the holes. Durkin also presented a depth profile for silver-gold specimens made in the single-step process. The profiles, prepared by Auger electron analysis and argon ion machining, show that specimens usually have a silver-enriched free surface, followed by zones which have approximately the composition predicted from deposition data, with variations accounted for by the diffusion of silver to the free surface and into the supporting gold film. The boundaries between the various layers are therefore not sharp, and are broadened by diffusion; furthermore, there is significant concentration of silver throughout the gold substrate.

Durkin observed that the specimens prepared by this evaporation technique must be considered to be graded into silver-rich and gold-rich zones, rather than composed of discrete layers, with consequent reduction in significance of the stated alloy compositions. It is likely that the high temperatures required during 'bake-out' for the Auger spectroscopy somewhat broadened the diffusion layers that Durkin measured, however, so the specimens used for his corrosion studies would have included narrower interdiffusion bands than those measured by Auger profiling. The two-stage method of sample production used in this work would also lead to narrower interdiffusion bands, particularly between gold and alloy.

The paddle-shaped specimens consist only of alloy deposited directly onto mica with no intermediate silver and gold substrates. These specimens share none of the compositional uncertainties caused by interdiffusion in multi-layer specimens, but they are expected to have some variation in composition with depth. A feature of many binary alloys is some surface segregation of one of the metals; for gold-silver, it has been demonstrated by Tokutaka et al (1981) that one or two monolayers of silver segregate on the surface. Although this level of segregation would not significantly alter the overall alloy composition, one or two monolayers of surface silver could play a part in both the initial electrochemical potentials displayed by the specimens, and in the initial mechanisms of corrosion.

CHAPTER THREE

ELECTROCHEMICAL METHODS AND MICROSCOPY

3.1 Electrochemical Control Requirements

There are many different modes of control of electrochemical systems, from the relatively straightforward static or dynamic control of current or potential to more sophisticated methods which employ, for example, measurement of a.c. impedance of electrodes at various potentials (Makrides, 1962), the imposition of potential steps on a working electrode (Thompson, 1979), or fast response oscillographic measurements (Birke and Roe, 1965). These are just a few of the wide range of experimental systems, but they all share the same fundamental requirements. These are the ability to measure and control currents around an electrochemical circuit, and to measure and control the potential of the working electrode. Additionally, though to varying degrees according to the aims of the particular experiments, there is a need to determine and control the nature of the electrolyte itself.

The measurement of a net current through an electrochemical cell may be achieved with any standard ammeter of suitable sensitivity. The control of this current with a suitable power supply also causes no problems when the power supply can be externally programmed. The main factor is that the current should be derived uniformly (or in a known manner) over the

whole electrode surface, and this is determined by the geometry of the electrochemical cell, and not by the control instrumentation. It is in the realm of the measurement and control of electrode potentials where a more sophisticated approach is needed. When devising electrochemical tests the major considerations are therefore the nature of the control instrumentation and the design of the electrochemical cell and reference electrode system.

3.2 The Electrochemical System

Electrochemistry is carried out under a variety of conditions. The design of the cell and the materials from which the cell is constructed must meet the general requirements of electrochemistry, as well as any additional factors arising from the nature of each investigation. The basic requirements (Sawyer and Roberts, 1974) are related to the precision of measurement, the optimum electrode geometry, the chemical reactivity and the working temperature and pressure of the system. The scale of the system (in other words, the volume of electrolyte, and electrode areas) and the need to reduce contaminants and the ease of changing the electrolyte as well as the ease of cleaning the cell between measurements must also be considered. The additional factors will depend upon the type of auxiliary experimental equipment being used, such as systems for controlling temperature and pressure, for spectroscopic or for ellipsometric analysis. A full discussion of the optimisation of cell design for various electrochemical conditions and requirements would be outside

the range of this work; descriptions and over 17 designs of a number of different cells are given by Sawyer and Roberts (1974).

As has been discussed in chapter 1, the electrochemical corrosion undertaken for this work is designed to complement the chemical corrosion of gold-silver alloys undertaken by Forty and Durkin (1980), Forty (1981) and Durkin and Forty (1982). The chemical corrosion was carried out on a range of thin alloy films (400 to 500 Å thick) in concentrated nitric acid. The corrosive attacks on the samples were undertaken at room temperature, and whilst high-grade 'Analar' reagents and doubly-deionised water were used to make up the acids, atmospheric oxygen was not excluded from the system. Although it is common in electrochemical research to take extensive precautions to exclude oxygen from the cell by means of various environmental systems, for this work it was considered that to do so would reduce the comparability between the two approaches, electrochemical and chemical. It does, however, mean that where an oxide layer is thought to be produced on an alloy, there is no indication as to whether the oxygen atoms are provided by the breakdown of the aqueous electrolyte, or are provided by molecular oxygen dissolved in the electrolyte.

The electrolyte used is 0.1M, pH 1.5 HNO_3, prepared from deionised water (1.5 megohm-cm) and 'Analar' reagents. The acid concentration is found to be non-aggressive within the 300s timescale of most experiments, since specimens immersed

for 1 hour in open-circuit conditions show no measurable silver removal nor any evidence of corrosion morphology. The nitric acid electrolyte has a similar level of purity as the more concentrated (and hence chemically aggressive) nitric acids of Forty and Durkin, so again the systems may be considered directly comparable. The extreme measures of electrolyte purification and pre-electrolysis required for some research work were not used here.

Two designs of electrochemical cell were used. The simpler of the two, shown in figure 3.2.1, is the glass cell for the treatment of the 'paddle-shaped' specimens (chapter 2) used to provide electrochemical and analytical data. The main considerations of this cell are to provide an even distribution of potential over the circular test area of the specimen, and to prevent contamination of any species (particularly chloride ions, which readily form complexes with gold) which may influence the dissolution behaviour of the alloys under test. The potential distribution is made as uniform as possible by the planar configuration of the working electrode and the counter electrode, and is helped by the high conductivity of the electrolyte (the 0.1M nitric acid). The distribution of potential is also influenced by a meniscus, so the connecting-strip to the test area of each specimen is protected by a lacquer coat from the edge of the test area, across and just above the liquid surface.

The reference electrode used is a saturated calomel electrode (SCE). This is a very stable and commonly used reference

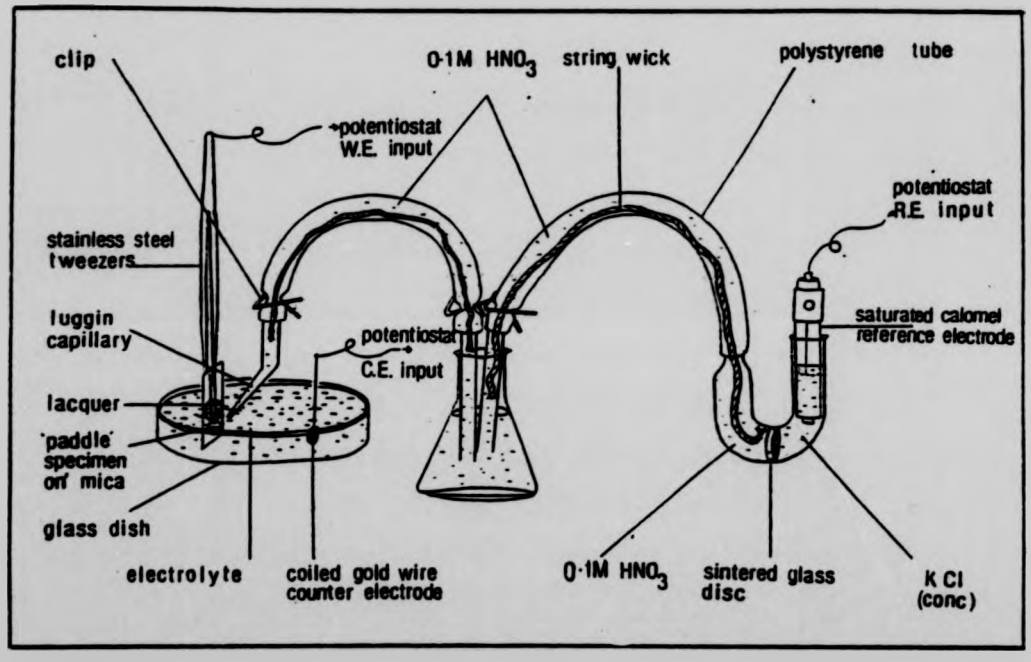

Figure 3.2.1 The glass cell and reference electrode system for use with mica-mounted specimens. Two HNO_3 bridges reduce the risk of electrolyte contamination by KCl.

electrode with a potential of +241mV compared with the zero of the hydrogen scale. To prevent the contamination of the electrolyte with chloride ions from the SCE, it is placed some distance from the electrochemical cell. The potential sampled by the SCE is that of the electrolyte which is at the opening of a luggin capillary placed about 10mm in front of, and to the side of the working electrode. Since the HNO_3 electrolytes used are of high conductivity, the problem of uncompensated solution resistance does not arise: there is only a range of a few millivolts (under 5mV) wherever the capillary tip is located in the cell.

The electrical path from the capillary tip to the SCE is via two bridges of 0.1M HNO_3; each bridge is clamped at each end to prevent both syphoning and any significant ionic diffusion from SCE to cell. Each bridge contains a wick to maintain conductivity across the clamps. The total resistance of the pathway from capillary tip to SCE is about 80 kilohms which, being in series with the 10^{12} ohm reference input impedance of the potentiostat, does not introduce a significant error into the measurement of potentials.

The electrochemical treatment of the thin, grid-mounted specimens intended for transmission microscopy presents an additional problem because of their fragility. Furthermore, there is the extra problem of how the electrical contact to the specimens should be made. Another consideration is where and how the reference take-off should be located.

The positioning of the reference take-off is discussed by Cahan et al (1972). In that work they examine some alternatives to the Luggin capillary, and discuss the use of the Piontelli electrode and the sidehole electrode (figure 3.2.2). The cell used in this work is a modification of the design of Cahan et al and is made of teflon, which is easy to machine and is inert at room temperature. The cell has a 1mm diameter sidehole electrode for the reference take-off point, and the SCE is placed some distance from the cell with two salt bridges, in an arrangement similar to that used in the cell for paddle-shaped specimens.

The grid-mounted specimens are held in the cell using a modification of a system described by France (1967) for polarisation measurements on metal sheets. The grid is held against the body of the cell by gentle back-pressure provided by a 3mm diameter gold sheet which also acts as an electrical contact to the grid. With this system, little physical damage occurs during electrochemical treatment to specimens as thin as 200Å, enabling them to be examined by transmission microscopy following anodic treatment. The cell designed and built for the electrochemical treatment of grid-mounted specimens is shown in figure 3.2.3.

Despite differences is cell design and specimen preparation, potentiodynamic current/voltage curves taken with paddle-shaped specimens correspond with current/voltage curves of similar alloy compositions provided by grid-mounted specimens. It is inferred that the links between

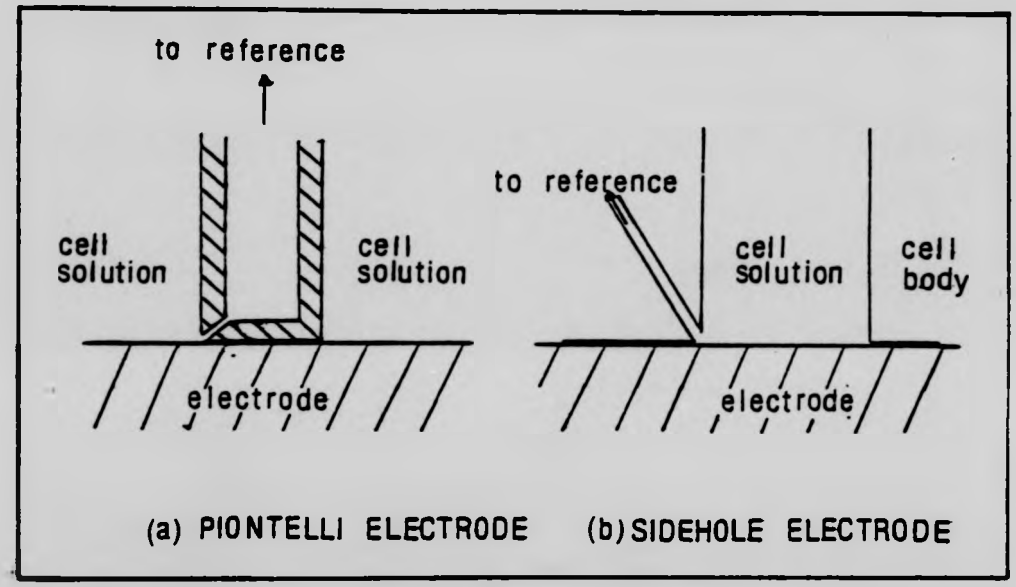

Figure 3.2.2 Two alternatives to the luggin capillary: the piontelli and sidehole electrodes.

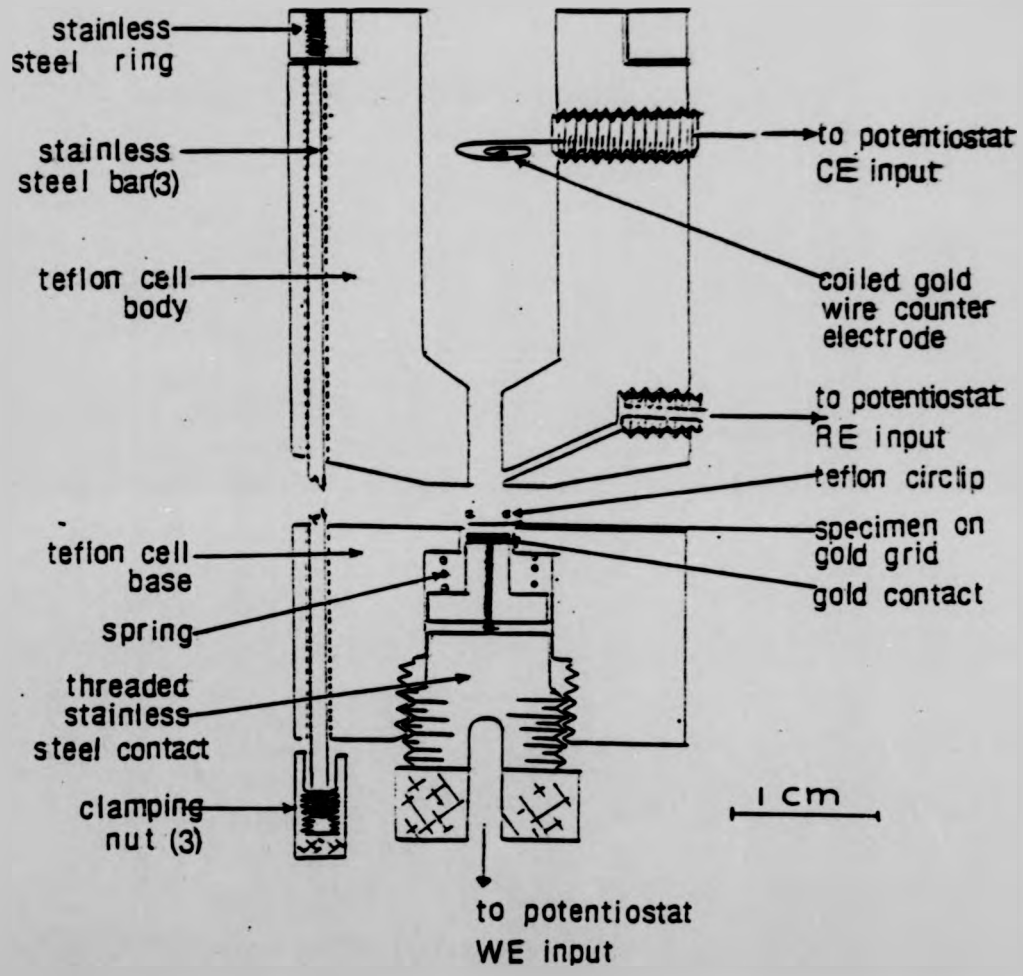

Figure 3.2.3 Section through the teflon cell designed for the electrochemical treatment of thin alloy specimens mounted on electron microscope grids.

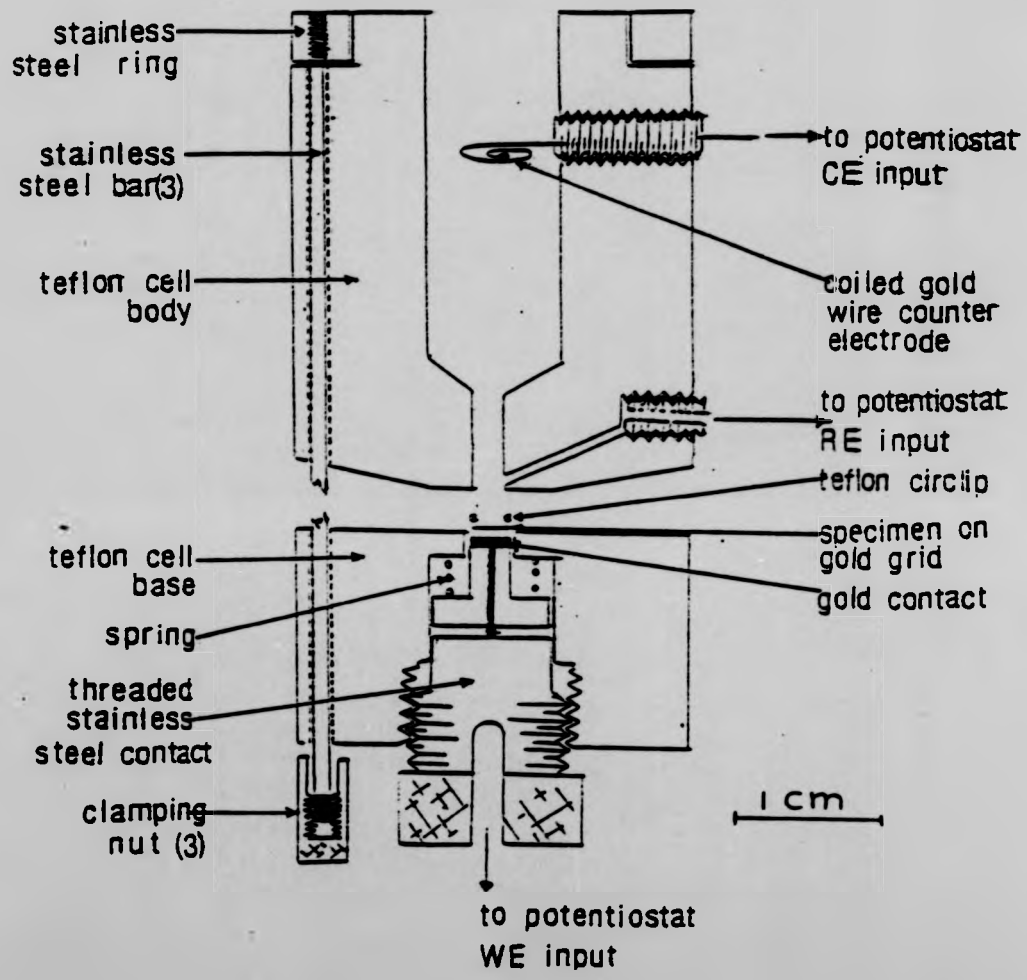

Figure 3.2.3 Section through the teflon cell designed for the electrochemical treatment of thin alloy specimens mounted on electron microscope grids.

electrochemical and analytical observations provided by paddle-shaped specimens apply equally to the grid-mounted alloys.

3.3 Electron Microscopy and Diffraction

The electron microscope employs the wave properties of electrons in a manner comparable with the optical microscope. The electron beam is focused using magnetic lenses; illumination from the source is focused by a condenser lens onto the specimen. A magnified image is formed by the objective lens and this image is then magnified by one or sometimes two projector lenses onto a fluorescent screen.

The electron microscope is capable of far better resolution than the optical microscope. The wavelength of an accelerated electron beam is given by:

$$\lambda = \sqrt{\frac{150}{V}}$$

where V is the accelerating potential. The accelerating voltage of the transmission electron microscope used for this work is 100kV, and for this the wavelength of the electron beam is 0.04Å. Lens aberrations, however, reduce this theoretical limit to between 1Å and 10Å.

Whereas in a light microscope contrast is due to absorption of light by the object, in the electron microscope it is due to the processes of electron scattering. Electrons may be

scattered elastically or inelastically. When elastic scattering takes place and if the object is crystalline a coherent beam of scattered electrons, which suffer no energy loss, is formed. When inelastic scattering occurs some fraction of the energy of incident electrons is transferred to the atoms of the object. Inelastic scattering is mainly confined to small angles, and has a small effect in thin crystals, causing comparatively little effect on image contrast. In general, heavier atoms (those with larger atomic number, Z) are better scatterers than light ones. In the case of silver-gold alloys, those parts of the object with higher proportions of gold will appear electron deficient (darker) in the image.

Electron diffraction patterns enable the operator to determine quickly whether a sample is polycrystalline or is a single crystal, and whether more than one phase is present. Electron diffraction patterns are easy to obtain using the transmission electron microscope; a crystalline specimen will diffract electrons at well defined angles, θ, dependent on electron wavelength, λ, and crystal lattice spacings, d, in accordance with Bragg's law:

$$n\lambda = 2d\sin\theta$$

Diffraction patterns are obtained by bringing diffracted electrons to focus in the back focal plane of the objective lens. The image formed by the objective lens lies in the object plane for the intermediate lens (the first projector

lens); the strength of this lens is reduced until the object plane coincides with the back focal plane of the objective lens. When this condition is achieved the diffraction pattern from the object will be imaged by the intermediate lens and then magnified by the remaining projector lens. An aperture can be placed at the objective lens image plane to isolate a small region of the object, so the diffraction pattern is produced from a restricted area of the object.

The micrographs and diffraction patterns recorded in this work were obtained with a conventional transmission microscope ('Cambridge JEOL 100C'). This has a side-entry eucentric tilting goniometer stage, and operates at 100kV. It is fitted with an energy-dispersive X-ray analyser.

3.4 X-Ray (E.D.X.) Analysis

X-rays are produced when electrons strike a metal surface. These X-rays are characteristic of each element, and if the X-ray emissions are analysed information is provided as to which elements are present in the specimen. The relative intensity of the X-rays provides quantitative information about the elements present.

The system used here is known as an E.D.X. system (Energy Dispersive Analysis of X-rays). The equipment is used in conjunction with the transmission electron microscope or a scanning electron microscope (Cambridge 'Stereoscan'), and it can detect and display simultaneously the intensities of all

X-ray energies leaving the specimen. The systems use lithium-drifted silicon crystals kept at liquid nitrogen temperatures to detect the X-rays; the X-rays entering the detector crystals create electron-hole pairs, the number of which is proportional to the X-ray energy. The associated charges are collected and passed into a multichannel analyser which separates pulses in terms of amplitudes and which stores the signals in memory channels corresponding to these amplitudes. The resulting energy spectrum is then displayed on a cathode ray oscilloscope forming a VDU output from the multichannel analyser.

Statistical uncertainties can be high, because the number of X-rays counted at any one time is only a fraction of the total emitted due to the small size of the detector. Corrections for detector efficiency and X-ray absorption and fluorescence losses in the specimen make absolute determination of concentrations difficult to measure, so the procedure usually adopted is to determine the ratio of two or more components.

Associated computer software is programmed to make corrections for absorption, fluorescence, detector efficiency and differences in ionisation cross-section. With this software reproducible ratios of silver:gold can be obtained; in practice it is found that reliable and reproducible results are obtained with gold-silver alloys down to about 10% silver. There is an excellent correlation between the expected alloy composition calculated from codeposition rates during specimen preparation and the alloy compositions measured by E.D.X. ;

this is shown in figure 3.4.1. This confirms the accuracy of E.D.X. analyses for these thin specimens, confirming that the technique is appropriate for the subsequent analysis of anodically corroded specimen from which quantitative information can be obtained.

The quantity of silver in each alloy tested is calculated from deposition data on the basis that the gold thickness t_{Au} is the same as that deposited in the original (uncorroded) alloy. For example, in the case of an uncorroded mica-mounted (paddle-shaped) specimen having an original thickness of 450Å and an original composition Au66Ag, the original gold in this alloy is equivalent to a thickness t_{Au} = 150Å, and the original silver is equivalent to a thickness t_{Ag} = 300Å. Following an electrochemical corrosion, the ratio of silver:gold is measured by E.D.X. to be 'r'. In other words:

$$\frac{t_{Ag}}{t_{Au} + t_{Ag}} = r$$

So that:

$$t_{Ag} = \frac{t_{Au} \cdot r}{(1 - r)}$$

If, for the example given, the ratio of silver:gold is found to be (say) 1:1.5 following corrosion, then using the reasonable assumption of no net loss of gold from the alloy, a remaining silver thickness of 100Å is calculated, hence 200Å of silver have been lost during the corrosion process.

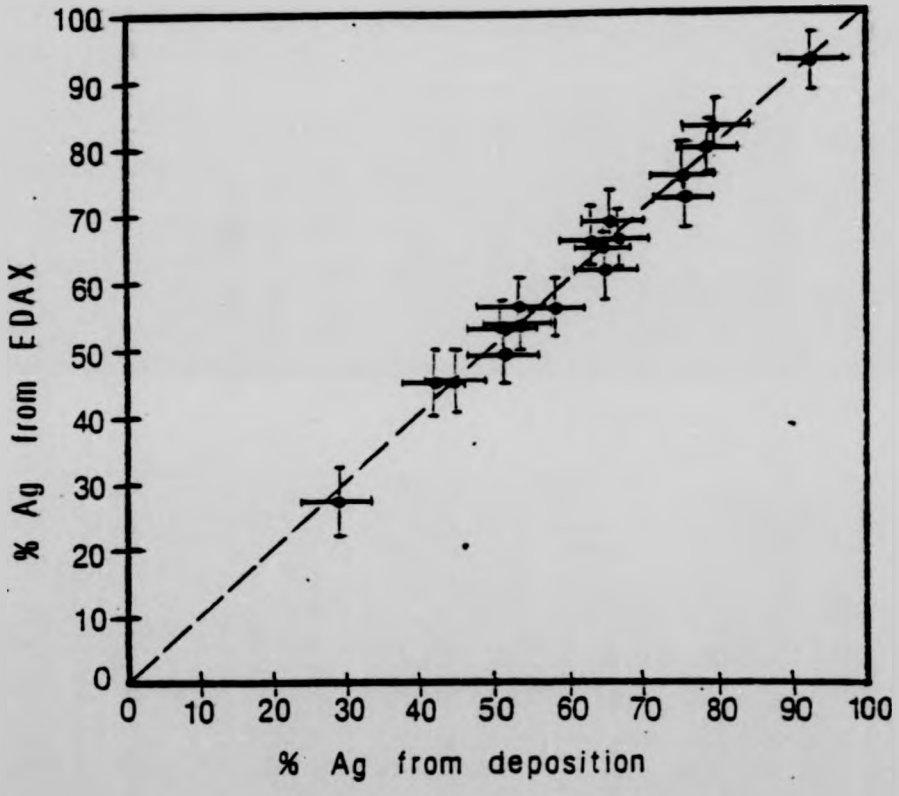

Figure 3.4.1 Comparison of silver percentage measured by E.D.A.X. with that calculated from the relative rates of deposition of silver and gold during sample preparation, showing the close correlation of the two approaches.

3.5 Aspects of Experimental Procedure

Mica-mounted (paddle-shaped) and grid-mounted specimens have been made by the vapour deposition method described in Chapter 2. It is important to ensure that the silver wire and the gold wire are properly cleaned and dried before being mounted on their tungsten sources to avoid contaminants. Care also has to be taken to heat the substrate to the correct temperature (285^{o}C); there is some 'lag' between altering the supply current and measuring the temperature, so overshooting the required temperature is easily done. Depositions carried out at too high a temperature or too low a temperature produce films with small crystal sizes and a large number of holes.

When the substrate is at the required temperature (285^{o}C) the next difficulty is to achieve a stable evaporation rate of the first element, then a stable combined evaporation rate by adding the second element. The problem is that, as material evaporates from each source, the evaporation rate alters; this is particularly the case for the small bead of gold. The first source to be evaporated (with the substrate covered by a shutter) is silver, because the tungsten 'basket' holds enough silver to allow the evaporation rate to stabilise without a large fractional loss of silver from the source. The gold evaporation is then commenced as well, and as soon as the combined rate is stable the shutter is opened to expose the substrate to the evaporating sources. It is generally better to evaporate to an approximate composition and calculate the exact composition later rather than try to

produce an exactly predetermined composition, because so much time can be lost adjusting evaporation rates that one of the sources (usually gold) can run out of material.

The electrochemical treatment of the prepared specimens calls for particularly careful handling. In the case of the 'paddle-shaped' specimens the mica backing provides valuable support, but the cutting of each specimen from the strip can introduce hairline cracks in the connecting strip; these cracks render the specimens unusable. When lacquer is painted over the connecting strip care has to be taken not to touch the strip with the brush: the specimens are so thin that even a light touch can cut and damage the connecting strip. When used in the glass cell (figure 3.2.1) these specimens have proved to be surprisingly robust, and able to withstand not only the electrochemical treatment, but also subsequent dipping in distilled water to wash. They can also safely be introduced into the scanning electron microscope for X-ray microanalyses, although to prevent charging of the mica substrate adjacent to the specimen the exposed mica is coated with conducting paint which is earthed to the specimen holder.

Different problems arise in the case of grid-mounted specimens. These are extremely fragile, and the thin alloys are easily lifted away from the supporting grids. Even with the greatest of care, sometimes less than one specimen in four will survive the handling of electrochemical and electron microscopical treatments. When mounted in the teflon cell (figure 3.2.3), the pressure of the back contact can lift the

film away from the grid, especially if any liquid is present as the back contact is being screwed up. The specimen can be damaged when the lower part of the cell is tightened onto the upper part, and it is also liable to damage when the electrolyte is introduced into the cell. The best way to fill the cell is slowly to pipette the electrolyte in, holding the pipette end close to the specimen. This also ensures that the cell is properly filled, and that no air bubbles remain in the lower part of the cell.

The electrochemical treatments usually lead to thinned specimens, so they are even more liable to be damaged afterwards. The electrolyte has to be pipetted slowly out of the cell, for if the lower part of the cell is removed with the electrolyte present, the outflow across the specimen will destroy it. No attempt can be made to wash the specimen, since this almost invariably causes the alloy to float off the grid and fold up. Specimens which have survived this treatment are dried gently on absorbent (filter) paper, which has the effect of drawing the specimen back down onto the grid. They are then introduced into the transmission electron microscope. The final difficulty is the softness of gold which makes the gold grids more difficult to handle than grids made of other materials, and gold grids are easily crumpled.

Appendix I to Chapter 3

Electrochemical Current/Potential Relationships

An expression for the potential of an electrode was derived by Nernst in 1904. He made the assumption that a fixed diffusion layer of thickness d exists at the electrode surface, and the potential-determining ions can only pass through this layer by diffusion, since no convection takes place. He also made the assumption that concentration varies linearly with distance from the electrode, hence the concentration of ions for both the cathodic (i.e. depletion) and anodic (i.e. augmentation) cases may be calculated from Fick's first law. The well-known Nernst equation relates the potential of the electrode versus the normal hydrogen electrode (NHE) as a function of the activities of the oxidised [O] and reduced species [R]:

$$E = E^{o} + \frac{RT}{ZF} \ln \frac{[O]}{[R]}$$

E = electrode potential T = temperature

E^{o} = standard potential Z = valence state of ion

R = gas constant F = Faraday's constant

As discussed by Bard and Faulkner (1980), the Nernst equation provides a linkage between the electrode potential E and the concentration of the participants in the electrode process:

$$O + ne \rightleftharpoons R$$

A reversible (or 'Nernstian') process is one in which an infinitesimal reversal of the driving force causes the reaction to reverse itself.

The electrode may be disturbed from its equilibrium potential by having an additional external current superimposed by means of a suitable counter electrode. The electrode will assume a potential E_i which differs from the equilibrium value E; the difference between E_i and E is known as the overpotential η:

$$\eta = E_i - E$$

For electrodes with low currents and efficient stirring (so that mass transport is not a factor determining the current) the current is limited by interfacial kinetics. The exponential relationship for such systems between current and overpotential was given by Tafel in 1905:

$$\eta = a + b\log i$$

where a and b are constants

There are, however, many other processes which might cause an overpotential at an electrode. These include (Kortum, 1965) transition overpotential, concentration overpotential, crystallisation overpotential, resistance overpotential, diffusion overpotential and reaction overpotential. The total overpotential is the algebraic sum of these, and it is possible, by close consideration of experimental details, to distinguish between them; Kortum provides some methods for

doing so.

The overpotentials thought to arise in this work are crystallisation overpotential, concentration overpotential and resistance overpotential. The crystallisation overpotential is a term describing the reaction hindrance created by the incorporation of metal ions into or removal of metal ions from the crystal lattice of the electrode (and may itself be limited, in the case of alloys, by bulk diffusion of the less noble element). Resistance overpotential is caused when insulating surface films are formed on the electrode. These films, which play an important part in passivity, may be able to maintain high electric fields and the electrode processes will be dominated by the size and nature of conduction across the films: whether charge is carried by ions or by electrons.

Concentration overpotential takes place when the concentration of the dissolving species is increased (or decreased) at the electrode. The activity term [O] in the Nernst equation is equal to a mean activity coefficient (a thermodynamic term) multiplied by the concentration of the species. When the concentration of the oxidised species (Ag^+ in this case) is increased in the electrolyte, the electrode potential E will be increased. This causes problems for workers who wish to determine electrode potentials accurately, since stationary electrodes are, by their nature, subject to non-stationary environments. To overcome this, a number of non-stationary electrode systems have been produced, notably the dropping mercury electrode for electrolyte analyses and the rotating

ring-disc electrode. Ring-disc electrodes have well-defined hydrodynamic behaviour which allow for the accurate control of electrolyte concentration, but such a system would destroy the delicate, thin-film specimens of this work and so could not be used here.

The concentration of the reduced species, [R], is normally taken as unity for solid metal electrodes, but in these two-component alloys the concentration of the dissolving species (silver) is dependent upon alloy composition, hence the activity of silver in the alloy would be expected to be composition-dependent and E should increase with reducing silver concentration.

Measurements of potentials and overpotentials are nowadays invariably made with a three (or more) electrode system. Any cell voltage measured between working and counter electrodes is of little practical value for elucidating single-electrode processes, since the potential measured is the sum of that developed across the working electrode/electrolyte interface, plus those developed across the electrolyte and the electrolyte/counter electrode interface. Furthermore, all three values alter (and by different amounts) when current flows. The introduction of a third electrode (the reference electrode) which does not take part in the current path and so has a stable potential, is used to determine the electrode potentials. The positioning of this electrode will depend upon the expected distribution of potential in the cell.

The distribution of potential in a three-electrode cell depends upon the concentration of the electrolyte (Albery, 1975). Figure I(1) demonstrates this relationship; from this figure it can be seen that the effect of uncompensated solution resistance is greatest for the least concentrated (most resistive) electrolytes. This solution iR drop between working electrode and reference is only significant for high-current, low-conductivity cells, and is not large enough to introduce significant errors into the low-current, high conductivity cells of this work.

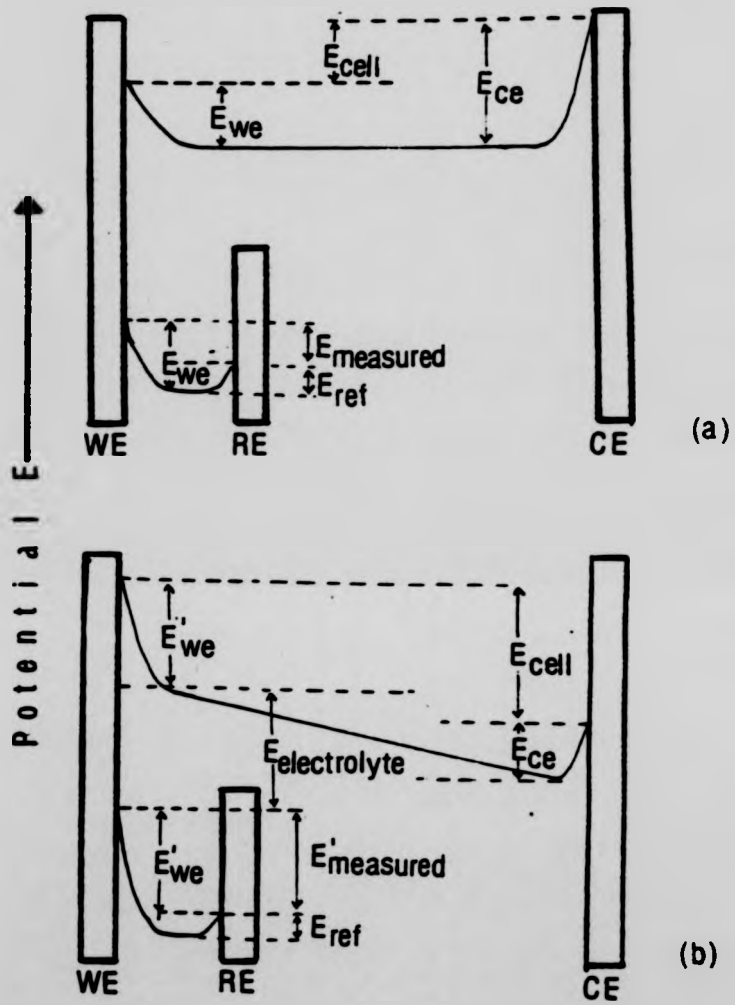

Figure I(1) The distribution of potential in a 3-electrode cell: WE (working or test electrode), RE (reference electrode) and CE (counter electrode. (a), under zero-current, open-circuit conditions; (b) with an applied current, taking the convention that an anodic current is positive. The overpotential is $E'_{we}-E_{we}$ which is equal to $E'_{measured}-E_{measured}$ since the reference potential E_{ref} remains unaltered.

Appendix II to Chapter 3

The Potentiostat

A potentiostat is a device for the controlling of the potential between a working electrode and a reference electrode, making it equal to an externally set value (Hickling, 1942). This value may be static or time-varying. The potentiostat control system is usually a differential operational amplifier with high open-loop gain; this provides an output when there is a difference in potential between the externally set potential and the potential difference which exists between working and reference electrodes. As is shown in figure II(1) of a simple single-amplifier potentiostat circuit, this then drives a negative feedback circuit between the counter electrode and working electrode in such a way as to reduce the operational amplifier input to zero. The potentiostat may be modified for constant-current function by generating a potential across a resistance in line with the counter electrode when current flows. This potential is fed into the differential amplifier as before.

West (1970) outlined the principal variables of importance for the electrochemical control circuitry. These are: the closeness of control of the applied potential, and whether it can be measured; the provision or otherwise for scanning the potential, and the rates of scan available; the ease by which output current can be changed from positive to negative, and how sensitively current can be measured; the rise-time (speed

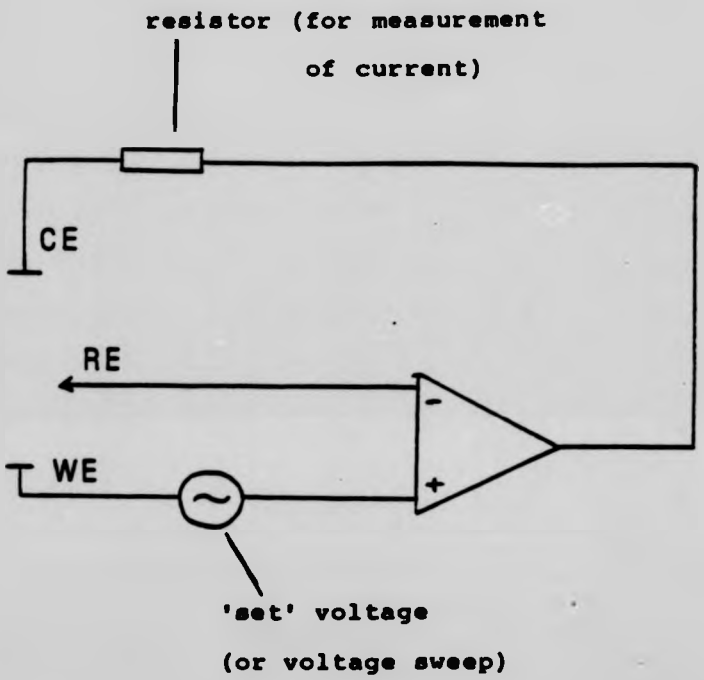

Figure II(1) Single amplifier potentiostat circuit.

of response), long-term stability and (for commercially available potentiostats) the servicing facilities.

The optimum design of a potentiostat should meet several standards (Sawyer and Roberts, 1974): a) the circuit should provide accurate control of potential, with no iR drops through the signal generator or current-measuring resistor that lead to potential control errors; b) a design which uses a single-ended rather than differential amplifier is preferred due to the lower drift of the former; c) because it is most convenient to refer all signal inputs and outputs to a common ground, a circuit design that allows the signal generator and the current measuring device each to have one terminal grounded is desirable.

Commercial potentiostats typically have an output power of 15W (1A at 15V) or more, and are designed for a wide range of metal tests and analyses, corrosion studies, fuel cell and battery investigations. Such 'general-purpose' facilities are not required for the physically small samples of this work, and it was anticipated that this work or future work would involve measuring very low currents (perhaps under 100nA) with a minimum of electronic noise. It was decided to design and build a potentiostat here, around the specific needs of the electrochemical corrosion of small specimens.

The circuit of the potentiostat designed and built for this work is shown in figure II(2). It is essentially a differential amplifier system of the type discussed above. It

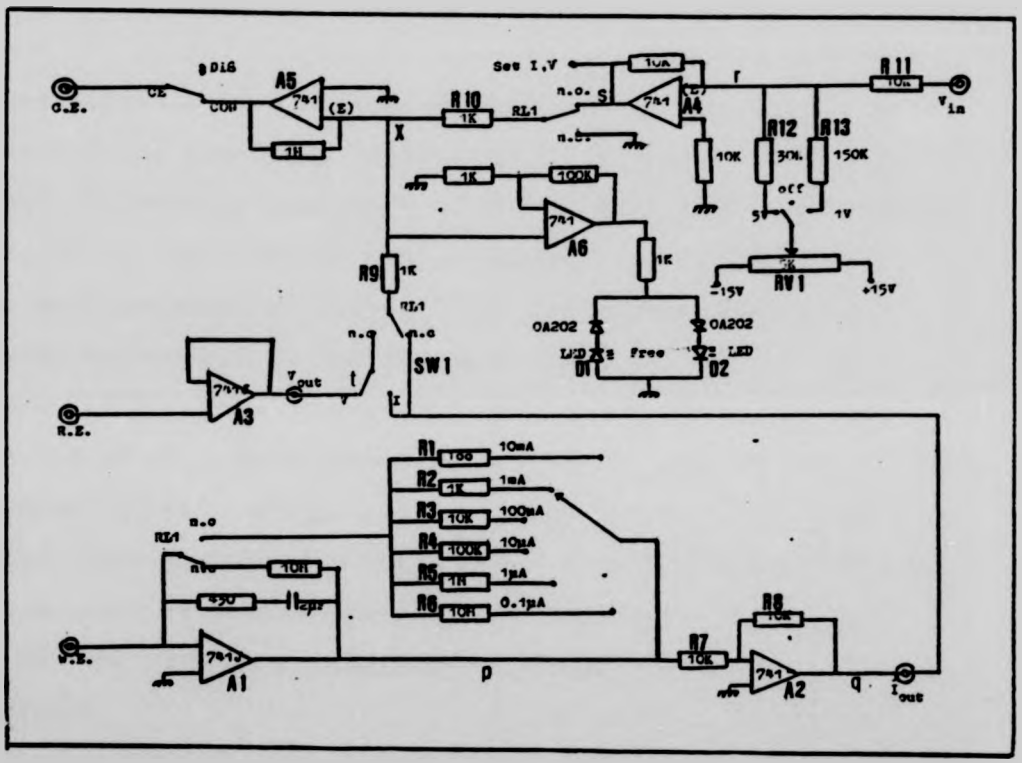

Figure II(2) The potentiostat circuit.

can be used for potentiostatic and galvanostatic work, and has an internal ramp generator for time-varying potential and current clamping. The maximum cell voltage which the potentiostat can maintain is about $\pm$14V, and the maximum current about 20mA.

A significant feature of this circuit is the 'virtual earth' of the current measuring and control system. The current through the working electrode passes to the JFET operational amplifier 1. This has an input impedance of 10^{12} to 10^{13} ohms, and produces a voltage at (p) proportional to the current, and scaled by the feedback resistors R_1 to R_6 (for example, if 1 kilohm is selected on the current range, then an output of 1V will be produced by an input current of 1mA). Amplifier 2 has unity gain (R_7=R_8), and re-inverts the voltage; this current-derived voltage at (q) is a non-inverted voltage which is proportional to the current. It is used to provide the current measurement output, and for current clamping.

The voltage at which the working electrode will be set is the sum of any voltage input at V_{in}, plus the voltage from RV_1. The series resistors in this part of the circuit (R_{11} to R_{13}) produce a current at (r) proportional to the total set voltage. The purpose of amplifier 4 is to re-invert, and produce a voltage at (s) proportional to the current at (r) (and hence proportional to the total set voltage). R_{10} turns this voltage into a current i' at the summing point 'X'.

The voltage from the reference electrode feeds into amplifier 3. This is a high input-impedance JFET (10^{12} to 10^{13} ohms): a high impedance here is desirable because the passage of significant currents would disturb the equilibrium potentials of reference electrodes. This amplifier produces an output voltage at (t) equal to the input voltage, and so provides the voltage output measuring signal

Switch SW_1 selects voltage derived from the current, or voltage from the reference, according to whether the system is to operate in galvanostatic/galvanodynamic or potentiostatic/potentiodynamic mode respectively. Whichever voltage is used is then converted to current i'' by R_9. Currents i' and i'' are added at the summing-point X. If the reference voltage (or current-derived voltage) equals the total set voltage, then the two currents produced will be equal and opposite, hence there will be no current at point X, so the power amplifier 5 will not produce an output voltage. If; on the other hand, the currents are not equal (set voltage is smaller or larger than reference voltage or current-derived voltage) then there will be a non-zero current at X. Amplifier 5, which is set with a gain of 1000, will respond by producing an output voltage which goes to the counter electrode. If the cell is operating normally, the voltage applied to the counter electrode will act on the working electrode so as to return the current summed at X to zero.

On occasions the conditions may be too extreme for the potentiostat. The voltage required at the counter electrode

for the balance conditions may be greater than the supply voltage if the electrodes or electrolyte are of low conductivity, or (an extreme example of low conductivity) there may be an electrical discontinuity such as a poor contact or loss of electrolyte between counter and working electrodes. When these conditions occur, the potentiostat will not produce current balance at X, and amplifier 6 produces a voltage at (u). This drives the indicator LED D_1 or D_2 according to the sign of the voltage.

Maximum output current is 20mA anodic or cathodic, and maximum cell voltage (counter electrode/working electrode) is 14V; the reference electrode/working electrode voltage could also be clamped to near 14V if the cell voltage maximum is not exceeded. As is normal with potentiostats, the use of capacitors has been avoided since they damp the speed of response: the rise-time of the counter electrode for a step input of 1V is approximately 5 microseconds. The potentiostat is linked with a Bryans 26000 series A3 chart recorder for current and voltage recording. This system has been calibrated by comparing the current reading output with the current measured by a battery-operated milliammeter in series with a 'dummy-cell' made of resistors. Current-measuring output is accurate to better than 0.1%. A similar approach was taken with the calibration of V_{out} , and this, too, has an accuracy of better than 0.1%

Additional circuitry allows potential and current to be set, displayed and output with the cell in open-circuit conditions.

The internally-set voltage range is $\pm$5V, and an internal ramp-generator can provide linear anodic, cathodic or cyclic ramps within the range $\pm$4V. The integrator for measurement of total charge is an external unit into which is fed the I_{out} voltage.

CHAPTER 4

ELECTROCHEMICAL RESULTS

4.1 Introduction

The basis of electrochemistry is the investigation of the relationship between current and potential at a metal/electrolyte interface. The first step, therefore, is to determine whether to control the current and measure the potential, or whether to control the potential and measure the current.

One of the major aims of this work is the quantitative linking of electrochemistry with X-ray microanalysis. This suggests that current should be the controlled parameter, with the potential of the electrode being measured as a function of time. By controlling current it might be expected that correlations between silver lost (as measured by X-ray microanalysis) and charge passed (found by recording the time for which the steady current flowed) would be simple.

Early experiments were carried out in this manner, but results lacked consistency and reproducibility. This occurs because the potentiostat produces a 'set' current by raising the electrode potential until the set current is achieved. If the current is set to a value higher than that which the alloy is capable of achieving by dissolving out silver, the

potentiostat rapidly raises the potential until oxygen evolution occurs. When this happens, the current is produced solely by the electrolytic breakdown of water, and the size of the charge passed bears no relation to the silver dissolution current. Variations between the current-producing capability of different alloy compositions cause further complications, since there is no single value of current density that can safely be applied to all compositions without eventual oxygen evolution, particularly with gold-rich specimens.

The controlled parameter is therefore the electrode potential. This can be held at potentials where oxygen evolution is not significant, hence currents will be produced by mechanisms more likely to be pertinent to the corrosion processes. Whilst the potential is controlled, current or total charge are recorded; the particular conditions used are discussed individually in each section. Potentials are quoted on the saturated calomel electrode scale; the conversion to the standard hydrogen electrode scale is:

$$E_H = E_{sce} - 241 \quad mV$$

4.2 Cyclic Voltammograms

Voltammograms, which are arguably the most fundamental of the electrochemical characterisations and are the most frequently used, are produced by applying a linear ramp potential to the working electrode and recording the current produced against the potential. They are ideally 'steady-state' curves,

produced either with rate of change of potential which is infinitesimal, or with a series of potential steps, after each of which the current level is allowed to stabilise before being recorded. Neither of these approaches is appropriate for the small samples of this work; not only would the stabilised currents be too small to measure accurately, but the limited silver in the sample would be exhausted during the stabilisation of the current, and so would not be revealed in the subsequent current/voltage plot.

Cyclic voltammograms reveal anodic processes by the measurement of net anodic currents which arise at various potentials. These currents are ideally produced by a single mechanism, such as the monovalent dissolution of one electrode metal, or the deposition onto the electrode of a negative ion from the electrolyte. Frequently, the net anodic current is a mixture of two or more current-producing effects; by reversing the current sweep towards more negative potentials following the anodic run, cathodic processes which correspond with various anodic processes will then be observed. Cyclic voltammograms thus provide a method of monitoring anodic processes by looking at features on subsequent cathodic curves.

The rate of change of potential used here is 50 mV s^{-1}. Voltammograms taken of samples in the quasi steady-state which this constantly changing potential causes have clear, reproducible features which are large enough to be seen clearly. The size of a feature depends upon the sweep rate

for the following reason. The voltammograms are plotted as current as a function of potential. Since the potential is undergoing a linear increase with time, the curves are effectively current/time plots; for example, if the potential is plotted at 100mV per centimetre then, as an increase of 100mV takes 2 seconds at the potential ramp rate of 50mV s^{-1}, the axis also has the dimensions of 2s cm^{-1}. If the current scale is, say, 1mA cm^{-1} then an area under a curve of 1cm^2 represents 1mA x 2s = 2mC. Put another way, a current-producing phenomenon which causes a total charge of 2mC to pass will produce an anodic feature on this scale with an area 1cm^2.

This may be compared with the nature of the trace produced by the same phenomenon at the slower ramp rate of 5mV s^{-1} but with the same vertical current scale. In this case a 100mV increase will take 20s, so a 1 centimetre square will represent 1mA x 20s = 20mC. The 2mC phenomenon will now produce a much smaller feature, with an area of only 0.1cm^2. In order to produce adequately sized features, any decrease in ramp rate needs to be accompanied by an increase in the current-recording sensitivity, with the subsequent decrease in signal:noise that this entails. Apart from size, there is no discernible difference between features produced at the sweep rate of 50mV s^{-1} and those produced at rates as low as 1mV s^{-1}. On the other hand, more rapid potential change causes the features to spread and merge, although they still commence at potentials comparable with the slower rates.

The robust, mica-mounted specimens are used for this work. Being of uniform composition throughout, there can be no contributions to electrochemical behaviour from other elements. Furthermore, all parts of each specimen are protected with a lacquer mask, other than the contact which is above the electrolyte and the 3mm diameter test area which is immersed in the electrolyte. Using test areas which are identical in size, meaningful comparisons of currents (i.e., current densities) may be made between different specimens.

The specimen to be tested is held vertically in the glass cell (figure 3.2.1) employed for 'paddle' specimens, in fresh electrolyte under open-circuit (zero-current) conditions. On immersion, potentials of 300 to 400 mV are measured for all alloy specimens, but this drops during the first minute or two to 50 to 100 mV. The change is rapid at first, but soon slows. When the potential has achieved a steady value potentiostatic control is applied, with the initial clamp potential set equal to the open-circuit potential of the test electrode. Because these potentials have been carefully matched, the test electrode is still effectively under open-circuit conditions, having been subjected to neither an anodic nor a cathodic overpotential which could cause respectively dissolution of or deposition onto the specimen.

The potential is then swept at the set rate (50mV s^{-1}) and the current/potential curve is recorded. Cyclic voltammograms are produced with a triangular, repetitive voltage waveform which rises first to a preset anodic limit, then falls to a preset

cathodic limit before commencing to rise again. Sweep rates are equal in both the anodic and cathodic directions.

Figure 4.2.1(a) shows a cyclic voltammogram for a vapour-deposited gold film. This curve is typical not only of vapour-deposited gold specimens, but also of relatively impure (99%) rolled gold sheet. The first anodic feature is seen to be a low-current plateau (around 100μA cm^{-2}) which commences at 1200mV. One possible cause of such a plateau is a parasitic effect brought about by impurities in, or breakdown of, the electrolyte. Comparison of this curve with a similar curve produced with platinum (4.2.1(b)) shows that the latter has no equivalent peak or plateau, hence the plateau is specific to the gold electrode. The nobility of gold rules out dissolution as the likely current-producing effect, hence it is speculated that the plateau is caused by the formation of a surface film, probably an oxide, a hydrated oxide, or a chemisorbed oxygen layer.

At higher potentials the plateau runs into a region where current increases rapidly with potential. This is the anodic electrolyte breakdown of oxygen evolution, commencing at about 1500mV. If the specimen is subjected to higher potentials than this, bubbles of oxygen can be seen to form on the electrode and, after removal, the gold takes on a distinctly reddened appearance which might be associated with the formation of an oxide.

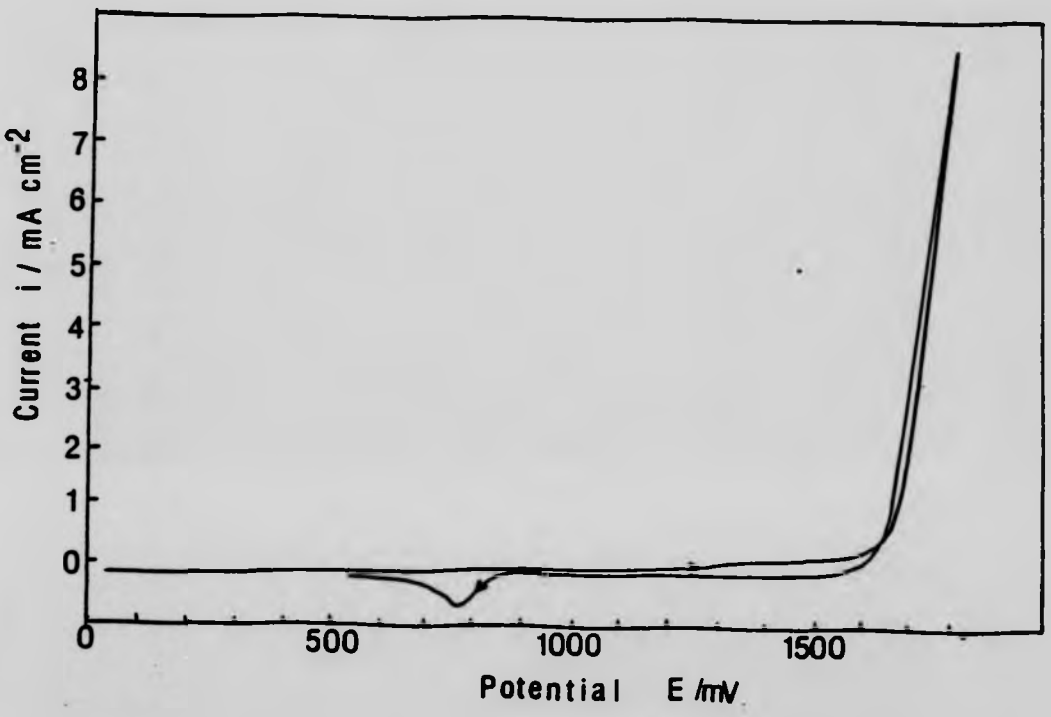

Figure 4.2.1(a) Cyclic voltammogram for vapour deposited gold in 0.1M HNO_3. Voltage ramp rate: 50mV s^{-1}.

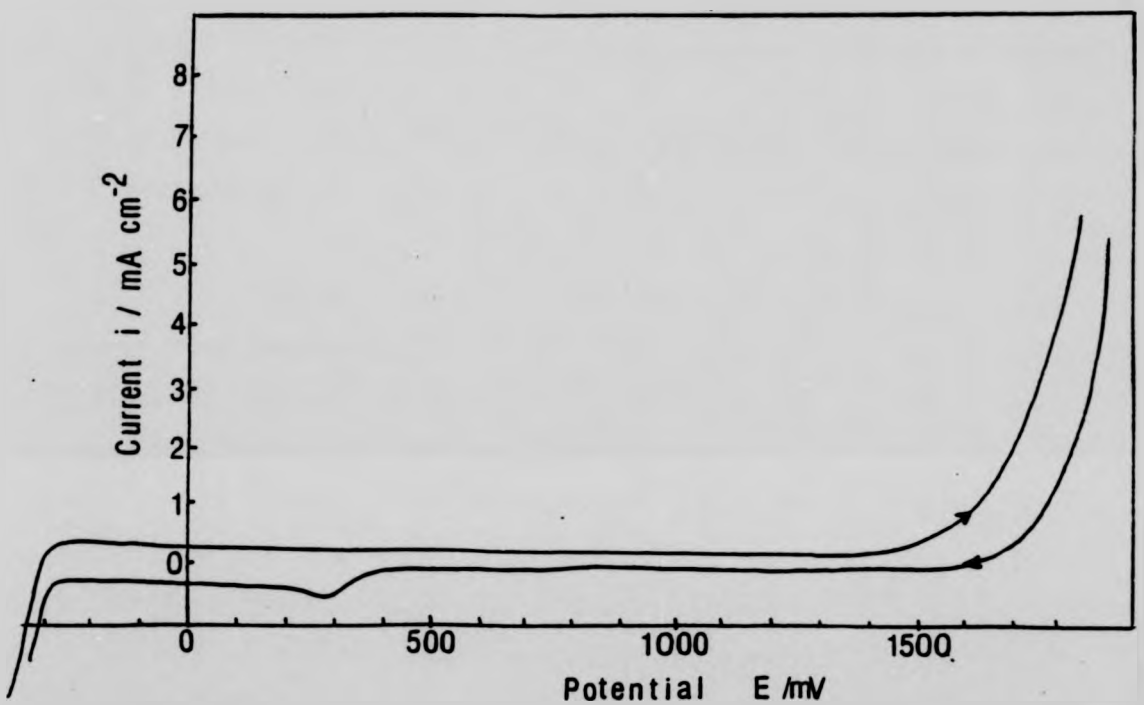

Figure 4.2.1(b) Cyclic voltammogram for Pt foil in 0.1M HNO_3. Voltage ramp rate: 50mV s^{-1}.

The main feature of the cathodic curve, produced when the potential is ramped in the negative direction, is a reduction peak which commences at between 900 and 950mV. Its presence may be explained by the reduction of surface species (such as anodically formed oxides) produced on gold by potentials above 950mV. The negative limit on the cathodic curve is approximately -250mV, where hydrogen evolution takes place on the electrodes.

Figure 4.2.2 shows a voltammogram for pure silver. Silver dissolution commences at about 350mV and causes a rapidly increasing current at and above this potential. The single cathodic feature is the redeposition of dissolved silver; there is no change in either the deposition or the dissolution potentials upon repeated cycling, which is evidence against the formation of a reaction-inhibiting surface film; the high solubility of silver nitrate mitigates against the formation of such films.

When gold-rich alloy specimens are tested, the voltammograms produced are identical to those produced and discussed above for pure gold. A typical alloy voltammogram is shown in figure 4.2.3, where the specimen was Au35Ag (35% silver, 65% gold). Like the curve for gold (4.2.1(a)) this curve has a current plateau of about 100μA which commences at about 1200mV and which runs into the oxygen evolution current; the cathodic curve also features a single reduction peak commencing at 950 to 900mV.

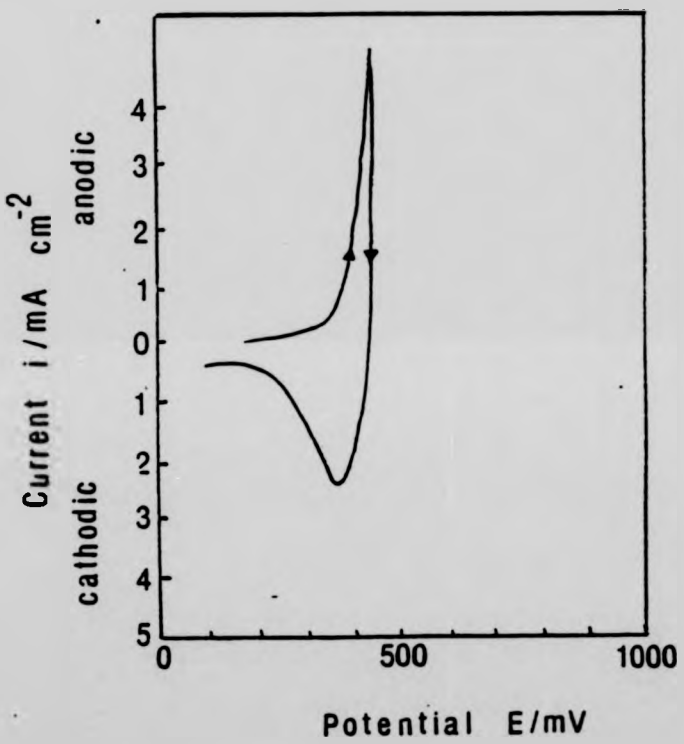

Figure 4.2.2 Cyclic voltammogram for vapour deposited silver in 0.1M HNO_3. Voltage ramp rate: 50mV s^{-1}.

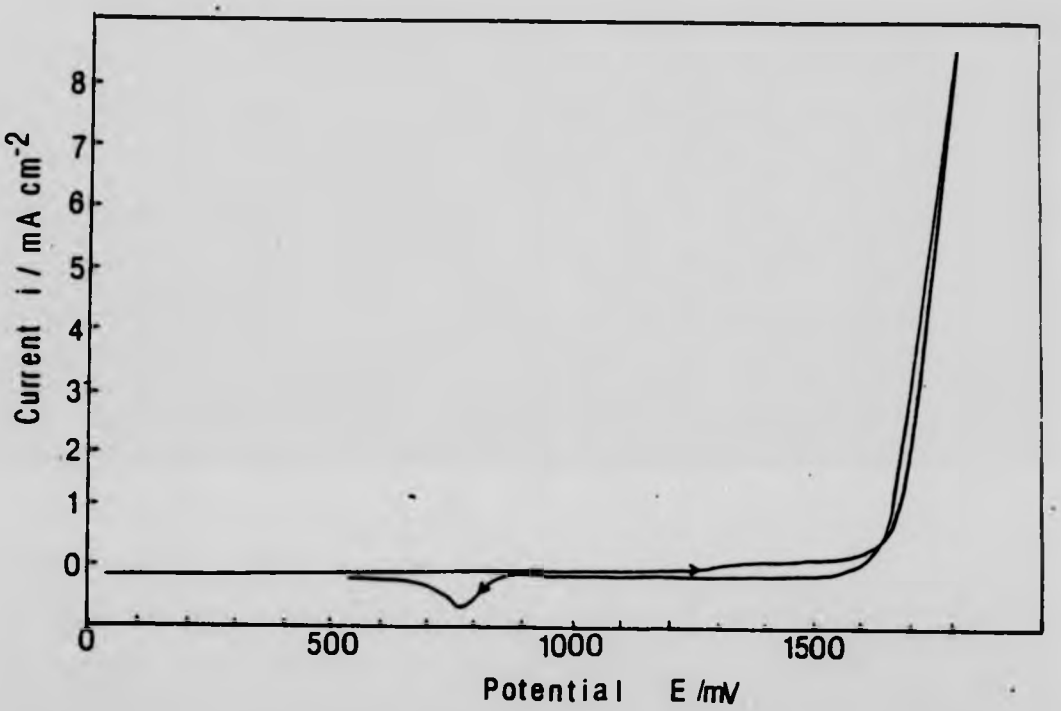

Figure 4.2.3 Cyclic voltammogram for Au35Ag in 0.1M HNO_3. Voltage ramp rate: 50mV s^{-1}

Voltammograms have been made with a range of alloy compositions in order to assess the influence of composition on the current/potential trace. A striking result is that all alloy specimens with compositions which lie between pure gold and Au55Ag produce gold-like curves. Any electrochemically driven silver dissolution from these specimens is thus too small to be detected, there being no evidence of anything other than gold-like nobility.

A different form of electrochemical behaviour is observed for specimens with over 55% silver in the alloy. A typical curve for silver-rich specimens is shown in figure 4.2.4, which was produced with Au60Ag. These alloy specimens have a single large anodic current peak or, as in this case, a pair of merged peaks, superimposed upon a gold-like curve. This particular curve has two cathodic peaks. The first small peak at 1500mV is thought to be the reduction of a surface oxide produced at a potential above 1500mV, and it is not a feature generally present in cyclic voltammograms of these alloys. The major cathodic feature, present in all cyclic voltammograms of silver-rich specimens, is the large reduction curve commencing at about 950mV.

Anodic and cathodic peaks such as these are often associated with, respectively, dissolution of the electrode material, and redeposition of the dissolved material. Since the anodic peaks are not observed on pure gold and gold-rich alloys, it may be inferred (and later tested directly) that silver is dissolved during the the anodic sweep.

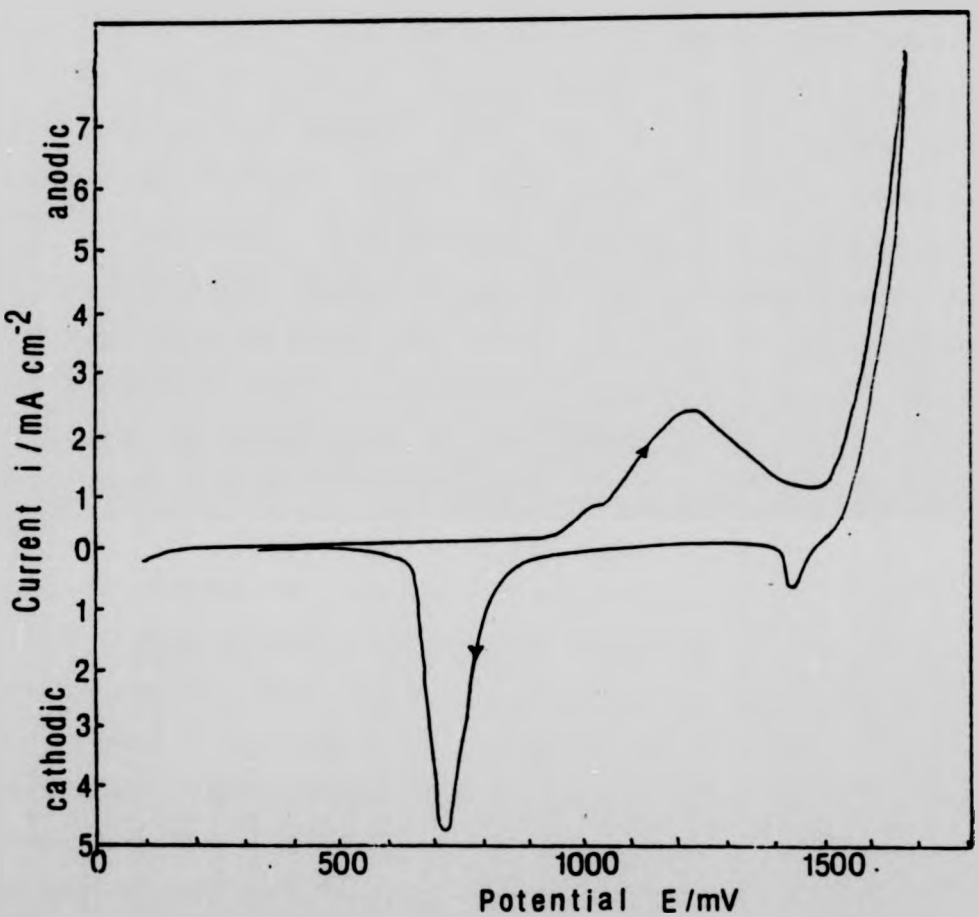

Figure 4.2.4 Cyclic voltammogram for Au60Ag in 0.1M HNO_3. Voltage ramp rate: 50mV s^{-1}.

One might now be tempted to identify the cathodic peak as a redeposition of previously dissolved silver, but if this is the case the initially very silver-rich specimens would be expected to produce even larger cathodic peaks. That this is not the case is shown by figure 4.2.5, which is a cyclic voltammogram of Au85Ag. This has a large anodic peak, followed by a cathodic peak considerably smaller than that produced by Au62Ag. Furthermore, there is an overlap of about 400mV: the anodic current starts to rise at about 500mV, with the major peak commencing at about 650mV, but the cathodic peak commences at 950 to 1000mV. A single potential within this overlap would not be expected to lead to silver dissolution on the one hand (during the anodic run) and silver deposition on the other hand (during the cathodic run). It might be possible to explain both curves as arising from silver dissolution and deposition currents, by postulating various changes which might take place in the specimen during the anodic run. This is unlikely to be the correct explanation, and whilst the anodic peak arises from dissolution and oxidation, the cathodic peak is thought to be due only to the reduction of surface oxides.

The next graph in this section, figure 4.2.6, shows three cycles produced with Au62Ag. The first anodic and the first cathodic peaks (labelled '1' on the figure) are large and clear, and are followed by successively smaller anodic and cathodic peaks. The second anodic peak is only produced when the specimen has been cycled through the first cathodic peak; this is confirmed in figure 4.2.7, for a similar Au62Ag

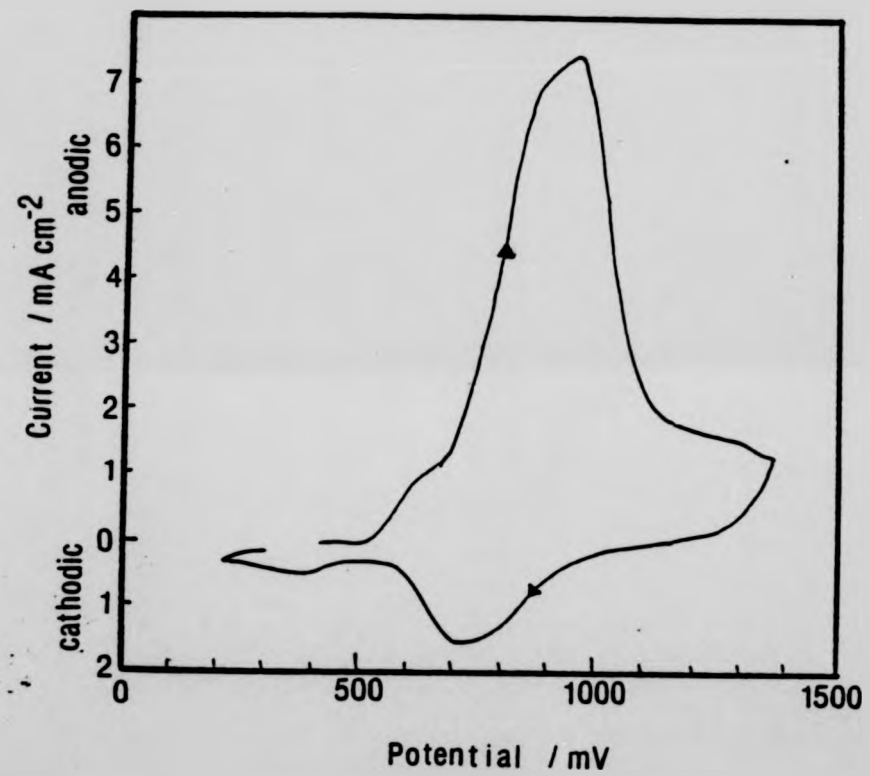

Figure 4.2.5 Cyclic voltammogram for Au85Ag in 0.1M HNO_3. Voltage ramp rate: 50mV s^{-1}

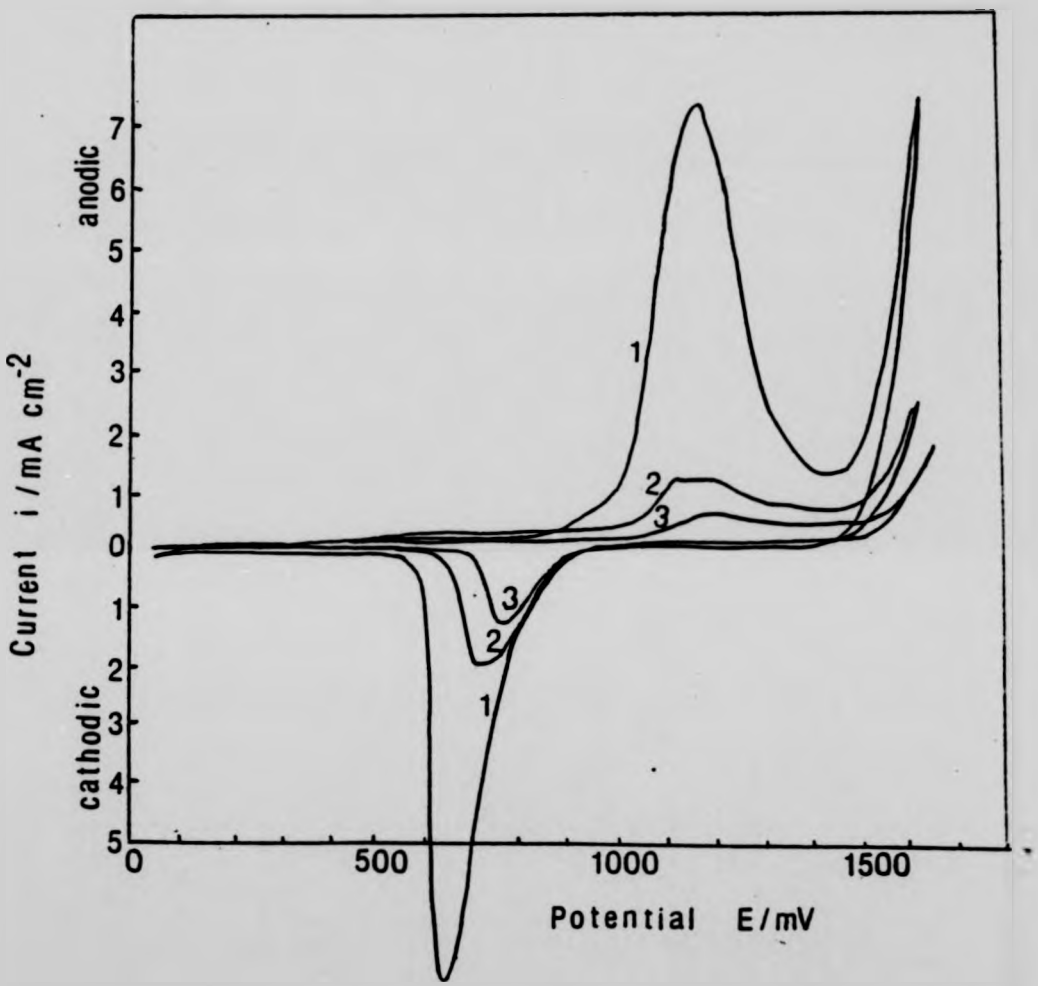

Figure 4.2.6 Cyclic voltammogram for Au62Ag in 0.1M HNO_3. Three consecutive sweeps from +50 to +1600mV; voltage ramp rate: 50mV s^{-1}.

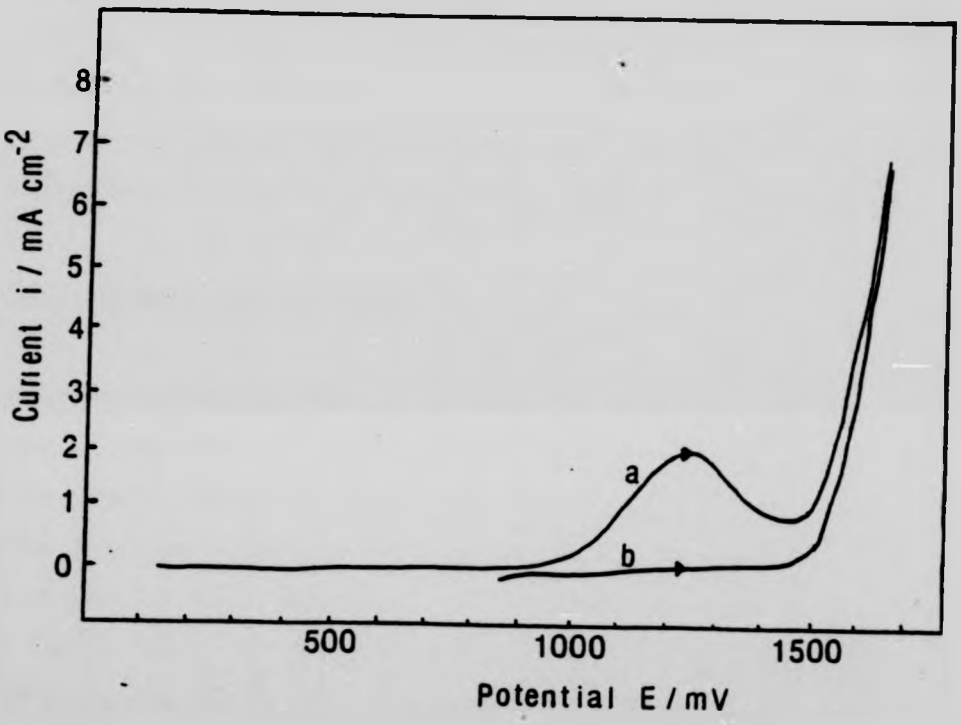

Figure 4.2.7 Single anodic sweeps for Au62Ag. Sweep (a) is the first sweep undertaken; sweep (b), on the same specimen immediately after the first sweep, shows that no silver dissolution current can be produced on subsequent anodisations of these thin films.

specimen cycled between 900 and 1500mV. In this case, there is no anodic peak on the second cycle, hence anodic peaks 2 and 3 (figure 4.2.6) arise from cathodic peaks 1 and 2 respectively. The detailed processes which produce these peaks are not thought to be parallel and independent dissolution and oxidation processes, followed by reduction and perhaps deposition, but it will instead be shown in this thesis that the processes are linked. The nature of this interrelationship will be further discussed in chapter 6.

4.3 Single-Sweep Voltammograms

The cyclic voltammograms presented in section 4.2 are essentially two separate, though associated, phenomena. The first is electrochemical dissolution of a metal to produce solvated M^+ ions; this may be accompanied by an oxidation reaction and by the deposition of negative ions from the electrolyte. This takes place during the anodic sweep when the electrode potential is raised above an equilibrium value. The second phenomenon is reduction, and this takes place during the cathodic sweeps, when the potential is reduced below some reduction value. The single-sweep voltammograms discussed in this section are produced in the same manner as cyclic voltammograms, but the sweep is a single voltage ramp which goes from the open-circuit value to a preset anodic limit (1600 mV). Since the test electrodes are driven in the anodic direction, the electrochemical curves produced are associated with metal dissolution, and not with metal deposition.

X-ray microanalysis (E.D.A.X.) has been undertaken on alloy specimens covering the whole range of compositions. This has shown that a marked reduction in silver content occurs only after the specimens have been subjected to a voltage sweep across the anodic peak. Although it cannot be stated that the anodic peak is solely the result of a silver dissolution current, the converse - that measurable silver dissolution does not occur in the absence of the anodic peak - is indeed the case. The observation has already been made in section 4.2 that specimens which have under 55% silver do not produce the anodic peak, and E.D.X. examination of such specimens following a single anodic sweep reveals that very little or no silver has been dissolved. Similarly, E.D.X. examinations of silver-rich specimens shows that if the anodisation is stopped before the commencement of the peak, the alloy composition has not altered; the specimen becomes silver-depleted only when the anodic peak has been reached and entered.

Figure 4.3.1 shows a set of single-sweep anodic voltammograms, displaced according to silver percentage. Although different alloys produce differently shaped voltammograms, overall, this graph reveals marked trends between the voltammograms. The first observation is that the onset potentials of the major anodic features vary according to the initial alloy compositions: the less silver-rich is the specimen, the higher is the onset potential of the feature. The first large peak of the Au89Ag specimen (curve (b) commences rising at about

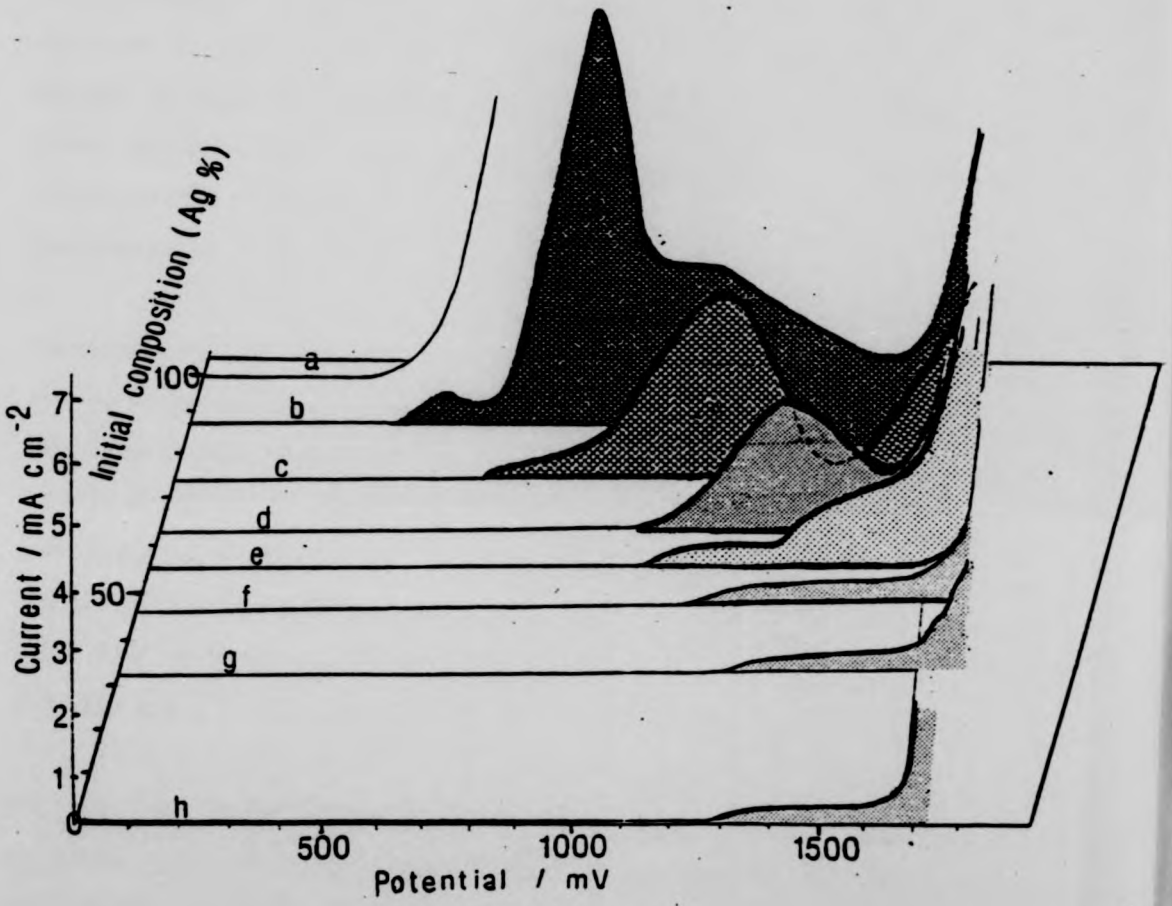

Figure 4.3.1 Single-sweep anodic voltammograms for silver, gold, and a range of silver-gold alloys.

500mV, for example, compared with 950mV for Au64Ag, curve (d). The trend towards higher onset potentials for this feature with decreasing silver content suggests that for gold-rich specimens (those with under 55% silver, which do not show the anodic feature) the onset of this feature requires a potential more noble than that for water breakdown, so would be supplanted by oxygen evolution as the current-producing phenomenon.

Examination of figure 4.3.1 also reveals that the more silver-rich is the specimen, the larger is the anodic feature. The first and obvious reason for this is that the more silver-rich is a thin film specimen, the greater is the quantity of silver which might be dissolved. Another reason, which is supported by evidence given in the next section, is that the more silver-rich is the specimen, the greater is the percentage of alloyed silver which can be removed.

As is shown in figure 4.3.1, different alloy compositions produce differently shaped single-sweep anodic voltammograms. The curve for pure silver (curve (a)) is that of silver dissolution, commencing at about 350mV. Curve (b), produced by the most silver-rich of the specimens shown on this graph, Au89Ag, is by comparison a very complex one. The first feature is a small peak commencing at about 380 mV which merges into a large peak which, by extrapolation, commences at about 500 mV. This peak merges with a third peak which is lower but seemingly broader than the second peak. All three of these anodic features are probably associated with silver

dissolution, but their presence indicates that, on these very silver-rich specimens, silver either dissolves in various modes or from different types of atomic sites.

Curve (c) was made with Au73Ag, and although it shows two anodic features, the first is a low plateau somewhat reminiscent of that formed by pure gold, though at a lower potential (commencing at about 600mV, compared with 1200mV for gold). The plateau runs into a clean anodic peak. Curve (d) has only one anodic peak, no plateau being visible for this Au64Ag sample. This peak is not seen in its entirety because it merges with the oxygen evolution current. The merging of this peak with the oxygen evolution current is more noticeable with Au57Ag used for curve (e); this peak is preceded by a low-current plateau.

A low-current plateau is the only feature on the remaining (gold-rich) specimens (f) and (g), and on pure gold (h). The plateau commences at the lower potential of about 1100mV for Au48Ag (curve (f)) compared with 1200mV for gold. An interesting possibility which now arises is that, if these low-current plateaux represent the formation of a surface species such as gold oxide, then the formation potential of this oxide appears to exhibit some dependence on the alloy composition. It could also follow that the rate of formation and decomposition of such a film might influence the dissolution characteristics of various silver-rich alloys.

4.4 Potentiostatic Coulometry and Microanalysis

Microanalysis of specimens which have been subjected to single anodic sweeps of potential reveals that the anodic current feature is associated with the dealloying of some silver from the original specimen. The anodic feature covers a few hundred millivolts and it cannot be assumed that silver dissolution necessarily takes place over the whole of the potential range covered by the anodic feature. The nature of the relationship between potential, alloy composition and the extent of silver dissolution is investigated in this section.

Each specimen was subjected to a fixed anodic potential for 300s whilst the current output signal was fed into an electronic integrator. The integrator produces a voltage output proportional to the total charge represented by the current signal; fed to a chart recorder, direct measurements of total charge as a function of time were made. Following this treatment the specimen was analysed for the silver:gold ratio; the amount of silver dissolved out of the alloy was found by comparing this value with that for the untreated specimen.

Up to ten specimens of each composition were subjected to a single anodic potential, in order to provide a series of potentials which includes and overlaps the position of the anodic feature of that specimen. Following the anodic treatment, each specimen was washed by dipping in distilled water, so preventing any silver precipitation upon drying (any

silver precipitation would lead to erroneous E.D.A.X. analyses of gold:silver ratios in the alloys). Each specimen was then placed in the scanning electron microscope and gold:silver ratios determined by E.D.A.X. analysis. This final ratio was compared with the initial gold:silver ratio using the gold as a standard, and the amount of silver removed by the electrochemical treatment was calculated; quantitative information on the silver lost was obtained by referring to deposition data using the method shown in section 3.7.

Figure 4.4.1 shows a typical family of charge/time curves, produced by Au84Ag specimens which have each been subjected to a fixed potential for 300s. At low anodic potentials (500mV and 600mV in this case) very little charge was passed, and subsequent analysis reveals that very little silver was lost (equivalent to two or three atomic layers of silver). When higher potentials were imposed then significant quantities of charge were passed, and E.D.A.X. analysis reveals that the passage of significant charge was accompanied by silver depletion from the alloy. A significant quantity of charge is passed, and a significant quantity of silver is removed from specimens whose current/voltage curves show the anodic feature discussed in sections 4.2 and 4.3. The less silver-rich is the specimen, however, the greater is the potential required for the passage of significant charge and for the associated silver removal. This is illustrated by comparing the potentials required by different alloys to produce a specified charge at 300s. For instance, the Au84Ag specimen shown in figure 4.4.1 required 300s at 800mV to produce a total charge

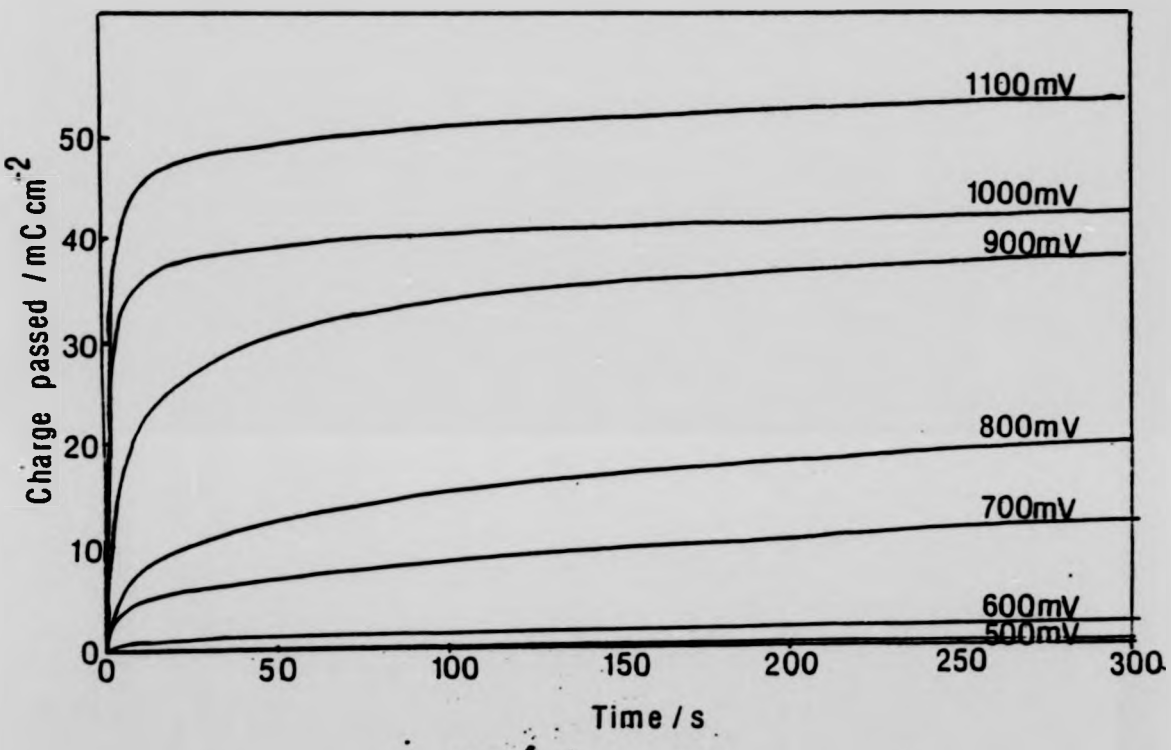

Figure 4.4.1 Charge/time curves for Au84Ag held at various potentials in 0.1M HNO_3. Significant silver dissolution currents, leading to measurable charge passage, occur with anodisation potentials as low as 700mV with this composition.

of 18mC cm^{-2}, but the same charge was passed in a more silver-rich specimen (Au92Ag) at the lower potential of 650mV. Conversely, a less silver-rich specimen (Au66Ag) required 1050mV to pass the same charge.

The charge/time curves for silver-rich alloys (those over 55% silver, for which the anodic feature is produced) are all similar, though the families of curves are shifted towards more noble potentials as the silver percentage is decreased. Alloys with under 55% silver, for which the anodic feature is not seen, all produce charge/time curves of the type shown in figure 4.4.2 for Au40Ag. The charge passed for these specimens is very small.

Having been subjected to fixed anodic potentials for 300s, specimens were analysed for their final compositions. Each alloy composition thus yielded a set of final compositions for specimens each of which had been anodised at a different potential. The family of curves shown in figure 4.4.3 compares sets of final composition values obtained with a series of initially silver-rich alloys; although gold-rich alloys were treated similarly, their final compositions are not shown on this graph since the composition change was always under 2%.

Figure 4.4.3 shows that there are three categories into which the dissolution behaviour of the alloys falls. The first category is where anodisation appears to remove all of the silver from the alloy (E.D.X. analyses of specimens with

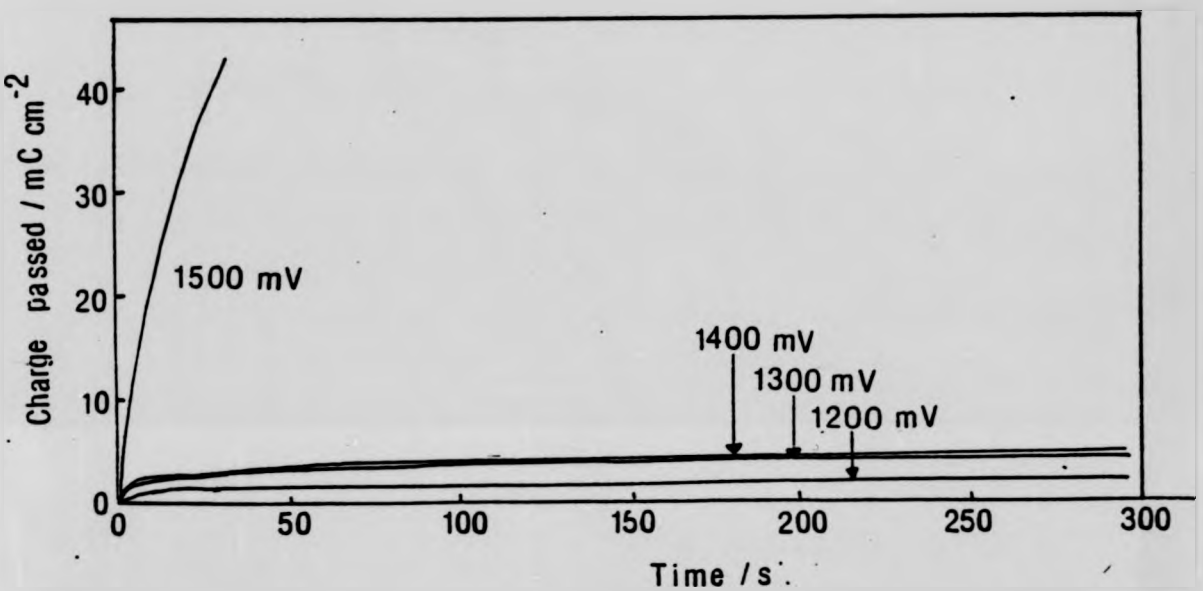

Figure 4.4.2 Charge/time curves for Au40Ag held at various potentials in 0.1M HNO_3. Very little charge is passed even by potentials as high as 1400mV. The high current produced by 1500mV is due to oxygen evolution.

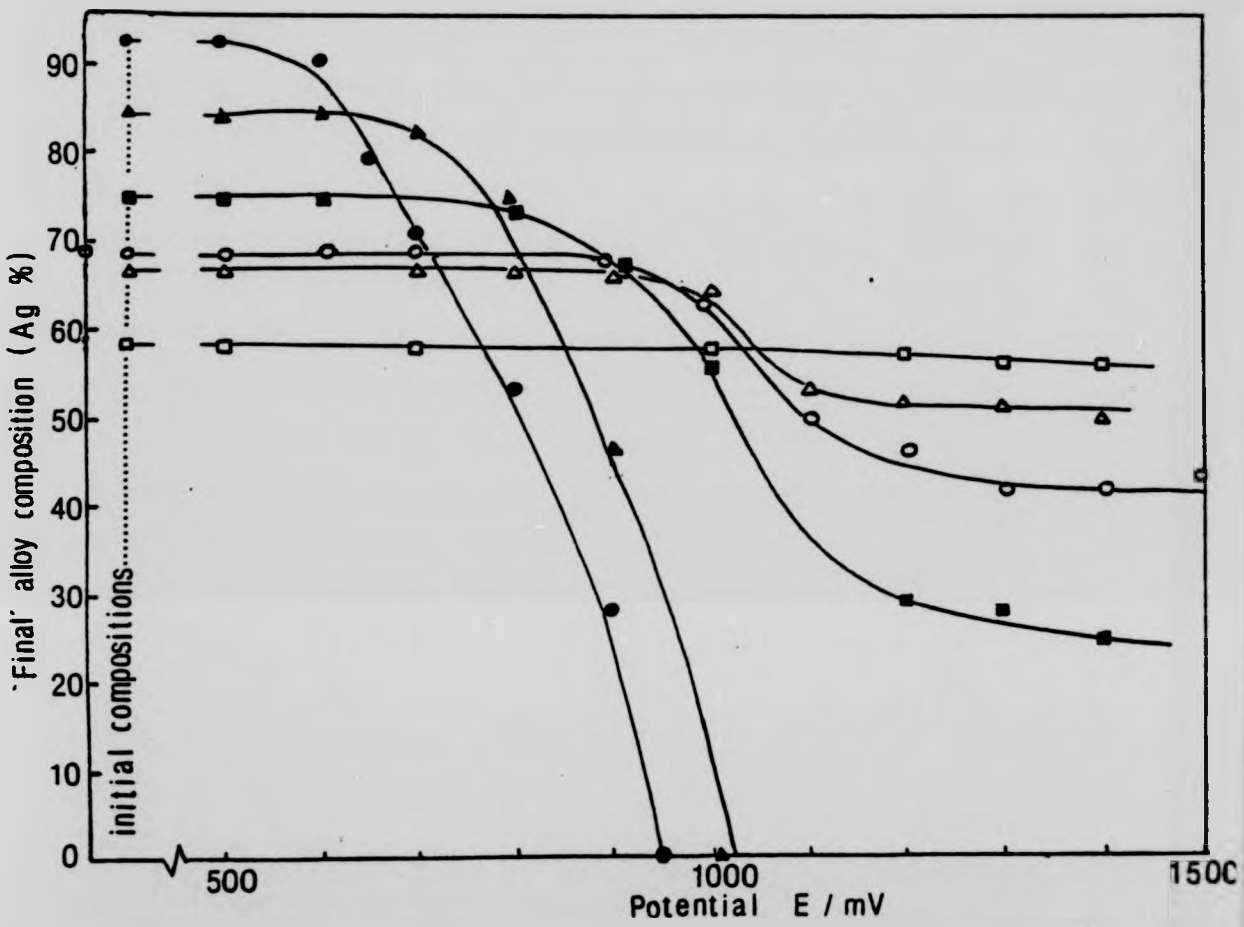

Figure 4.4.3 The relationship between the 'final' compositions of the alloys (following 300s anodisation time) and the static anodisation potentials; 0.1M HNO_3. Alloys whose initial silver concentration is 85% or over can be completely dealloyed in these conditions; alloys whose initial compositions lie between 55 and 85% silver can undergo partial dealloying; alloys with under 55% silver can undergo virtually no dealloying, so are not shown on this figure.

very low silver proportions do not yield reliable results: measurements of 'zero' silver concentration are better regarded as under 10% silver). This category is occupied by alloys whose initial silver percentage is 80% or over.

The next category is where a 300s anodisation (even at the relatively high potential of 1400mV) fails to remove all of the silver from the alloy. Specimens whose initial silver compositions lie between 55% and 80% fall into this category but, as the figure demonstrates, a lower final silver percentage is achieved by the initially more silver-rich specimens. There is no implication here that silver is uniformly distributed throughout the bulk of the specimen. E.D.A.X., not being a surface-sensitive technique, simply measures the total silver in these thin specimens without regard to any depth profile of composition. In fact, evidence that the final silver distribution is not uniform emerges by examining two specimens with the same initial composition but different thicknesses: 400Å and 1200Å. It was found that the final composition of the thicker specimen was more silver-rich than the final composition of thinner specimens, even though more silver was removed from the former. The implication is that silver is removed preferentially from layers close to the surface, with progressively less silver being removed from deeper regions.

The third category shown in figure 4.4.3 is occupied by specimens whose compositions are changed very little by anodisation. These are the alloys with under 55% silver and

so fall into the group which does not produce the anodic feature on a current/voltage curve. Although large silver depletion does not occur, anodisation at 1300mV or 1400 mV does give rise to a small silver depletion of between 0.5% and 1.5%. This was measured in all but one of over 200 separate tests, so is thought to be a significant result. The silver depletion measured would accord with the stripping of one or two layers of surface segregated silver, leaving the composition of the underlying alloy unaltered. The formation on silver-gold alloys of one or two monolayers of silver has recently been demonstrated (Tokutaka et al, 1981) using quantitative Auger electron microscopy.

4.5 Coulometry and Potential Decay

This series of experiments consisted of applying a constant anodic potential until a predetermined charge had been passed. The applied potential was then removed, and the potential/time curves were recorded under open-circuit conditions. The charge passed for all specimens was 7mC cm^{-2}. The use of this low charge satisfied two conditions: all specimens should be able to pass the predetermined charge by silver dissolution, without running out of available silver, and all specimens should reach this charge in a similar, fairly rapid time, in order to avoid complications in some specimens due to ageing effects. The potential chosen was 1200mV; this is sufficiently far from the anodic limit (1500mV) to avoid oxygen evolution yet, as figure 4.4.3 shows, total silver dissolution appears to be potential independent for all alloys

at and above 1200mV.

The potential/time curves (figure 4.5.1) are markedly similar for all alloy specimens. Each curve, other than that for pure silver, falls rapidly to a potential arrest at 890 $\pm$ 20mV. Following a measured time at this arrest the potentials begin to fall away again. This behaviour is characteristic of the dissolution of a chemically unstable surface species, perhaps an oxide formed during the previous anodic treatment.

The intercept of the extrapolated horizontal and vertical portion of each decay curve provides a nominal turning point known as the Flade potential, E_f. Anodically produced metastable films which are chemically unstable under open-circuit conditions will produce a potential arrest plateau from which E_f may be measured; furthermore, any particular surface species will exhibit a particular value of E_f. The value of E_f determined from these curves for gold and for the whole range of silver-gold alloys is 860 $\pm$ 40 mV. This implies that an anodic species is formed on gold during anodisation, and the same species (or a very similar species) is formed during the anodic dissolution of silver from silver-gold alloys.

Silver-gold alloys which are allowed to corrode freely in 35% HNO_3 produce potential/time curves as in figure 4.5.2. Alloys reached a stable potential of 820 $\pm$ 10 mV, and it is interesting to observe that this value is composition-independent. It is also close to the

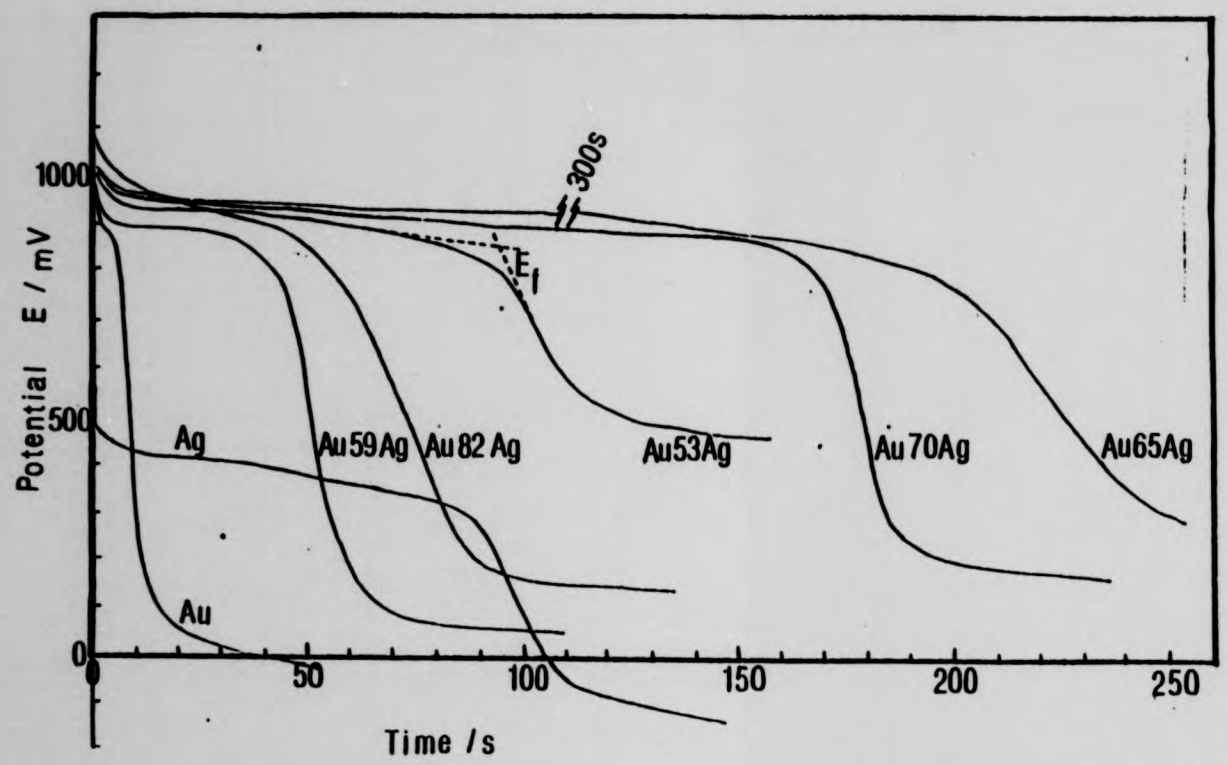

Figure 4.5.1 Open circuit potential/time curves for various silver-gold alloys following potentiostatic anodisation at 1200mV. All alloy specimens and gold produce a potential arrest at 890±20mV.

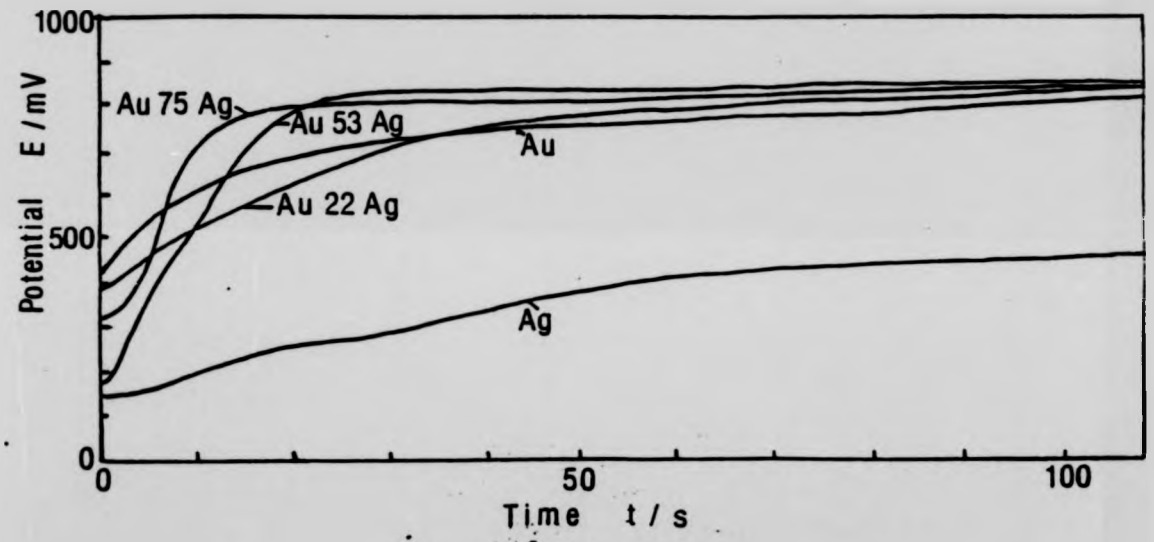

Figure 4.5.2 The variation of potential with time of silver-gold alloys corroding under open circuit conditions in 35% HNO_3. The potential reached by all alloy specimens - even the very silver-rich alloys, is the same as that reached by gold: 820±10mV.

composition-independent value of the Flade potential following electrochemical corrosion in 0.1M HNO_3. The correspondence of the potential values for these two approaches could suggest that there is also a correspondence in the nature of the alloy surfaces produced by open-circuit chemical corrosion and by anodically driven electrochemical corrosion. However, the difference in potentials is thought to indicate different processes; this concept will be discussed further in Chapter 6.

CHAPTER 5

MICROMORPHOLOGICAL OBSERVATIONS OF ANODICALLY CORRODED SPECIMENS

5.1 Introduction

When thin films of gold-silver alloys are immersed in concentrated nitric acid, a micromorphology is observed to develop on the surface (Forty and Durkin, 1980). This micromorphology consists of an island-and-channel structure, and the formation of this structure is dependent upon the initial composition of the alloy as well as the acid concentration. The chemically aggressive nitric acid environment causes corrosion, with localised anodic regions balanced by relatively large cathodic areas on the same surface. The metal dissolution takes place from the anodic regions, and it leads to a micromorphology which is observable in the transmission electron microscope.

The essential difference between chemical and electrochemical dissolution is that whilst in the former case anodic and cathodic sites lie on the same surface, and electron transfer takes place within the metal, in the latter case anodic and cathodic sites are separated, and electron transfer takes place via an external circuit. The nature of the electrical control system for electrochemical corrosion (the potentiostat) is such that it should be possible to produce a

micromorphology similar to that which develops during chemical corrosion, by making the alloy specimen anodic with respect to a suitable counter electrode. Furthermore, it should also be possible to control the extent (and possibly the nature) of the corrosion micromorphology and, by integrating the measured silver corrosion current, to quantify the silver removed from the alloy, and relate this with the extent of the micromorphology.

The main thrust of the work for this chapter was to apply the appropriate electrochemical conditions (as determined in the previous chapter) to thin silver-gold alloy films, and to examine these films under the electron microscope. In particular, the aims were to determine whether it would indeed be possible both to produce and control the development of corrosion micromorphologies, and to assess how these micromorphologies relate to the net silver loss.

5.2 Electrochemical Treatments

Following the two-stage film deposition (described in section 2.4) each specimen, already mounted on a supporting gold electron-microscope grid, was placed into the specially designed teflon cell. The electrolyte (0.1M HNO_3) was carefully pipetted into the cell, and a single-sweep voltammogram was produced with the first specimen of a batch to check the alloy composition (the basis between the relationship between voltammograms and alloy composition is discussed later in chapter 6, section 6.5). This specimen and

the electrolyte were then discarded,and a fresh specimen and fresh electrolyte were used for each of the series of tests.

The electrochemical conditions to be used were those indicated by the results from chapter 4. Thus, the electrolyte was 0.1M HNO_3, the control method was potentiostatic, and the standard anodic potential used was 1200mV; this potential is far enough from the anodic limit of the electrolyte to avoid oxygen evolution, yet is high enough to ensure the complete removal of all the available silver in all specimens used. The composition reached can be described as the 'final' composition of the specimen. The total charge passed was determined as before by integrating the current; the integrator output was fed to a chart recorder as a function of time. After each specimen had been potentiostatically corroded, the electrolyte was carefully pipetted out of the cell and the grid-mounted specimen was removed. Specimens were dried by drawing off moisture with a filter paper, but unlike the firmly mounted paddle-shaped specimens used for E.D.A.X., these specimens were not washed, since washing generally caused the specimens to float off the grids and be destroyed. Each specimen was finally examined under the electron microscope.

5.3 The Micromorphology Developed on Silver and on Gold

Figure 5.3.1(a) shows the result of producing an anodic current with a specimen consisting of 220Å of silver, on a gold substrate of similar thickness. The potential used for

(a)

0·1 μ

(b)

Figure 5.3.1 Electron micrographs of silver specimens (220Å thick) on a gold substrate, following anodic stripping at 500mV. (a) after removal of about 75% silver (calculated from total charge passage). (b) following 'complete' silver removal.

(a)

0·1 μ

(b)

Figure 5.3.1 Electron micrographs of silver specimens (220Å thick) on a gold substrate, following anodic stripping at 500mV. (a) after removal of about 75% silver (calculated from total charge passage). (b) following 'complete' silver removal.

(a)

0·1μ

(b)

Figure 5.3.1 Electron micrographs of silver specimens (220Å thick) on a gold substrate, following anodic stripping at 500mV. (a) after removal of about 75% silver (calculated from total charge passage). (b) following 'complete' silver removal.

(a)

0·1μ

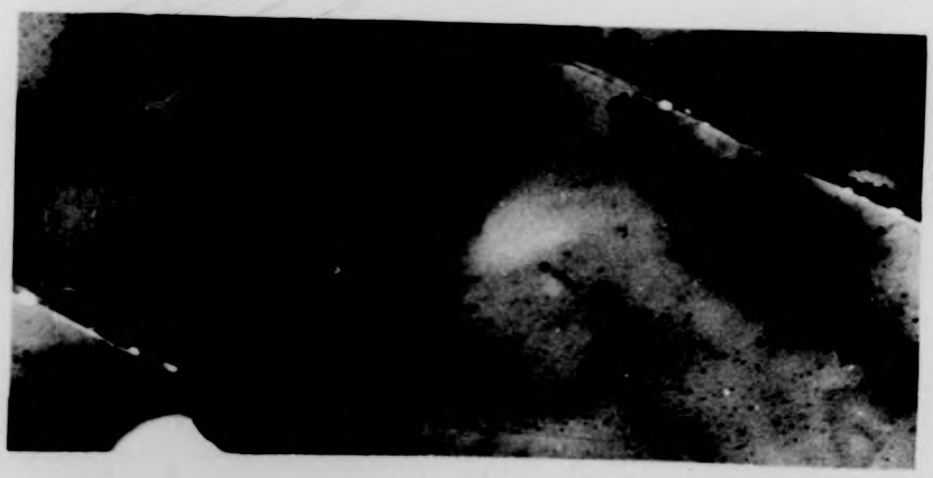

(b)

Figure 5.3.1 Electron micrographs of silver specimens (220Å thick) on a gold substrate, following anodic stripping at 500mV. (a) after removal of about 75% silver (calculated from total charge passage). (b) following 'complete' silver removal.

this was 500mV, since when higher potentials were used the silver loss was too rapid to control. In this case, the total charge passed indicated a loss of about 75% of the silver, if the current is assumed to be solely caused by silver dissolution. The main feature of this photograph is of large regions of fairly uniform brightness which appear to be encroaching upon other, darker, uniform regions. This has the appearance of a layer of silver being stripped from the gold in the light regions, which are spreading laterally over the surface, with some isolated islands of silver (dark spots) remaining on the light, gold, regions.

Figure 5.3.1(b) shows the film when most of the silver has been stripped. It now consists of large, rather featureless light areas in which the silver has been stripped from the gold substrate. There remain small darker islands in the light areas which are thought to be either islands of silver or regions of a silver-gold alloy formed on the surface; E.D.X. examination of this specimen detected some silver even after anodisation at the higher potential of 1200mV.

When gold is anodised at 1200mV for 300s (the potential used to dissolve silver electrochemically out of the alloys) no microstructural changes can be seen, as is shown in figure 5.3.2(a). The diffraction pattern of this specimen is indistinguishable from the diffraction patterns produced by all uncorroded specimens of silver, gold, and silver-gold alloys. The pattern, also shown in the figure, is that of a good, single f.c.c. crystal in a (111) orientation, having

Figure 5.3.2(a) A gold specimen anodised at 1200mV for 300s, and the associated diffraction pattern. These are indistinguishable from gold, silver and alloy specimens.

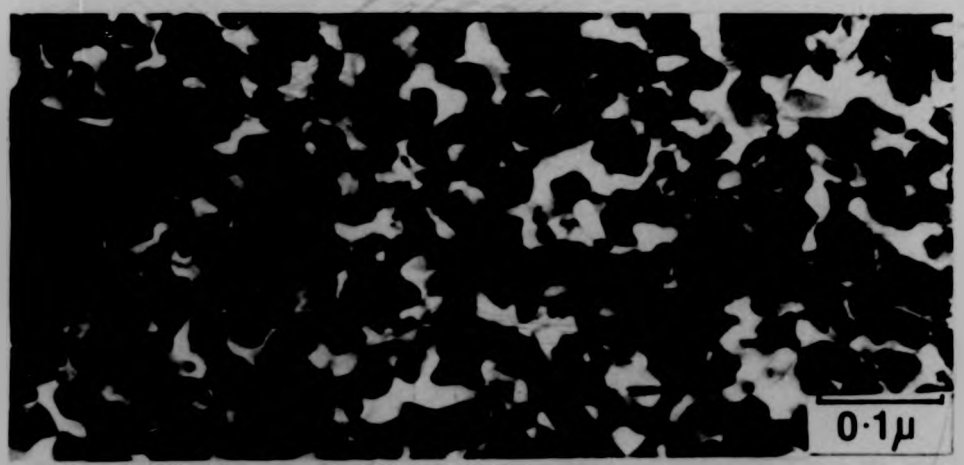

Figure 5.3.2(b) A similar gold specimen placed at a potential of 2.6V for 60s in 0.1M HNO_3, showing the considerable pitting and tunnelling which takes place at sufficiently high anodisation potentials.

Figure 5.3.2(a) A gold specimen anodised at 1200mV for 300s, and the associated diffraction pattern. These are indistinguishable from gold, silver and alloy specimens.

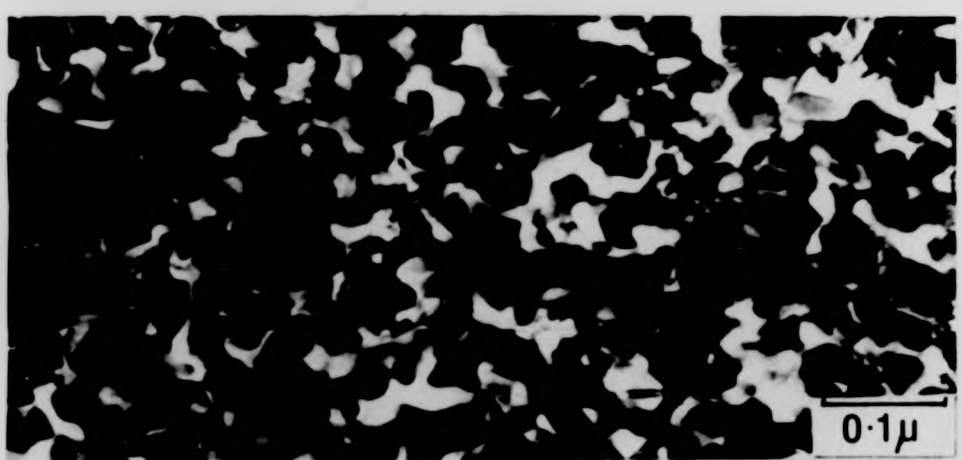

Figure 5.3.2(b) A similar gold specimen placed at a potential of 2.6V for 60s in 0.1M HNO_3, showing the considerable pitting and tunnelling which takes place at sufficiently high anodisation potentials.

strong spots corresponding to $2\bar{2}0$-type reflections. The weak spots which occur at positions close to those expected for 'forbidden' $1\bar{1}1$ reflections are thought to arise from double diffraction effects due to double-positioning twinned structures (Pashley and Stowell, 1963); they are probably therefore $1/3(2\bar{2}4)$ reflections.

When gold is anodised to a sufficiently high potential, however, considerable damage takes place. The gold specimen shown in figure 5.3.2(b) was placed at a potential of 2600mV for 60s, in 0.1M HNO_3. These were very strongly oxidising conditions, and streams of oxygen bubbles could be seen forming on the specimen during the anodisation. The figure shows that the gold film has become grossly pitted and tunnelled; similar morphologies develop where the anodisation potential is above about 1800mV. The development of this morphology is not specific to the nitric acid environment; when another gold specimen was anodised with the same conditions but in 0.05M H_2SO_4 it too developed a similar morphology.

Figure 5.3.3 shows the diffraction patterns which these corroded specimens produce. After 2.0V anodisation in 0.1M HNO_3, slight spreading of the $2\bar{2}0$ spots can be seen (5.3.3(a)), suggesting some polycrystallinity developing in the specimen. There is considerable polycrystallinity in the two specimens which were subjected to a 2600mV anodisation. These are shown in 5.3.3(b) and (c), where anodisation was carried out in H_2SO_4 and HNO_3 respectively; similar degrees of

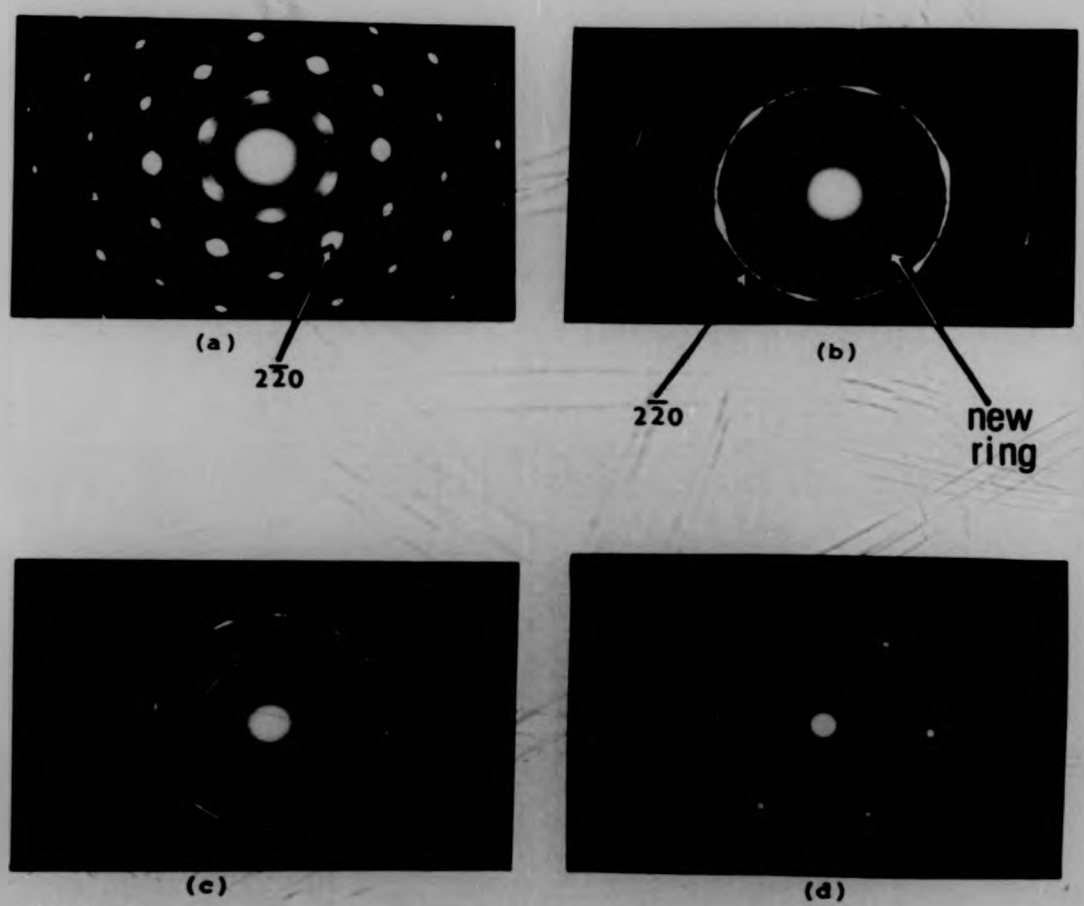

Figure 5.3.3 The diffraction patterns produced by gold specimens following various anodisation conditions: (a), 2.0V in 0.1M HNO_3, showing slight spreading of the $2\bar{2}0$ spots; (b) and (c), 2.6V in 0.1M H_2SO_4 and 0.1M HNO_3 respectively, showing considerable polycrystallinity and an extra ring within the $2\bar{2}0$ ring; (d) the diffraction pattern of an uncorroded specimen for comparison.

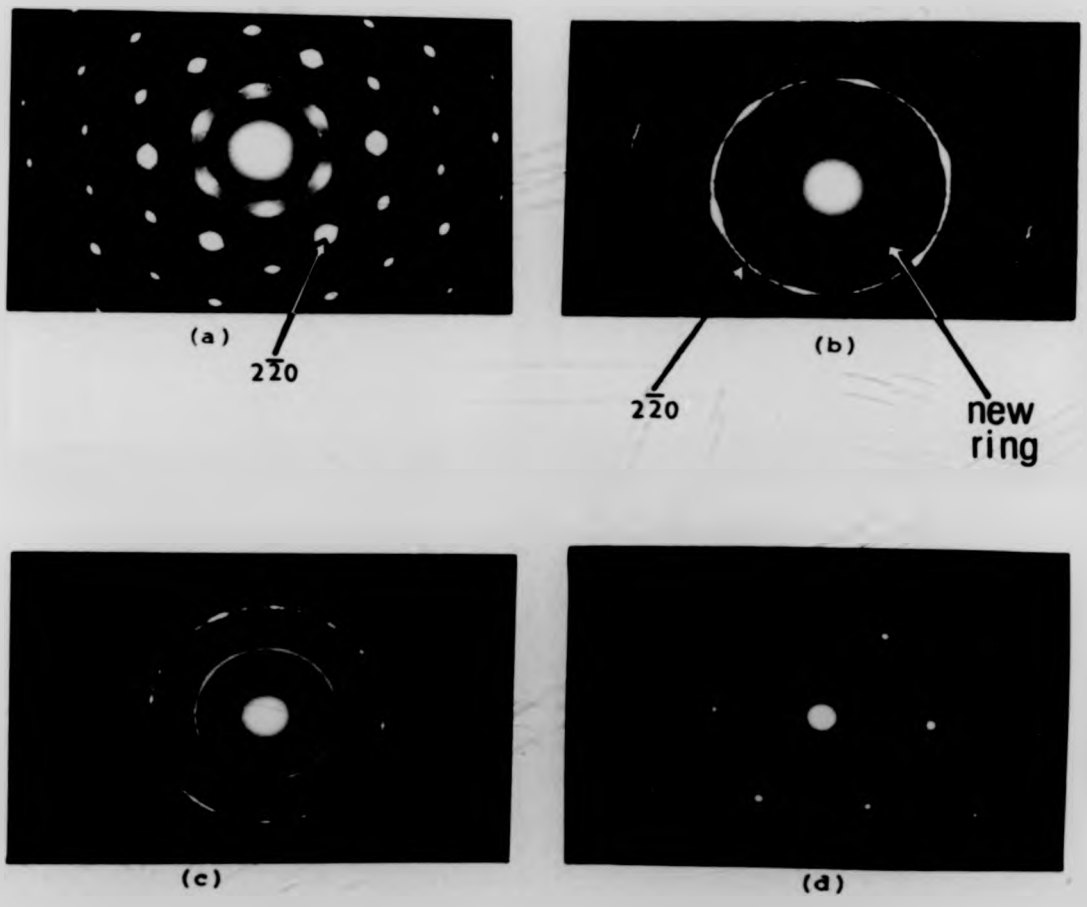

Figure 5.3.3 The diffraction patterns produced by gold specimens following various anodisation conditions: (a), 2.0V in 0.1M HNO_3, showing slight spreading of the $2\bar{2}0$ spots; (b) and (c), 2.6V in 0.1M H_2SO_4 and 0.1M HNO_3 respectively, showing considerable polycrystallinity and an extra ring within the $2\bar{2}0$ ring; (d) the diffraction pattern of an uncorroded specimen for comparison.

polycrystallinity have occurred in both specimens, as evidenced by the complete rings of $2\bar{2}0$ and $1/3(2\bar{2}4)$ spots. Some of the original $2\bar{2}0$ spots may still be seen, however, indicating that some of the original crystal structure remained after the anodisation. What is of interest in these photographs is the evidence of new polycrystalline phases or species, shown by the extra ring formed within the $2\bar{2}0$ ring, close to but outside the ring formed by the $1/3(2\bar{2}4)$ spots. This ring is just visible on the pattern obtained following 2000mV anodisation, but there are no corresponding spots on the diffraction patterns produced by any corroded specimens of gold, silver or alloys where the corrosion potential has been 1200mV or less. These patterns are the same as that shown in 5.3.3(d) for an uncorroded specimen.

5.4 The Development of a Corrosion Micromorphology on Au55Ag

Figures 5.4.1 (a) to (e) show how, with greater passage of charge, the micromorphology develops in this alloy. Each specimen was taken from the same deposition batch, and was anodised at 1200mV whilst the charge passed was measured with the current integrator.

The first of this series of photographs, 5.4.1(a), is a transmission micrograph of the uncorroded specimen. There is no structure but, as with many uncorroded specimens, a mottling in the surface can be seen. The difference in electron transmission indicated by the mottle may be caused by uneven thicknesses of the surface (the lighter areas being

(a), uncorroded

0·1 μ

(b), after 1.5mC cm^{-2}. A few isolated pits and channels are visible

Figure 5.4.1 The development of an electrochemically produced corrosion micromorphology on Au55Ag held at 1200mV in 0.1M HNO_3. The mottled appearance of the uncorroded specimen (a) is occasionally seen on these alloys.

(a), uncorroded

0·1 μ

(b), after 1.5mC cm^{-2}. A few isolated pits and channels are visible

Figure 5.4.1 The development of an electrochemically produced corrosion micromorphology on Au55Ag held at 1200mV in 0.1M HNO_3. The mottled appearance of the uncorroded specimen (a) is occasionally seen on these alloys.

(c) after 3mC cm^{-2}

0·1 μ

(d) after 6mC cm^{-2}

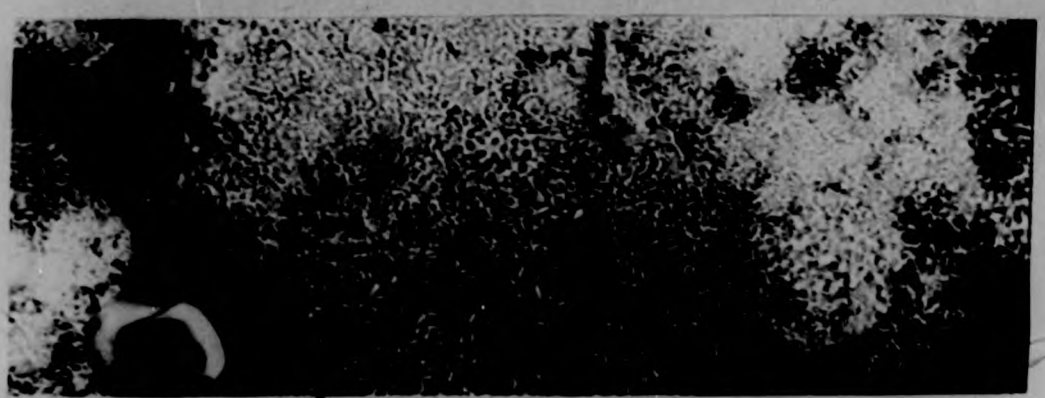

(e) after 20mC cm^{-2}

(c) after 3mC cm^{-2}

0·1 μ

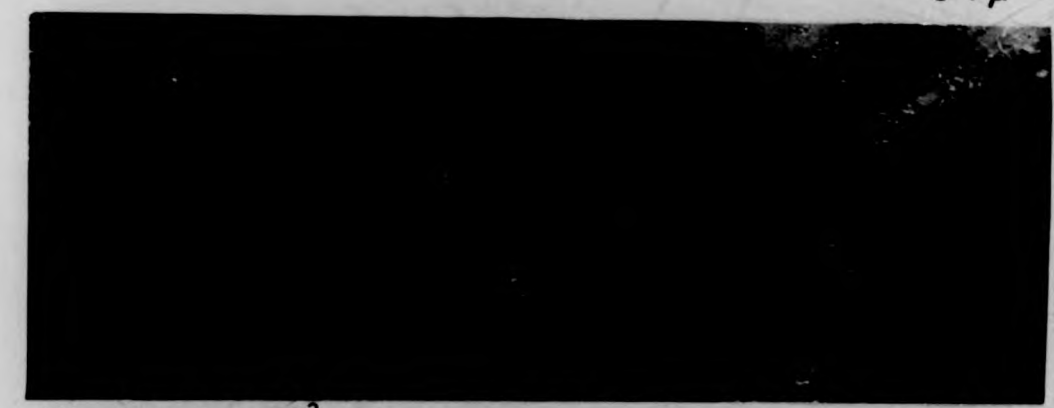

(d) after 6mC cm^{-2}

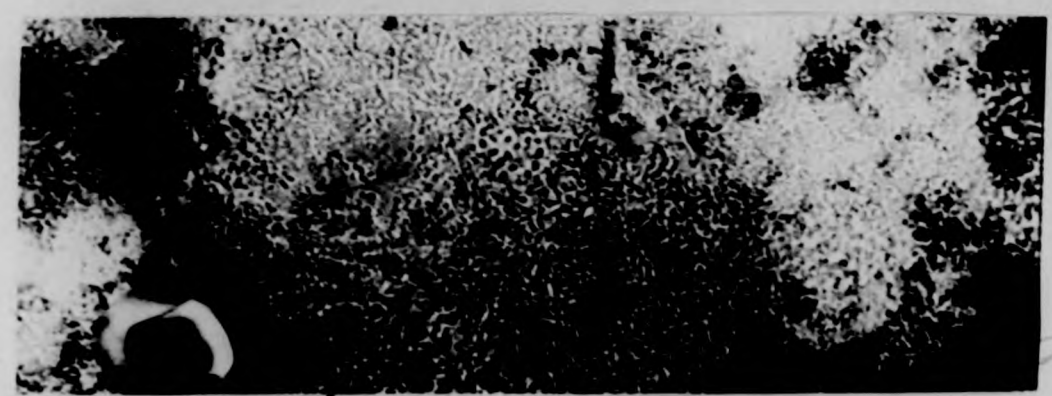

(e) after 20mC cm^{-2}

thinner) or by compositional variation. Gold is more electron absorbent than silver, so a gold film will appear darker than a silver film of the same thickness. The darker areas of this specimen may thus represent regions of gold-rich alloy. Compositional inhomogeneities, if they are present in these films, may play a significant part in the initiation and development of corrosion micromorphologies.

Figure 5.4.1(b) shows a specimen following anodisation to a charge of 1.5mC cm^{-2}. Small, bright pits with diameters of about 50Å are thinly scattered over the surface; a few of these pits appear to have joined to form channels in the surface. By doubling the charge to 3mC cm^{-2}, as in figure 5.4.1(c), and again to 6mC cm^{-2}, shown in figure 5.4.1(d), the pits and channels appear to be spreading laterally over the surface. The width of the channels which form each network remain about 50Å, the same as the initial pit diameters, and it can be seen that some new individual pits have nucleated in between the developing channel networks.

The maximum charge that this alloy composition passed was 20mC cm^{-2} after 300s at 1200mV. The 'final' morphology developed, shown in figure 5.4.1(e), is that of a network of interconnected, irregularly-shaped channels with widths of about 50Å. These channels do not entirely cover the surface: between them are darker, featureless regions where channels or pits have not encroached. The interpretation of the lighter structures as channels over the surface and not as tunnels through the bulk is due to the contrast of the micrographs.

The channels are uniformly light, with no change in the lightness where they cross. This indicates that there is no change in depth (or composition) where channels cross; if the light strips had been tunnels, where one tunnel crossed above another a brighter spot would have been seen.

5.5 The Development of a Corrosion Micromorphology on Au65Ag

After 1.5mC cm^{-2} a specimen of this alloy composition has, like the less silver-rich specimen shown in figure 5.4.1(b), developed small pits with diameters which are again about 50Å. As can be seen in figure 5.5.1(a), these are distributed over the surface, though the density of distribution is about double that for the less gold-rich specimen discussed previously, indicating that the pits are more easily nucleated in the more silver-rich alloy.

The way in which the pits develop on the surface with increasing charge can be seen from the sequence of micrographs in figure 5.5.1. The behaviour is similar to that for the Au55Ag specimen discussed in the previous section. At 3mC cm^{-2} the morphology again consists of networks of connected channels, with individual pits between the networks; this is shown in figure 5.5.1(b). At 6mC cm^{-2}, 5.5.1(c), the channel network continues to spread. It is interesting to observe that the networks are developing in the intragranular regions, rather than at holes or double-positioning boundaries.

(a), after 1.5mC cm^{-2}, small, isolated pits form

0·1 μ

(b), after 3mC cm^{-2}, the morphology now consists of a loose network of channels, plus some isolated pits

Figure 5.5.1 The development of an electrochemically produced corrosion morphology on Au65 Ag held at 1200mV in 0.1M HNO_3

(a), after 1.5mC cm^{-2}, small, isolated pits form 0·1μ

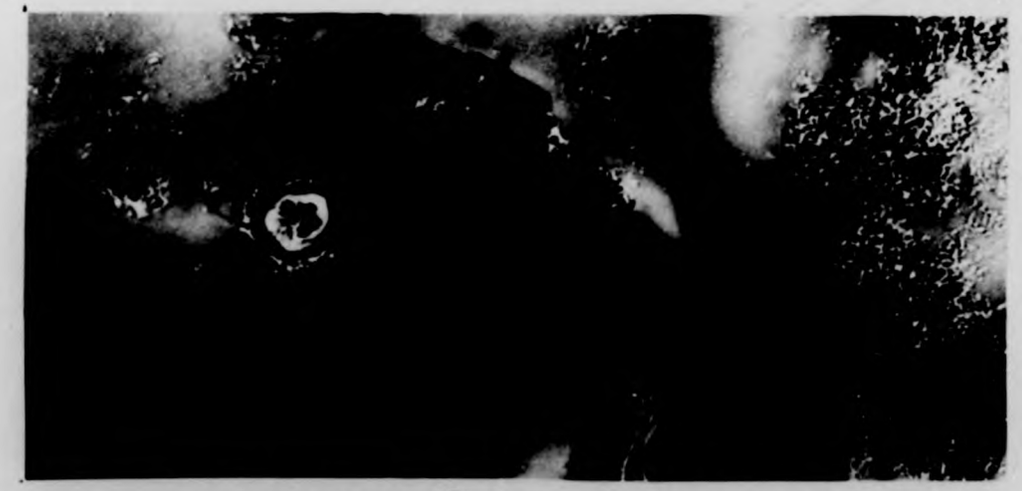

(b), after 3mC cm^{-2}, the morphology now consists of a loose network of channels, plus some isolated pits

Figure 5.5.1 The development of an electrochemically produced corrosion morphology on Au65 Ag held at 1200mV in 0.1M HNO_3

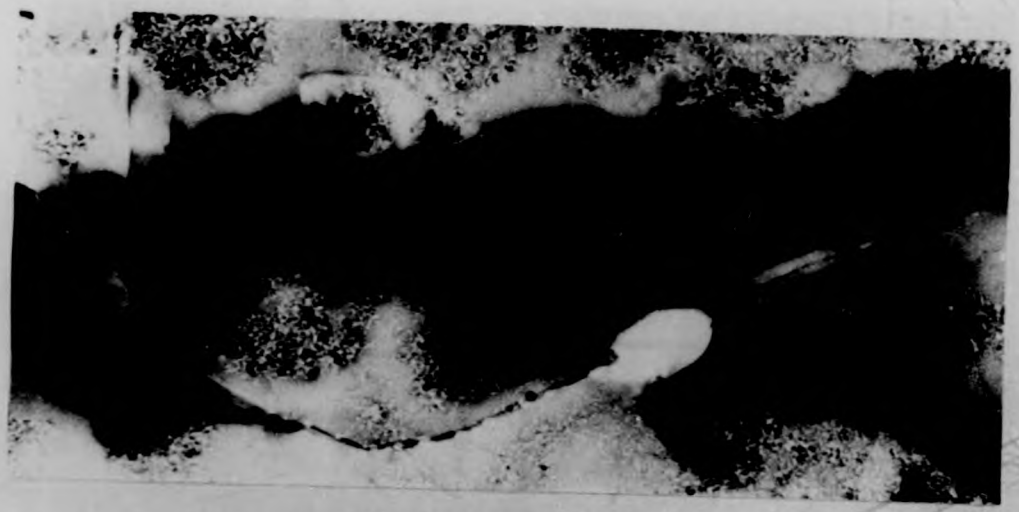

(c), 6mC cm^{-2}: continuing spread of the channels in the intragranular regions

0·1 μ

(d), 12mC cm^{-2}: surface coverage by a channel morphology is nearly 100%

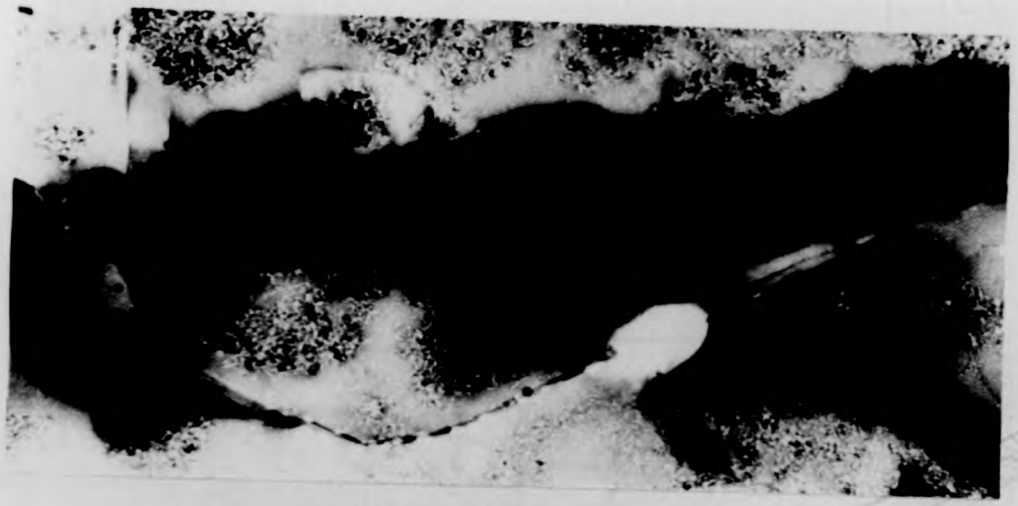

(c), 6mC cm^{-2}: continuing spread of the channels in the intragranular regions

0·1μ

(d), 12mC cm^{-2}: surface coverage by a channel morphology is nearly 100%

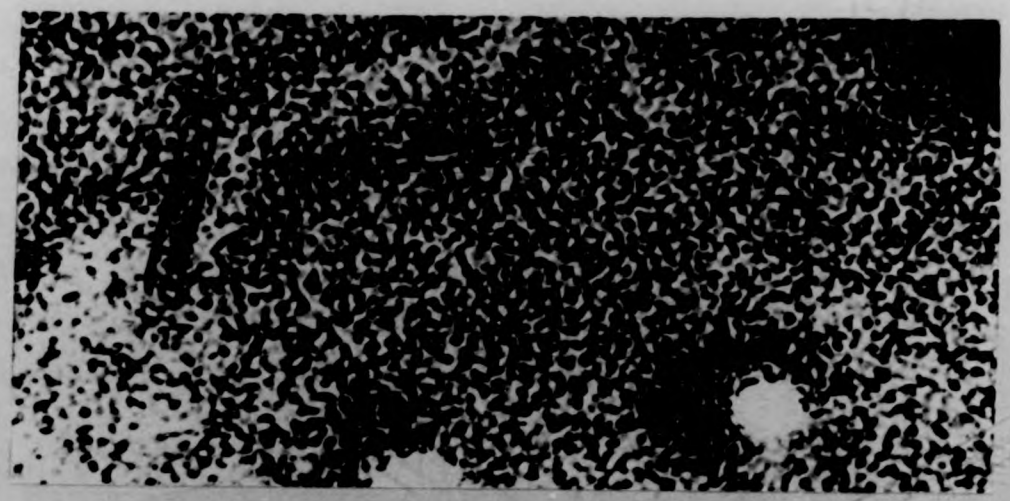

(e), 24mC cm^{-2}: the morphology has developed to a densely tunnelled structure

0·1μ

(f), 36mC cm^{-2}: the 'final' structure following 300s at 1200mV

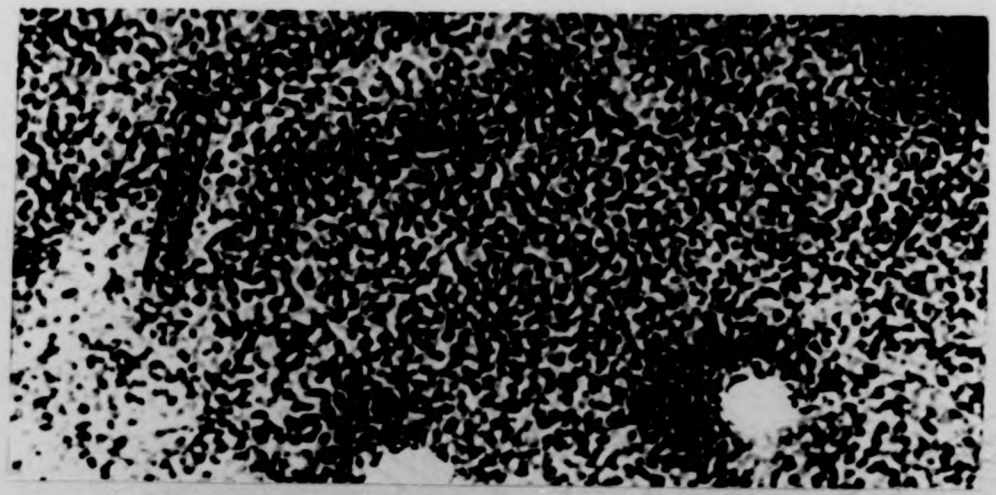

(e), 24mC cm^{-2}: the morphology has developed to a densely tunnelled structure

0·1μ

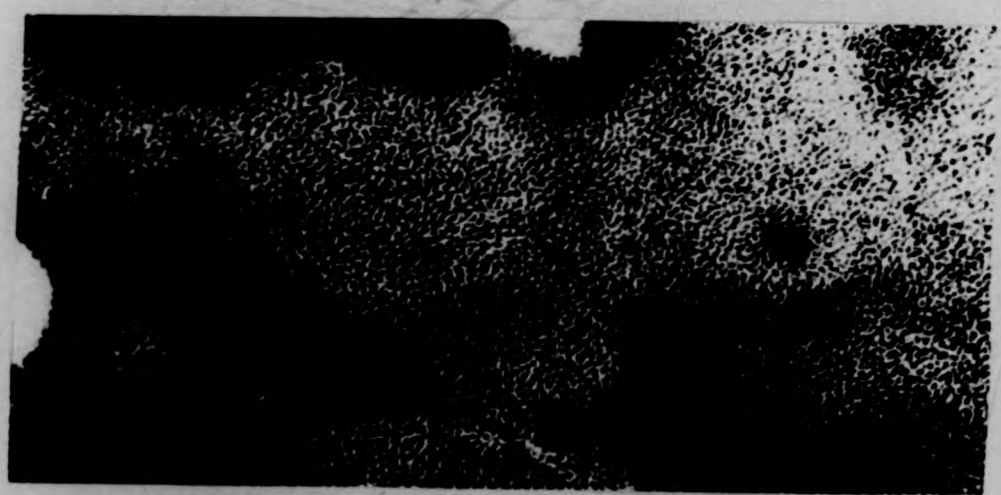

(f), 36mC cm^{-2}: the 'final' structure following 300s at 1200mV

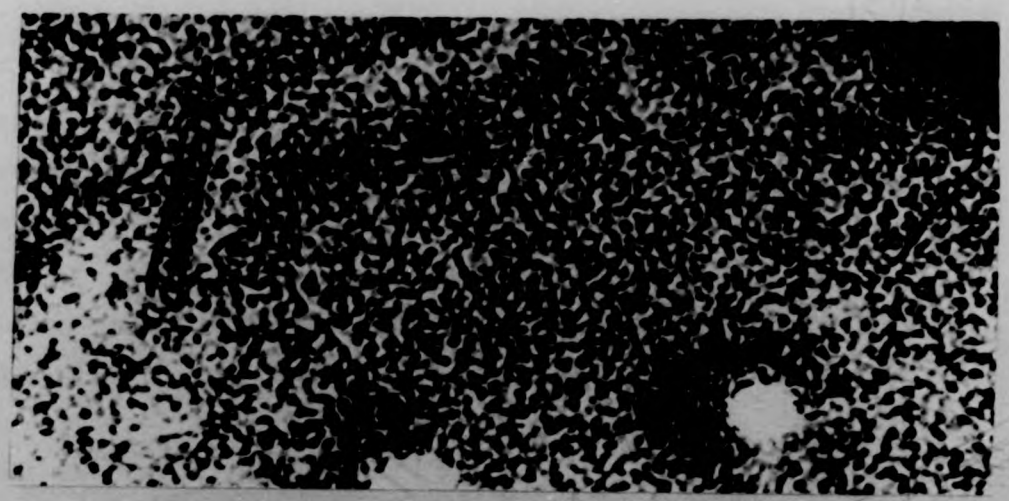

(e), 24mC cm^{-2}: the morphology has developed to a densely tunnelled structure

0·1 μ

(f), 36mC cm^{-2}: the 'final' structure following 300s at 1200mV

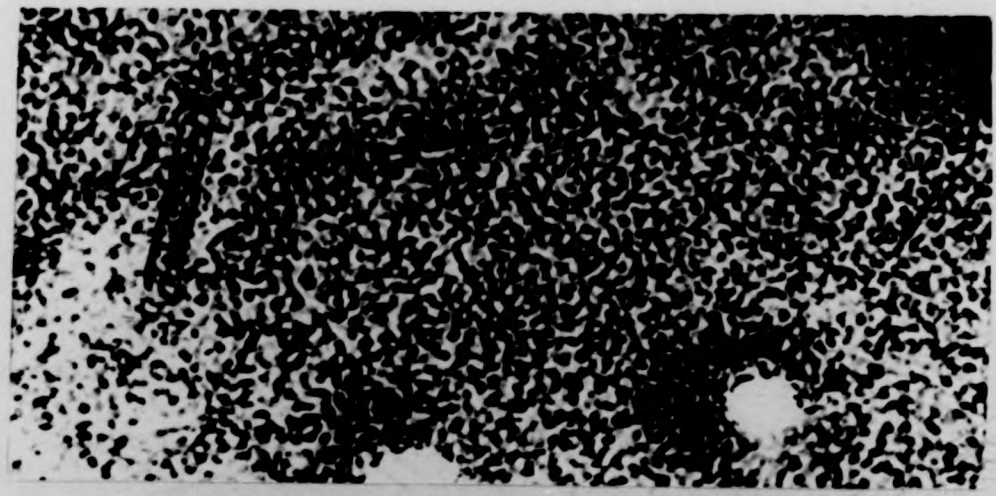

(e), 24mC cm^{-2}: the morphology has developed to a densely tunnelled structure

0·1 μ

(f), 36mC cm^{-2}: the 'final' structure following 300s at 1200mV

Figure 5.5.1(d) (12mC cm^{-2}) shows further development of the channels with surface coverage of the networks approaching completion. The morphology retains the appearance of channels rather than tunnels. However, a different structure is observed in 5.5.1(e) for a specimen anodised to 24mC cm^{-2}. This amount of charge is about twice that needed for full surface coverage of the channel network, and the specimen is now seen to be considerably tunnelled. The tunnels have a diameter of about 100Å, and are smoother and more rounded than the rather jagged channels from which they appear to have developed.

The maximum charge passed by this specimen was 36mC cm^{-2} after 300s at 1200mV; the corresponding micrograph is 5.5.1(f). The entire surface is covered with channels or tunnels; the diameter of these is 50Å, so the structure is somewhat finer than that shown in 5.5.1(e).

5.6 The Development of a Corrosion Micromorphology on Au72Ag

The corrosion channel networks start developing in the same way as previously described for Au55Ag and Au65Ag, with small pits nucleating independently over the surface of the film. Following a total charge of only 2.5mC cm^{-2} these spread and join up to form channel networks, as shown in figure 5.6.1(a).

As the corrosion proceeds, however, instead of spreading over the whole surface, as before, the channel network transforms towards a tunnelled morphology. Examination of 5.6.1(b),

(a) after 2.5mC cm^{-2} isolated groups of channel networks form

0·1μ

(b) after 4.mC cm^{-2} the spread of the channel networks is accompanied by some tunnelling

Figure 5.6.1 The development of an electrochemically produced corrosion morphology on Au72Ag, held at 1200mV in 0.1M HNO_3

(a) after 2.5mC cm^{-2} isolated groups of channel networks form

0·1μ

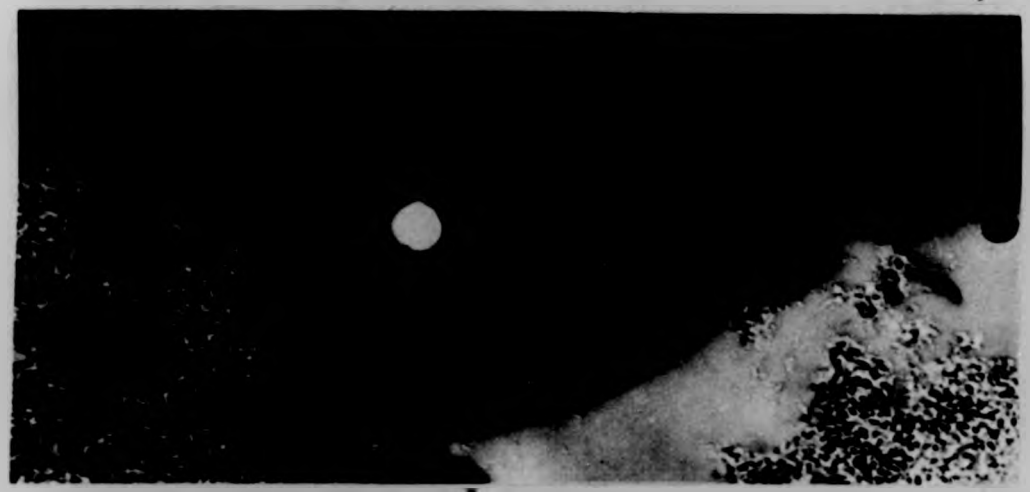

(b) after 4.mC cm^{-2} the spread of the channel networks is accompanied by some tunnelling

Figure 5.6.1 The development of an electrochemically produced corrosion morphology on Au72Ag, held at 1200mV in 0.1M HNO_3

(c)16mC cm^{-2}. An extensive structure of smooth, overlapping tunnels and channels

0·1μ

(d)45mC cm^{-2}: the 'final' micromorphology produced by anodisation at 1200mV for 300s. The fine structure covers the entire surface.

(c)16mC cm^{-2}. An extensive structure of smooth, overlapping tunnels and channels

0·1μ

(d)45mC cm^{-2}: the 'final' micromorphology produced by anodisation at 1200mV for 300s. The fine structure covers the entire surface.

after 4mC cm^{-2}, shows that a structure has developed which is midway between a tunnel and a channel morphology, with jagged and overlapping channels and tunnels. The more extensive corrosion produced by a charge of 16mC cm^{-2} is shown in figure 5.6.1(c). The structure of this corrosion is that of smooth, overlapping tunnels and channels. Regions around holes through the film and adjacent to many double-positioning boundaries tend to show less evidence of corrosion micromorphology than the regions within grains.

Figure 5.6.1(d) shows the micromorphology developed after 300s at 1200mV, when 45mC cm^{-2} had passed. Like the Au65Ag specimen anodised for a similar time (5.5.1(f)), the structure here has also become finer, with smoothly interlocking channels and perhaps overlapping tunnels. The micromorphology covers the entire surface, including regions adjacent to holes and double-positioning boundaries.

5.7 Comparisons of 'Final' Corrosion Morphologies

For this work the 'final' corrosion morphology is that which has occurred following a 300s anodisation at 1200mV. Figure 5.7.1 shows the morphology developed on Au52Ag; in this case it consists of widely scattered, jagged networks of channels. Large areas appear to be untouched, with no pitting or channelling.

Figure 5.7.2(a) shows that a channel morphology develops when the alloy contains slightly more silver. This specimen, which

Figure 5.7.1 The 'final' corrosion morphology of Au52Ag, following 300s at 1200mV in 0.1M HNO_3

Figure 5.7.1 The 'final' corrosion morphology of Au52Ag, following 300s at 1200mV in 0.1M HNO_3

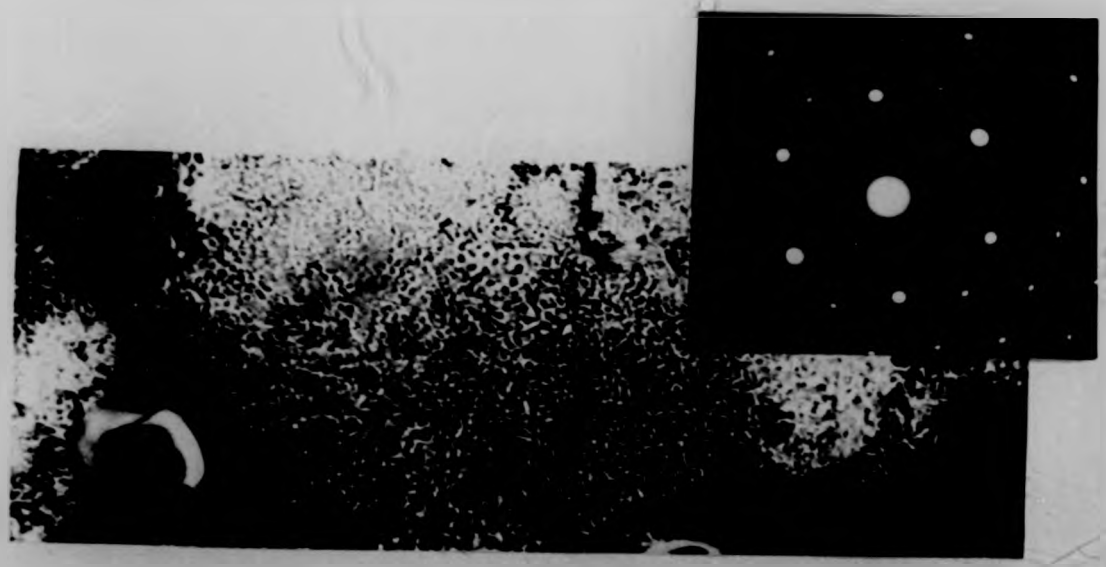

(a)1200mV; a loose network of fine channels is produced

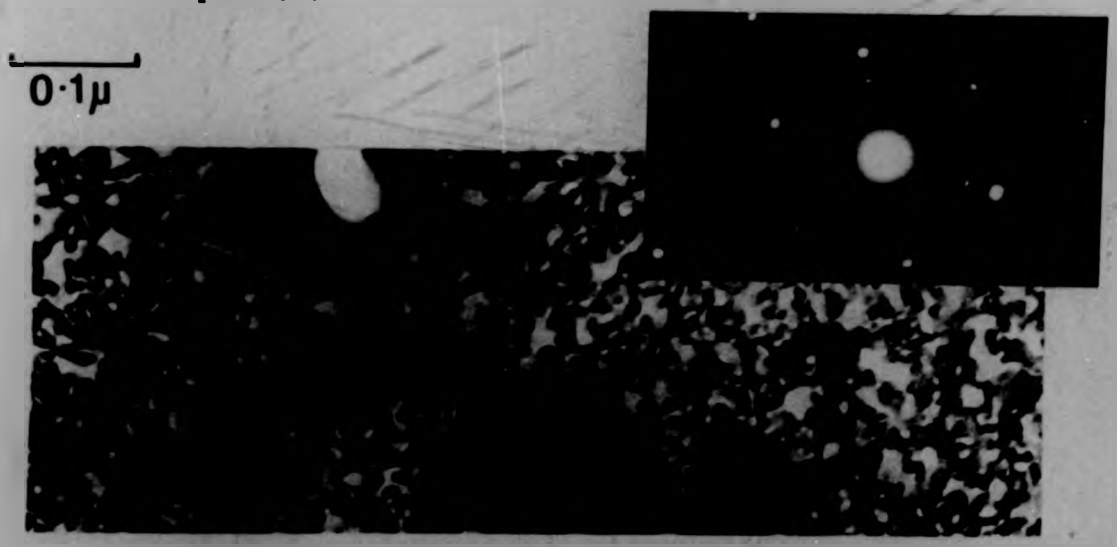

(b)1350mV; the structure is larger, smoother and overlapping

Figure 5.7.2 (a) the 'final' channel micromorphology for Au55Ag, and the associated diffraction pattern: (a) anodisation potential 1200mV for 300s; (b) anodisation potential 1350mV, 300s

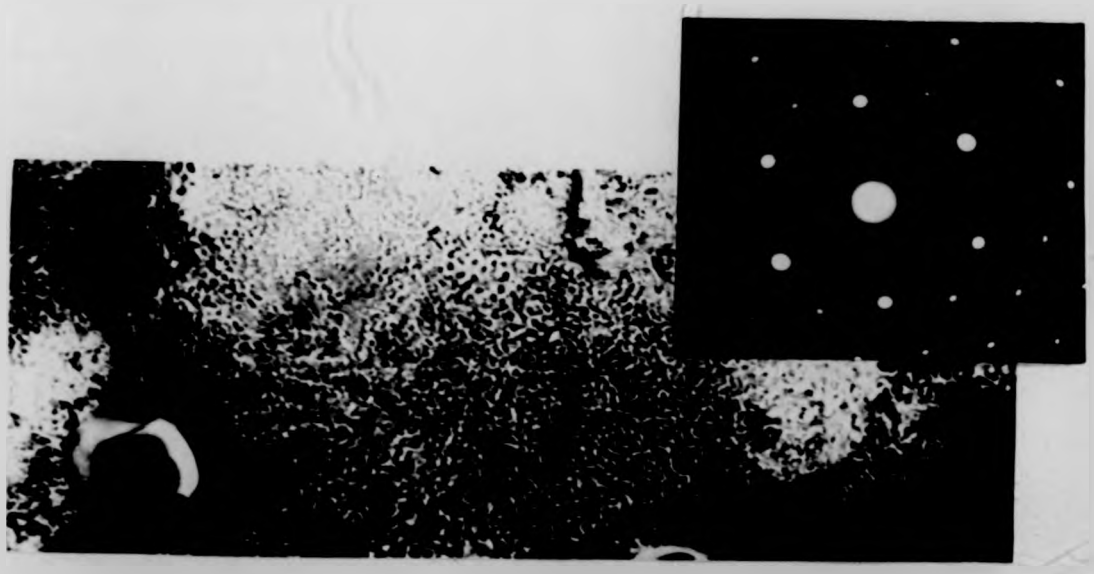

(a)1200mV; a loose network of fine channels is produced

(b)1350mV; the structure is larger, smoother and overlapping

Figure 5.7.2 (a) the 'final' channel micromorphology for Au55Ag, and the associated diffraction pattern: (a) anodisation potential 1200mV for 300s; (b) anodisation potential 1350mV, 300s

is Au55Ag, has developed a channel morphology which extends over the whole of the surface. Inset is the accompanying diffraction pattern, showing that the specimen remains a good f.c.c. single crystal. The total charge passed for this was 20mC cm^{-2}. It is particularly interesting to compare the corrosion structure which developed with a 1200mV anodisation with the morphology developed on a similar specimen after 1350mV anodisation. This is shown in figure 5.7.2(b). Although the total charge passed was only slightly greater for the latter case (23mC cm^{-2}) the morphology is very different. The alloy has a damaged appearance, similar to that produced with pure gold anodised at 2600mV, shown in figure 5.3.2(b). The light areas which represent tunnels, channels or holes are larger than those formed at lower potentials, with diameters of 200 to 400Å; these cover most of the surface, though some areas of apparently uncorroded alloy (dark areas on the micrograph) can be seen.

Inset in 5.7.2(b) is the associated diffraction pattern. Comparing this with the diffraction pattern of 5.7.2(a), extra spots lying within each of the $2\bar{2}0$ spots of the original crystal lattice can be seen. These could be the $2\bar{2}0$ spots of a new f.c.c. lattice; they are single, quite strong spots which are only slightly smeared. The new lattice which has given rise to these spots must be thick (over, say, 20 atomic layers) to produce the intensity of the spots, and is a good single crystal. By comparing the $2\bar{2}0$ spots of the two lattices, and using the lattice parameter a = 4.07Å for gold, the new phase has a lattice parameter of a = 5.52Å. The

positions of the new spots correspond exactly with the extra rings found on diffraction patterns of gold following 2.6V anodisation (figure 5.3.3), so it is evident that rings are formed by the same species or phase as are the spots. It is speculated also that this phase or species is associated with the characteristic damaged appearance of the gold film and of this Au55Ag alloy.

The corrosion morphology developed on Au65Ag, Au72Ag and Au82Ag are shown in figures 5.7.3, 5.7.4 and 5.7.5 respectively. For all of these compositions the structure consists of a fine network of overlapping tunnels which densely cover the entire alloy. This is especially clear in the micrograph of 5.7.5, for Au82Ag.

5.8 Some Additional Observations on the Development of Corrosion Micromorphologies

As discussed in section 5.4.1, gold is more electron opaque than silver, so a gold film will produce a darker micrograph image than a silver film of similar thickness. Regions of a specimen which are relatively gold-rich will thus appear darker than other regions which are more silver-rich. Another cause of darker regions is simply that of thickness; the thicker the film, the less electron transparent it will be. Additionally, Bragg diffraction can cause bright and dark regions in a thin film. Bragg diffraction contours are easily identified because tilting the object in the microscope goniometer causes fringes in the image to shift or to exchange

Figure 5.7.3 The 'final' corrosion morphology of Au65Ag, following 300s at 1200mV in 0.1M HNO_3

0·1μ

Figure 5.7.4 The 'final' corrosion morphology of Au72Ag, following 300s at 1200mV in 0.1M HNO_3

Figure 5.7.5 The 'final' corrosion morphology of Au82Ag, following 300s at 1200mV in 0.1M HNO_3

Figure 5.7.3 The 'final' corrosion morphology of Au65Ag, following 300s at 1200mV in 0.1M HNO_3

0·1μ

Figure 5.7.4 The 'final' corrosion morphology of Au72Ag, following 300s at 1200mV in 0.1M HNO_3

Figure 5.7.5 The 'final' corrosion morphology of Au82Ag, following 300s at 1200mV in 0.1M HNO_3

contrast.

Careful examination of micrographs taken of uncorroded specimens reveals two features which indicate that some specimens are either of non-uniform thickness, or of variable composition. The first is the mottling which a few uncorroded specimens exhibit (shown in figure 5.4.1(a) for a specimen of Au55Ag). The second feature consists of concentric rings of different contrast which are sometimes observed. Figure 5.8.1(a) and (b) show examples of such rings on a specimen of Au60Ag. These invariably occur in the centre of grains, with the rings becoming darker towards the central region, which is the darkest. There is no variation of darkness within each ring, but the divisions between rings are sharp and distinct.

It is well known that these alloys undergo silver enrichment around holes and at double-positioning boundaries. The silver atoms which migrate to these grain boundaries must of necessity be derived from within the grains, making the centres of the grains thinner and/or gold-enriched. If the centres are thinner, then the centres of the grains will appear lighter than the edges. Since, as figure 5.8.1(a) and (b) shows, those grains which show the rings become darker towards the centre, it may be inferred that the rings do indeed correspond to regions of gold enrichment towards the grain centres. Such an effect would, however, be expected to be graded, producing a continuous contrast change, rather than discrete, producing distinctly separated regions. An alternative explanation for the rings may be that they are

(a)

0·1μ

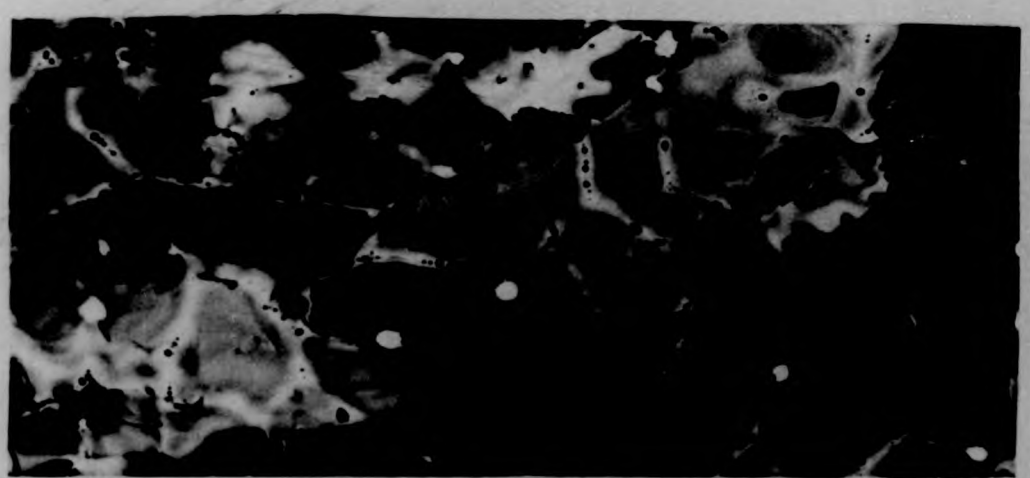

(b)

0·5μ

Figure 5.8.1 (a) and (b), the variation of contrast occasionally seen within the grains of uncorroded alloy specimens, seen here on a sample of Au60Ag

(a)

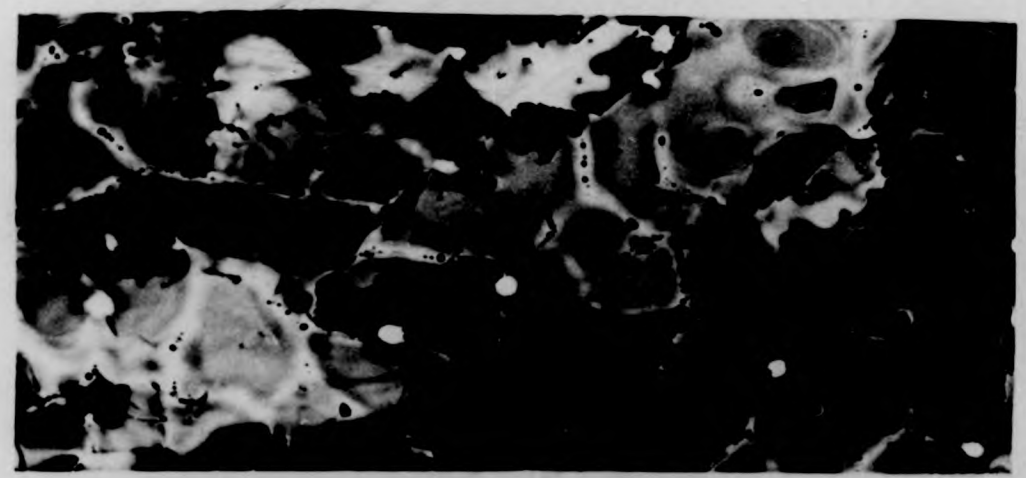

(b)

Figure 5.8.1 (a) and (b), the variation of contrast occasionally seen within the grains of uncorroded alloy specimens, seen here on a sample of Au60Ag

caused by the pile-up of steps into supersteps during specimen preparation; the high terraces so produced may in addition be non-uniform in composition.

Figure 5.8.2(a), (b), (c), (d) and (e) shows the spread of micromorphology over the surface as corrosion develops. Very occasionally, the early stages of channel morphology are seen as incomplete rings of pits within grains; such a ring is visible in figure 5.8.2(a), after charge passage of 3mC cm^{-2}. If the rings of enhanced contrast in the electron-microscope image represent regions of gold-enrichment, the presence of rings of pits suggests that there is an optimum composition (or a compositional range) for pit nucleation. On the other hand, if the rings of enhanced contrast represent supersteps the rings of pits could be due to increased nucleation at such steps. The corrosion structure spreads within the grains until, as 5.8.2(d) shows, the morphology covers all regions other than grain boundaries and holes. The lines of dark spots which delineate the grain boundaries on this micrograph are probably redeposited silver or silver salts from the electrolyte following the anodisation. The final stage of the development of the micromorphology is the encroachment of the channels to regions adjacent to pits and grain boundaries, as shown in figure 5.8.2(e).

Figure 5.8.3 shows that the nucleation and development of corrosion pits may also be related to the forementioned mottling which is thought to signify compositional variations on a microscopic scale. Figure 5.8.3 shows the early stages

(a) 3mC cm^{-2}, with a ring of pits (arrowed) developing within a grain: this ring possibly corresponds with the rings of contrast variation shown in figure 5.8.1

(b) 6mC cm^{-2}, showing isolated groups of channels

Figure 5.8.2, showing the typical manner by which the micromorphology spreads over the specimen (in this case, Au68Ag) with 1200mV anodisation potential

(a) 3mC cm^{-2}, with a ring of pits (arrowed) developing within a grain: this ring possibly corresponds with the rings of contrast variation shown in figure 5.8.1

(b) 6mC cm^{-2}, showing isolated groups of channels

Figure 5.8.2, showing the typical manner by which the micromorphology spreads over the specimen (in this case, Au68Ag) with 1200mV anodisation potential

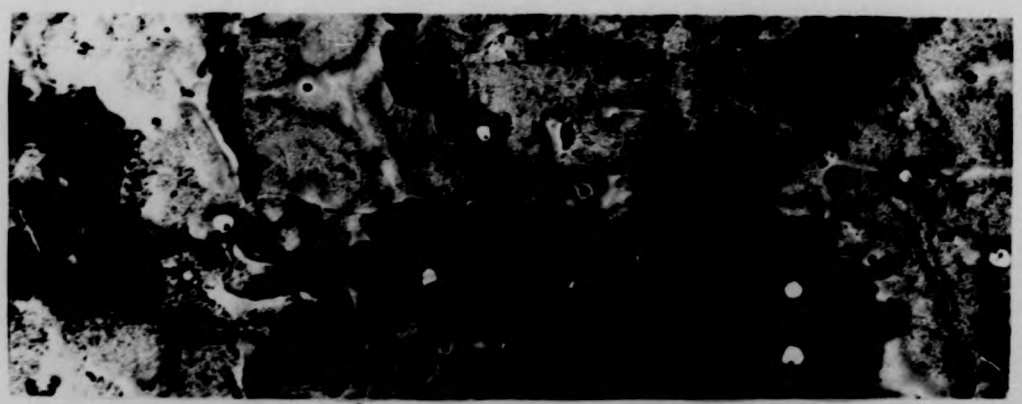

(c) 12mC cm^{-2}, spread of the corrosion structure

0·5μ

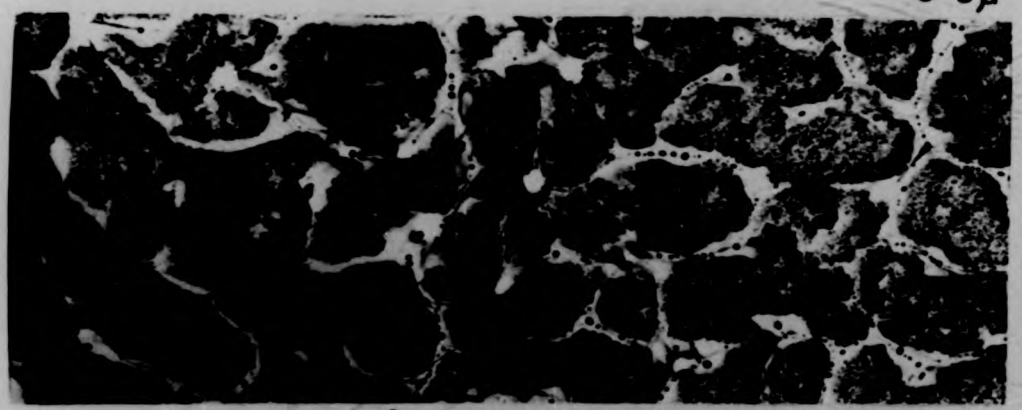

(d) 24mC cm^{-2}, showing clearly that the grain boundaries have no corrosion structure, despite considerable morphology within grains

(e) 34mC cm^{-2}: all of the specimen, including grain boundaries, is covered by a corrosion morphology

(c) 12mC cm^{-2}, spread of the corrosion structure

0·5μ

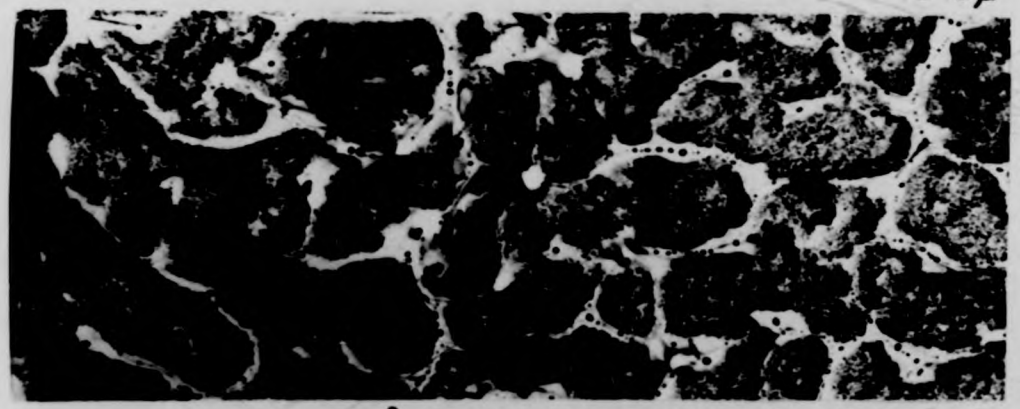

(d) 24mC cm^{-2}, showing clearly that the grain boundaries have no corrosion structure, despite considerable morphology within grains

(e) 34mC cm^{-2}: all of the specimen, including grain boundaries, is covered by a corrosion morphology

Figure 5.8.3 The early stages of corrosion in a specimen of Au67Ag, showing that the initiation sites of corrosion pits may be associated with sites which produce different electron micrographical contrast.

Figure 5.8.3 The early stages of corrosion in a specimen of Au67Ag, showing that the initiation sites of corrosion pits may be associated with sites which produce different electron micrographical contrast.

of corrosion of a sample of Au67Ag. The sample is evenly mottled, and there is a number of small pits visible in the upper part of the figure. It is striking that all of these pits are included within a dark (and therefore more gold-rich) region, as if the composition elsewhere is not suitable for pit initiation. In the lower part of this figure is a more extensively corroded region. The scale of the corrosion structures is the same as the scale of the mottling, indicating that not only the initiation, but also the development of the corrosion channelling may be strongly influenced by variations in microcomposition.

CHAPTER 6

DISCUSSION

6.1 Introduction

The potentiostatic and potentiodynamic behaviour of gold-silver alloys has been examined in chapter 4. The complementary microanalytical study, also reported in chapter 4, has provided direct evidence of the compositional changes which different alloys undergo following treatment at different anodic potentials. The information gained in this way has been applied to thin films of the alloys, to control the amount of corrosion and thus to examine the way in which the corrosion micromorphologies develop in a range of alloys. The results of such studies were presented in chapter 5.

The substance of this discussion is the combination of data obtained from the three techniques: electrochemistry, X-ray microanalysis and transmission electron microscopy. It will be shown that additional light has been shed upon the nature of the so-called 'parting-limit' of gold-silver alloys; at a silver concentration below the 'parting limit' (variously reported at being some 50 to 55% silver) it is confirmed that silver cannot be leached from the alloy by electrochemical means. More significantly, however, it will be shown that the development of corrosion pits and tunnels in these alloys is not, as had previously been thought (Forty and Rowlands,

1981), a straightforward dissolution-reordering process, but it involves the formation and decomposition of an intermediate metastable gold oxide species.

6.2 Discussion of Anodic Voltammograms

The results of X-ray microanalysis (chapter 4) show that there is a net removal of silver from a range of silver-rich silver-gold alloys during electrochemical treatment. Furthermore, this silver dissolution was shown to be associated with the major anodic current peak seen on anodic sweeps of single-sweep and cyclic voltammograms. This major anodic peak is not, however, the only anodic feature exhibited during the anodisation of these alloys, and further consideration needs to be given to the likely current-producing phenomena responsible for the additional structures on the anodic curves.

A series of single-sweep anodic voltammograms has been presented in figure 4.3.1. Curve (a) on this figure, produced by pure silver, shows a rapid rise in anodic current caused by silver dissolution. There is no evidence of any other current-producing process. A different picture is shown by curve (b) for a silver-rich (Au89Ag) specimen. As the potential is ramped the first feature observed is a small peak commencing at about 380mV. This merges into a major peak which commences at about 500mV. This peak merges with a third peak which is lower and possibly broader than the second. The first, small peak starts at approximately the same potential

and rises at the same rate as the silver dissolution shown in curve (a). It can therefore be associated with the dissolution of a small quantity (about three atomic layers) of silver from an unalloyed surface-segregated silver layer. Tokutaka et al (1981) have shown theoretically and demonstrated experimentally with Auger electron microscopy that there is segregation of silver on the surface of gold-silver alloys. Furthermore, the thickness of this segregated layer is related the the bulk composition; one atomic layer of silver forming on alloys of under 50% silver in the bulk, and between one and two layers forming on alloys which have over 50% silver in the bulk.

The major anodic feature of curve (b) consists of two merged peaks. As has been discussed in chapter 4, the area under each component peak should correspond to the total charge passed during its formation. In this particular case, the charge required to remove electrons from the silver was found to be larger than the charge equivalent to either of the two overlapping peaks. Both of the peaks must, therefore, be associated with silver dissolution from the alloy. However, it is interesting to note that the total charge passed during the formation of the double peak is slightly larger than could be accounted for by silver dissolution alone.

An interesting possibility now arises: the presence of the double peak associated with silver removal indicates that silver dissolution can take place from sites of differing silver activity. The first component of the double peak,

which commences at the lower potential, is produced by silver atoms which are more active and which lie in relatively shallow potential wells. Such atoms might lie on surface sites, or in double-positioning boundaries where the structure is more disordered. The supply of these active and mobile atoms is limited in these thin films, and consequently the first peak is also limited. Further dissolution can only be maintained by the removal of more firmly-bound atoms. The second component of the double peak should therefore represent the dissolution of these silver atoms from their deeper potential wells. The actual process by which the atoms leave the alloy is not clear; some may be ionised directly from within the grains, leaving a surface rich in vacancies; other atoms may then travel outwards from within the alloy as these vacancies flow inwards. Alternatively, silver atoms may migrate to crystalline discontinuities (such as grain boundaries) which provide established pathways out of the alloy.

The major anodic current peaks of silver dissolution for the less silver-rich specimens, (c), (d) and (e) of figure 4.3.1, which has also been shown to be related to silver dissolution, commence at higher potentials as the gold percentage is increased. The activity of the silver in these specimens is therefore reduced with increasing gold content, and this may perhaps provide an alternative explanation of the occurrence of the double peak shown in curve (b) for the Au89Ag specimen. Since the activity of the silver atom might be influenced by the nature of the surrounding atoms the two types of potential

well can be the result of a micro-ordering of the silver and gold during specimen preparation so that the alloy consists of some silver atoms in an environment which is relatively silver-rich, and other silver atoms in an environment which is relatively less silver-rich. There is some evidence for this kind of phase separation in silver-gold alloys from the mottled appearance in the electron microscope images of some specimens, already described in chapter 5. It is of course possible that micro-ordering takes place during the dissolution itself. Indeed, it has been proposed that reordering does take place when corrosion pits develop.

Whatever causes the variation in the activity of silver in specimen (b), whether it is associated with inter- and intra-granular effects, or whether it is associated with micro-ordering before or during corrosion, one significant question remains unanswered: the double-peak of silver dissolution shown clearly in curve (b) and possibly in curve (c) is only evident for the very silver-rich specimens. It is not clear why multiple silver-dissolution peaks are not observed in the case of less silver-rich specimens.

Turning now to curve (c), for Au73Ag, two components of the curve can be identified. The first is a low current plateau which commences at about 600mV; this merges with the major anodic peak which commences at about 800mV. Both the peak and the plateau are thought to be associated with silver dissolution. There are two possible causes for the plateau.

It might represent the dissolution of one or two surface layers of segregated silver; but, if so, the relatively high potential at which it commences would be rather surprising since pure silver commemces dissolution at a potential close to 350mV. Alternatively, and more interestingly, it might be caused by the dissolution of silver from a very silver-rich surface alloy phase. It is tempting to see this plateau as echoing the first large peak of curve (b), since they both appear to commence at about 600mV. The major anodic feature of curve (c) may now be thought of as corresponding to the second of the merged peaks of curve (b) but with a displacement of about 100mV towards more noble potentials.

The next curve to be considered is that produced by pure gold: curve (h). This curve, of course, lacks the silver dissolution peak, but it does have a low current plateau which commences at about 1200mV and which merges with the oxygen evoution current at about 1600mV. That this plateau is not due to electrolyte impurities is confirmed by comparing the anodic curve with that obtained using platinum in the same electrolyte, shown in figure 4.2.1(b); there is no corresponding current plateau when platinum is used. This current can therefore identified as arising from the oxidation of gold; other workers (for example: Shmid and O'Brien (1964), Brummer and Makrides,(1964); Ogura, Haruyama and Nagasaki (1971)) have produced evidence that an oxidation reaction takes place at potentials close to 1200mV (s.c.e.) producing Au_2O_3, Au-O, Au-OH, or other as yet unidentified oxide or hydrated oxide states. The area under the curve would be

consistent with the formation of one or two layers of trivalent gold oxide.

A similar plateau is also seen on the curves produced by the gold-rich specimens, curves (g) and (f), and these plateaux are similarly considered as arising from gold oxidation. The areas underneath the plateaux for the alloys are slightly greater than the area under the pure gold plateau, so perhaps there has been some contribution to the current by the dissolution of a surface atomic layer of segregated silver; it may alternatively indicate an increased oxidation current.

Close examination of these plateaux reveals a significant relationship between them. By comparing the curves for the gold-rich alloys it can be seen that the onset potentials of the gold oxidation plateaux are influenced by the alloy composition, commencing at less noble potentials as the gold content is reduced. For example, whereas the gold oxidation plateau commences at 1200mV on pure gold (curve (h)), the corresponding plateau commences at some 1150mV on Au34Ag (curve (g)), and at 1100mV for Au48Ag (curve (e)).

It is now apparent that there is a considerable shift in silver dissolution potential with alloy composition, and there is a relatively small, but nonetheless significant, shift in gold oxidation potential. Curve (e), for Au57Ag, clearly shows a situation where these potentials have 'crossed over'; the silver dissolution potential (about 1200mV) is higher than the gold oxidation potential (about 1000mV).

The final curve which remains to be discussed is curve (d), for Au64Ag. It has the least complexity of all the curves, having just one anodic feature. This is possibly the most significant of all the curves, since at this composition the potential for gold oxidation would appear to be the same as the potential for silver dissolution. Since both gold oxidation and silver dissolution are taking place, it is reasonable to suppose that they will interact. For alloy compositions such as this the interaction would be expected to be a maximum because the dissolution and oxidation potentials are the same, that is about 960mV. The implications of this will be discussed later (section 6.4).

6.3 Dealloying of Silver and the Parting Limit

The total silver which can be dissolved from each alloy is related to the imposed anodic potential: the higher the potential, the more silver is removed. This adds weight to the observation made in section 6.2 that silver is removed from different potential wells in the same alloy: deeper wells (more tightly bound silver) will require higher potentials to draw out and ionise silver atoms.

As was mentioned in section 4.4, figure 4.4.3 shows that there are three categories into which the dissolution behaviour of the alloys fall. The first category consists of specimens with over about 80% silver in the alloy, and these very silver-rich specimens can be completely dealloyed when anodised to a sufficiently high potential: 1000mV or even

less. The 'final' silver concentration for such alloys in this category is zero. The second category is where anodic treatment removes some, but not all of the alloyed silver. The specimens which fall into this category are those with an initial silver concentration of between 55% and 80%. The third category is those alloys for which even a prolonged anodisation at high potential (up to 1400mV) fails to remove a significant quantity of silver. For these specimens a very small amount of silver is, in fact, removed, but since this corresponds to only about 1% reduction in silver concentration, it is unlikely that the silver is removed from within the specimen, but rather from an atomic layer of surface segregated silver.

The direct measurement of silver removal equates with present knowledge of the dissolution behaviour of noble metal alloys. Previous studies have usually been carried out using chemical rather than electrochemical means, and there are no other published results on the direct measurement of the electrochemical parting of silver from silver-gold. It has been known for a long time that parting can only take place when the less noble element is present in sufficient quantity. The parting of silver from a gold-rich silver-gold alloy is important for jewellery makers who may wish to produce a more gold-rich alloy; straightforward chemical or electrochemical treatment will not be capable of refining a gold alloy of 14 carat or more (about 40% gold), and the technique used is normally to melt down the gold alloy with additional silver, so that complete parting can then be carried out.

The maximum gold percentage in the alloy from which some silver can be dissolved was originally described by Tammann and Brauns (1931) as the 'parting limit'. They studied annealed silver-gold alloys after immersion in hot H_2SO_4, and determined that alloys are unattacked when the alloy contains 50% or more gold, which they established as the parting limit of silver-gold. This is in good agreement with the parting limit of about 55% determined in this present work. As Shreir (1976) discusses, complete parting of silver-gold alloys in nitric acid can occur only when the Ag:Au ratio is greater than about 2.5:1 (i.e., about 70% or more silver). This may be compared with a silver composition of about 80% determined in this work for which complete silver dissolution was found. It should be mentioned, however, that this figure of 80% is almost certainly higher than the true value because of kinetic effects. Shreir also observes that, at lower silver:gold ratios, separation is incomplete; this, too, matches the results shown in figure 4.4.3.

6.4 Discussion of Kinetic Effects in Potentiostatic Coulometry

The charge/time curves presented in section 4.4 show the total charge passed by each specimen during anodisation at a fixed potential. Although the anodisations were carried out for a standard time of 300s, the greatest charge passage (in other words, the highest currents) generally took place in the first ten or twenty seconds, the curves later flattening out. In the case of the gold-rich specimens (for example, Au40Ag,

figure 4.4.2), this flattening-out corresponded to a current of up to 10μA cm^{-2}, even with high applied potentials (up to 1400mV). This current matches the current that would be expected to arise from impurities in an electrolyte which has not undergone any pre-electrolysis to sweep out impurity ions.

A slightly different picture is presented by silver-rich alloys, as illustrated by Au84Ag (figure 4.4.1). At low potentials the curve soon demonstrates very little charge passage; at 500 and 600mV, for example, the charge increase corresponds to a current of about 5μA cm^{-2}, after the initial region which is linked with the formation of the electric double layer. At these potentials, which are lower than the silver-dissolution onset potential (as indicated by the potential at which the major anodic current feature of anodic voltammograms begins to rise), the current is solely produced by electrolyte impurities. If the charge/time curves for the same specimen at high potentials (1000mV and 1100mV) are examined, these curves are seen to have a very rapid initial climb which has nearly levelled out at 50s. At around 200s anodisation, these curves have also levelled out to an electrolyte impurity-type current, so all silver dissolution appears to have taken place and be completed well before this time.

The growth of charge for specimens anodised at intermediate potentials follows a somewhat different behaviour. Following the initial rapid rise, the charge continues to rise at a rate greater than that which may be accounted for by impurity

currents. Silver dissolution under these conditions thus proceeds more steadily, though at a lower rate, for a longer time. Close examination of the 700, 800 and 900mV curves reveals that the curves are approaching a steady value of charge, and, extrapolated, they would not reach the same total charge as was passed at the high anodic potentials already discussed. This means that, although additional anodisation at these intermediate potentials might remove some additional silver, even after a very long anodisation the total quantity of silver removed would be less than the total quantity removed at higher potentials.

This behaviour is of some consequence when one wishes to relate silver dissolution currents to the removal of silver from different atomic sites in the alloy. The nature of the problem is illustrated by considering the ambiguities inherent in the interpretation of figure 4.4.3. The figure was produced by measuring the silver percentage of each specimen, after the specimen had been anodised for 300s at a fixed anodic potential. The composition thus achieved is regarded as a 'final' composition. It could be argued that the concept of a 'final' composition is improper for this system, on the basis that the anodisation time was arbitrary. In other words, what was measured was not a true final state, brought about by a surface passivation phenomenon or by the exhaustion of silver available at that potential, but was a kinetic phenomenon.

Figure 4.4.1 provides evidence that there is indeed a kinetic effect, but that the general argument, based upon 'final' compositions, does still apply. There is no kinetic contribution to the 'final' composition for the specimens anodised at high or at low potentials, since the current arises from the electrolyte and not from any further electrode dissolution. For these specimens, increasing the anodisation time would not produce any measurable change in the 'final' silver concentration in the alloy. The 'final' composition for the intermediate values does have some time-dependency, so these compositions should be regarded with some caution. Nevertheless, if the charge/time curves for the specimens anodised at intermediate potentials are extrapolated, they will clearly remain in the same relationship to each other and will not produce the same total charge as the high-potential (1000 and 1100mV) curves.

The implications on the 'final' composition/anodisation potential graph (4.4.3) are that low-potential and high-potential silver percentages do not reflect a dissolution rate, and the remaining silver percentage would be hardly if at all reduced by increasing the anodisation time. The silver percentage values obtained for each composition at intermediate potentials (those at the falling parts of the curves) would be reduced by increasing the anodisation times, but the curves would still retain their general shapes, though with slightly steeper gradients at these intermediate values.

Figure 4.4.1 provides evidence that there is indeed a kinetic effect, but that the general argument, based upon 'final' compositions, does still apply. There is no kinetic contribution to the 'final' composition for the specimens anodised at high or at low potentials, since the current arises from the electrolyte and not from any further electrode dissolution. For these specimens, increasing the anodisation time would not produce any measurable change in the 'final' silver concentration in the alloy. The 'final' composition for the intermediate values does have some time-dependency, so these compositions should be regarded with some caution. Nevertheless, if the charge/time curves for the specimens anodised at intermediate potentials are extrapolated, they will clearly remain in the same relationship to each other and will not produce the same total charge as the high-potential (1000 and 1100mV) curves.

The implications on the 'final' composition/anodisation potential graph (4.4.3) are that low-potential and high-potential silver percentages do not reflect a dissolution rate, and the remaining silver percentage would be hardly if at all reduced by increasing the anodisation time. The silver percentage values obtained for each composition at intermediate potentials (those at the falling parts of the curves) would be reduced by increasing the anodisation times, but the curves would still retain their general shapes, though with slightly steeper gradients at these intermediate values.

6.5 The Silver Dissolution Potential for Silver-Gold Alloys

Extension of the initial linear portion of each curve of figure 4.4.3 shows the potential at which the 'final' alloy composition begins to deviate from the initial composition. This is where silver dissolution commences; the associated potential for each alloy can be described as the 'silver dissolution potential', E_{Ag}. The variation of E_{Ag} with initial alloy composition is shown in figure 6.5.1. The silver dissolution potential for pure silver in 0.1M HNO_3 is 350mV, and the curve in figure 6.5.1 shows that there is a linear increase in silver dissolution potential with addition of gold of 18mV per cent of alloyed gold. If C_{Au} is the gold concentration in the alloy, expressed as an atomic percentage, the relationship is summarised as:

$$E_{Ag} = 350 + 18C_{Au} \quad mV$$

Also plotted on this graph are the potentials where the major anodic peaks in anodic voltammograms are estimated to commence. These potentials are not sharply defined, but they do lie close to the silver dissolution potential for each alloy composition. This confirms that the major anodic peaks are caused by silver dissolution, and has led to the following interesting and valuable result. Using the results shown in figure 6.5.1 it has proved possible to make a rapid assay of the composition of an alloy from an anodic voltammogram. Compositions estimated in this way have proved to be remarkably close to compositions measured by E.D.X. (which are

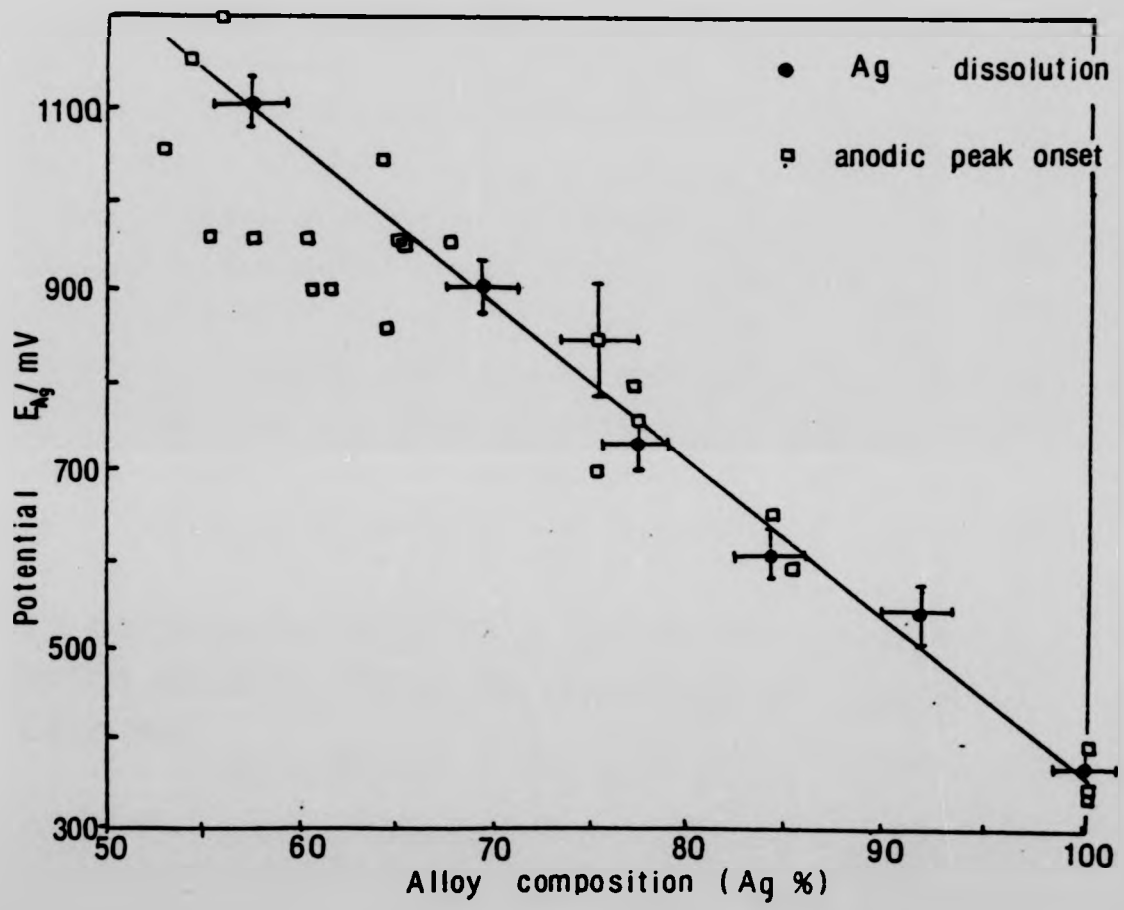

Figure 6.5.1 The variation of critical dissolution potential for silver, E_{Ag}, with composition. Also shown are the potentials at which anodic current peaks commence to rise.

themselves close to expected compositions from vapour deposition data), with a maximum error of 5%. This rapid assay method could be of some minor commercial use if an immediate approximate composition of a gold-silver alloy is needed. Additional tests have shown that the results obtained here with thin film specimens equally apply to polycrystalline bulk alloys. Because of the large amount of available silver, however, bulk alloys produce voltammograms similar to that produced by pure silver (figure 4.2.2), though displaced to more noble potentials for the less silver-rich specimens. They do not produce the anodic peaks which are seen on voltammograms of thin-film specimens (for example, figure 4.2.4) because the size of the area under each peak is limited in thin films by the amount of silver available

6.6 Electrochemical Evidence for the Formation of a Metastable Surface Gold Oxide During the Dissolution of Silver from Silver-Gold

It has been argued (Forty, A. J. and Durkin, P., 1980) that the corrosion channelling and tunnelling reported earlier for silver-gold alloys corroded in 35% nitric acid involves the surface mobility of gold atoms. The gold mobility is thought to be through the formation of an intermediate state of partially oxidised and solvated gold (Durkin and Forty, 1982) which decomposes, redepositing gold at the sides of developing pits and channels.

Further information on the processes involved may be obtained if the changing potential of the alloy is monitored during chemical attack. The 'corrosion potential' is the potential where the intercept of the anodic overpotential and the cathodic overpotential (which is otherwise termed an underpotential) produces equal (and opposite) anodic and cathodic currents. In these conditions net dissolution from anodic regions is balanced by an equivalent current from cathodic regions, so a network of local corrosion cells is formed which allows the electrochemical processes to continue without any external circuit. Since overpotentials will give rise to current density, and it is the total current which is of significance here, a small overpotential on a large area of cathode may be balanced by a large overpotential on localised anodes.

As Kortum (1965) observes, the overall rate of corrosion depends upon the steepness of the overpotential/current curves of the anodes and cathodes. As is demonstrated in figure 4.5.2, where the potential/time curves are shown for alloys corroding freely in 35% HNO_3, the potential of each corroding alloy increases with time - in other words, its overall surface activity is decreasing. A partial explanation could be provided by considering the shift of E_{Ag} with composition during anodic dissolution in non-aggressive acid concentrations shown in figure 6.5.1 and discussed earlier. The value of E_{Ag} increases with gold content, and as silver is being dissolved the proportion of gold in the alloy will rise. In other words, the rest potential of the anodes is becoming

increasingly noble, and it is essentially this which has been recorded in the potential/time plots of figure 4.5.2.

Whilst the change in specimen composition discussed above may have some bearing on the potentials measured, the largest factor is illustrated by considering evidence provided by transmission electron microscopy and E.D.X.. The development of corrosion pits in a range of specimens has been described in chapter 5. The manner in which these pits form has been shown to be similar for all silver-rich specimens. The first sign of corrosion damage is the formation over the surface of isolated corrosion pits with diameters of 30 to 50Å; these pits are visible when a charge density of about $1.5mCcm^{-2}$ has been passed. Despite this, E.D.X. analysis shows that silver has been removed from the specimen.

There are obvious differences between what are referred to here as 'chemical' and 'electrochemical' processes. Although both are essentially electrochemical effects, in the former case anodic and cathodic sites are found on the same specimen, whereas in the latter case anodic and cathodic sites are (largely) separated, and differences will also be found to exist in the electrolytes adjacent to the corroding alloys. Nevertheless, it may be appropriate to equate the early stages of electrochemical corrosion with the early stages of chemical corrosion. Rather than an increase in the anodic areas, most of the surface may be anodic to start with, then inactive (cathodic) regions extend over the surface whilst anodic regions diminish in size and develop as pits with increasing

current density. These pits might themselves become less active as the alloy becomes less silver-rich, and E_{Ag} rises, for the reason discussed above.

The stable potential reached by the alloys is 820 $\pm$ 10mV. It is interesting that this is the potential reached by all alloys, as well as by pure gold itself. The narrow range of this stable potential is a strong argument for the formation of the same surface species on all of the alloys, and since it also forms on pure gold itself, the surface species does not contain silver. The species is thought to be an oxide which might be hydrated. Figure 4.5.2 also shows that the alloys approach the stable potential more rapidly than does the pure gold. This means that the gold oxide formation is enhanced or driven by silver dissolution.

How this might come about is revealed by first considering the chemical dissolution of silver in nitric acid, which is thought to proceed as follows (Evans 1960):

Anodic Reaction:

$$Ag \longrightarrow Ag^+ + e^-$$

Cathodic Reaction:

$$H^+ + e^- \longrightarrow H \text{ initially, followed by:}$$

$$H + HNO_3 \rightleftharpoons H_2O + NO_2$$

$$NO_2 + e^- \longrightarrow NO_2^-$$

$$NO_2^- + H^+ \longrightarrow HNO_2$$

$$HNO_2 + HNO_3 \rightleftharpoons 2NO_2 + H_2O$$

Two molecules of nitrogen dioxide are formed for every silver atom dissolved. These are in turn reduced to NO_2^-, so that further protons can be oxidised , enabling still more silver to be dissolved. This reaction is said to be autocatalytic, and it would appear that the concentration of NO_2 would rise indefinitely as long as silver is dissolving. Alternative reactions which tend to reduce this concentration are:

$$H + HNO_2 \rightleftharpoons NO + H_2O$$
$$2HNO_2 \rightleftharpoons 2NO + H_2O$$

The potential/time curves (figure 4.5.1) are designed to reveal whether any oxide was produced (and remains) during a previous anodisation. It has been noted previously that all curves, other than that for pure silver, fall to a potential arrest at 890 $\pm$ 20mV. This behaviour is characteristic of the dissolution of a chemically unstable surface species, in this case possibly a metastable gold oxide.

An oxide is only stable if it can be formed at potentials below that of water breakdown. Otherwise, the reduction reaction of gold oxide to gold takes place. In the case of trivalent gold oxide, for example, the reduction reaction is summarised:

$$Au_2O_3 + 6H^+ + 6e^- \rightleftharpoons 2Au + 3H_2O$$

This reduction reaction proceeds by the oxidation of water:

$$2H_2O \rightleftharpoons O_2 + 4H^+ + 4e^-$$

The relevant potential for this to occur is given by Pourbaix (1973):

$$E = 1228 - 59pH + 14.1pO_2. \quad mV$$

The 0.1M HNO_3 used in this work for anodic dissolution of alloys has a pH of 1.5 so, neglecting the small contribution due to dissolved molecular oxygen, the potential for the breakdown of water to occur is calculated to be 898mV s.c.e. This calculated potential corresponds with the 890mV measured experimentally for the potential arrest, so it is considered that the potential arrest does indeed signify the reduction of a metastable surface gold oxide which has previously been formed by anodisation to high potentials and which is subsequently reduced by the oxidation of water.

The length of time spent under open-circuit conditions at the potential arrest in a given electrolyte depends mainly upon the thickness of the surface species being reduced. The time spent by each alloy at the potential arrest of figure 4.5.1 has been measured and is shown in figure 6.6.1. The arrest time is the time taken from the open-circuiting of the alloy (the removal of the applied anodic potential) to the turning point in figure 4.5.1 called the Flade potential, E_f.

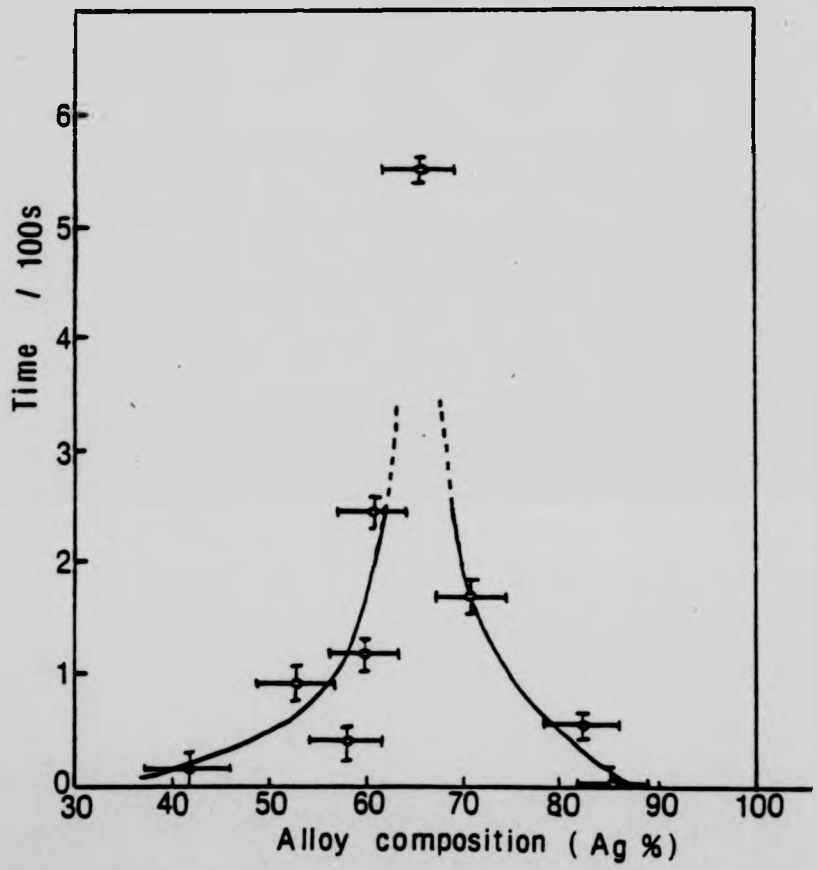

Figure 6.6.1 The time spent on the potential plateau of figure 5.5.1, as a function of alloy composition.

Figure 6.6.1 shows that there is a very significant maximum in the arrest time at about 65% silver, indicating that at this composition a relatively thick oxide layer has formed. With silver compositions above about 85% no arrest can be seen, so it appears that gold oxide is either transient or is not formed at all. Below about 50% silver, the arrest appears merely as a shoulder which is rapidly passed through; so for gold-rich specimens anodised to 1200mV only a small amount of gold oxide is formed.

The fact that Au65Ag has the longest potential arrest is most interesting, particularly when it is recalled that it is just this composition where the silver dissolution potential, E_{Ag}, was found to be coincident with the gold oxidation potential. This is the condition where an optimum degree of gold oxidation would be expected, because neither of the current-producing mechanisms (gold oxidation and silver dissolution) would be expected to dominate or supplant the other. Less gold oxide is produced by the more silver-rich specimens because the anodisation potential chosen for these measurements was 1200mV, which represents an increasingly greater overpotential for silver as the silver concentration increases. Additionally, of course, the very silver-rich specimens have a relatively small amount of gold with which to form an oxide.

The lessening of the time on the plateau (figure 4.5.1) for specimens having under 65% silver may signify a decrease in the oxide thickness, but for these specimens the silver

dissolution potential is higher than the gold oxidation potential. It might therefore be expected that gold oxidation would be, if anything, favoured, so it can be argued that the explanation lies in the kinetics of the formation and reduction of the oxides. Both the silver dissolution potential and the gold oxidation potential are higher on less silver-rich specimens than on more silver-rich specimens, so the anodisation potential of 1200mV represents a smaller overpotential on the former specimens than on the latter. This means that alloys which are less silver-rich will take longer to reach the predetermined charge density of 7mC cm^{-2} than those which are more silver-rich. If water breakdown is taking place at a constant rate, and this is reducing gold oxide to gold, then, although gold oxide will be formed on the less silver-rich specimens, considerably less oxide will be present at the end of anodisation.

Electrochemical currents, from which total charge passed may be found, are rarely caused by a solitary electrochemical reaction such as a metal ionisation. More than one current-producing phenomenon will often take place simultaneously; in the case of silver-gold alloys current-producing phenomena which are supported by the above discussion are silver ionisation and gold oxidation. Insight into current-producing phenomena is provided by the charge transfer efficiency of different alloy compositions, figure 6.6.2. The charge transfer efficiency is measured against silver, and is calculated from charge/time curves (such as in figure 4.4.1) in combination with E.D.X. analyses. The

charge/time curves give the total charge passed, from which the number of electrons n_t corresponding to that charge is calculated. E.D. X. measurements of the specimens before and after corrosion provide data from which the total number of silver atoms removed, n_{Ag}, can be found. The charge transfer efficiency is given by n_{Ag}/n_t.

Figure 6.6.2 shows that the charge transfer efficiency is unity at about Au85Ag. This suggests that for this composition, every electron removed at the anode has been provided by a silver atom. Less silver-rich specimens have a lower charge-transfer efficiency, meaning that more current is passed than can be accounted for by silver dissolution. The minimum charge transfer efficiency is about 0.5, indicating that only about half the electrons measured come from silver dissolution, the others being provided by alternative reactions. This minimum value of the charge transfer efficiency is found for alloys with compositions about 60-65% Ag, and it is thought that the additional current arises from the breakdown of water, releasing oxygen which combines with gold to form gold oxide.

Also shown on figure 6.6.2 is the calculated charge transfer efficiency curve for silver if gold is oxidised, as a specific example, to Au_2O_3 and if it is assumed that the ratio of oxidised gold atoms to ionised silver atoms is the same as the ratio of gold:silver in the alloy. In other words, this curve is drawn for the case where the current produced by a sample of Au60Ag consists of sixty silver atoms each releasing one

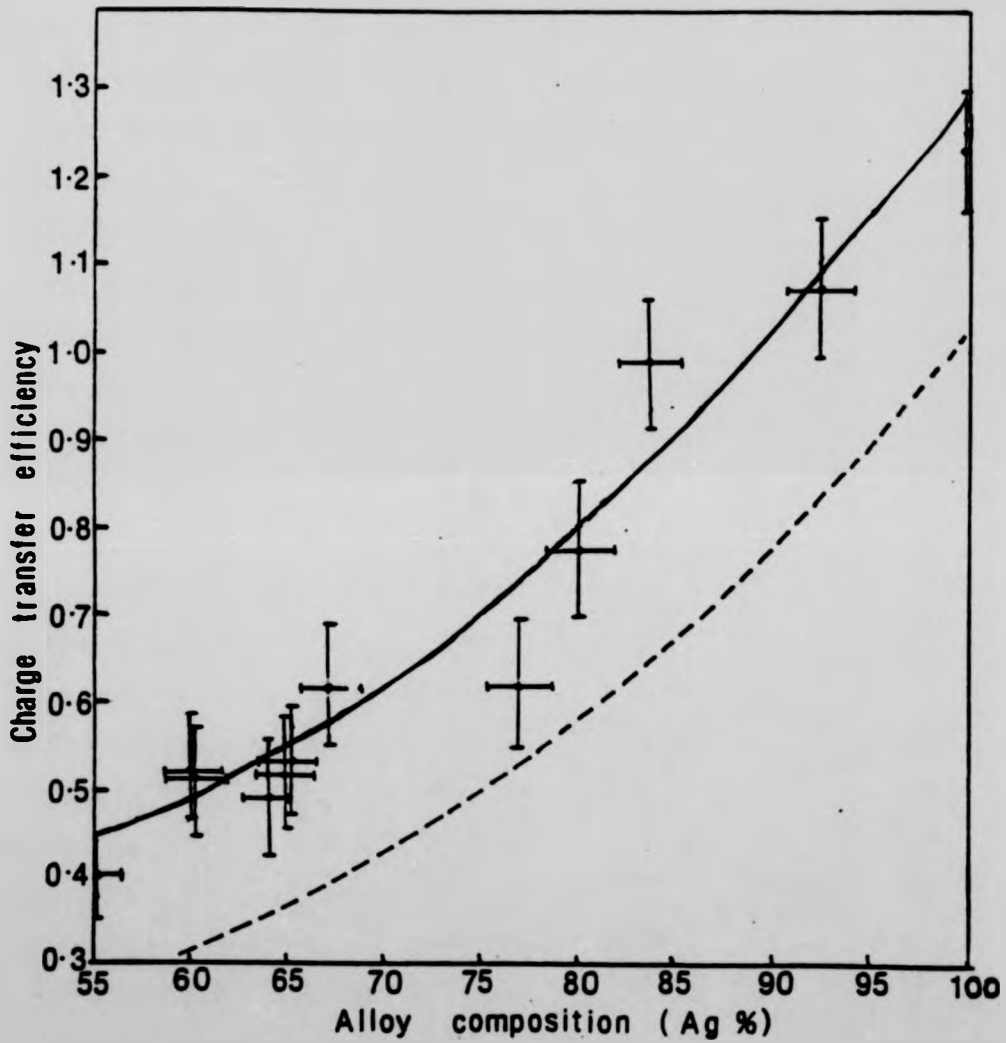

Figure 6.6.2 The relationship between charge transfer efficiency (for the anodic effect: $Ag \rightarrow Ag^{+} + e^{-}$) and alloy composition.

electron for every forty gold atoms which are oxidised to Au_2O_3 by the reduction of water. This very idealised theoretical curve lies alongside but below the actual curve, which in fact shows a charge transfer efficiency of over 1.0 for the very silver-rich specimens. This is almost certainly due to an associated autocatalytic process (more silver is removed than can be accounted for by charge passed), so chemical dissolution for these very silver-rich specimens seems to accompany electrochemical dissolution. If this is the case for the very silver-rich specimens, it may also be the case for the less silver-rich specimens, and if so it will bring the measured curve down, close to the idealised theoretical curve.

As was stated in section 4.2, cathodic processes in cyclic voltammograms can be used to provide evidence about previous anodic processes. The onset potential of the anodic peaks, which has been shown to equal E_{Ag}, has been shown to vary with alloy composition, and the charge transfer efficiency has been shown to be significantly less than unity for the less silver-rich specimens. Examination of the cyclic voltammograms shows that the onset potentials of the cathodic peaks is independent of the alloy composition, so this peak does need further consideration.

Figure 6.6.3 shows a series of cyclic voltammograms taken with a specimen of vapour deposited gold. Each run is to a different anodic limit, starting with (a) to 1050mV, up to (i) where the specimen was ramped to 1900mV. Each of the

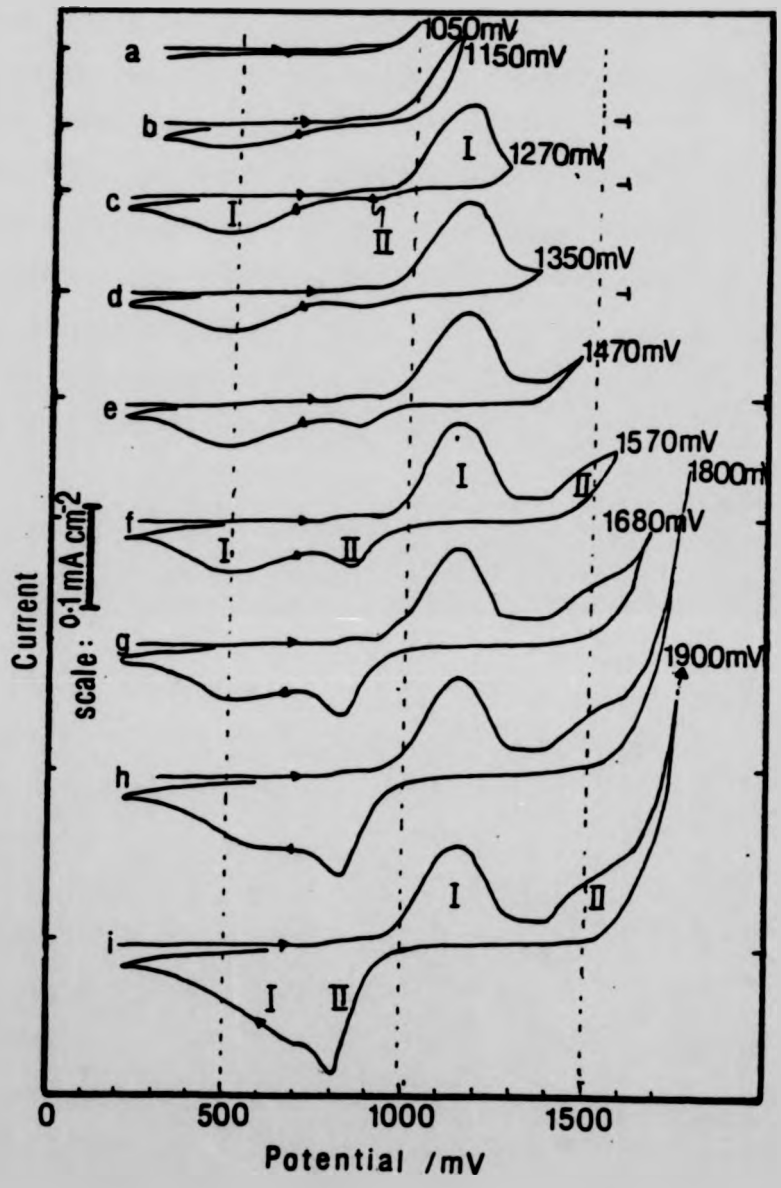

Figure 6.6.3 Cyclic voltammograms for gold in 0.1M HNO_3, showing the formation and reduction curves for oxides I and II (see text) when ramped to different anodic limits. Ramp rate: 50mV s^{-1}

specimens has a small plateau commencing at about 800mV. Whilst curve (a) has no discernible cathodic current, a small reduction peak can be seen in curve (b), which has been taken into the first part of an anodic peak. The reduction peak is larger for specimen (c), which has been taken through the anodic peak. The anodic peak, which starts at about 950mV, and the corresponding cathodic peak, which starts at about 750mV, have been labelled I on the figure, and are considered to show the formation and subsequent reduction of an oxide.

Curves (c) to (i) show a small reduction peak (labelled II on the figure) which commences at between 1000 and 950mV. This peak is not detectable on specimens anodised to a potential lower than 1270mV, and it grows larger as the anodisation potential limit is raised. The reduction peak labelled I also appears to grow when the specimen is taken to higher potentials.

The small plateau seen on the anodic sweep is probably due to a slow adsorption-desorption process which involves a small amount of charge (Nguyen Van Huong et al., 1980). This is generally referred to as an incipient oxidation, and has been shown by Nguyen Van Huong et al. to be an inherent property of gold electrodes, and not an impurity oxidation current. Watanabe and Gerisher (1981) investigated surface oxide layers on gold by illuminating specimens with visible light and measuring photocurrents. As well as detecting the incipient oxidation, they found that low-coverage surface oxides, or possibly hydroxides, formed between about 750 and 1150mV.

This corresponds with oxidation and reduction peaks I on figure 6.6.3. They also find that up to about 10Å Au_2O_3 forms at potentials between 1250 and 1550mV; this matches the peaks labelled II on figure 6.6.3. Although Watanabe and Gerisher identify what has been called here reduction peak II, the conditions they employed do not isolate peak I, which they see as a shoulder commencing at about 750mV (similar, for example, to the shoulder in (g) on figure 6.6.3).

The reduction peak which commences at 950 to 1000mV is now identified as arising from the reduction of Au_2O_3, but a further confirmatory test is needed to check that silver cannot be deposited at these potentials. This is shown in figure 6.6.4. A pure gold specimen was placed in 0.1M HNO_3 to which a little $AgNO_3$ had been added. The first run was in the cathodic direction, starting at a potential of 1200mV; as can be seen, there is no measurable cathodic current at about 950mV, showing that no silver is deposited at that potential. It also shows that no gold oxide is produced when gold is held at 1200mV (the potential chosen in this work for the anodic dissolution of silver). Indeed, no silver deposition takes place until a far less noble potential (about 500mV) is reached, labelled 'a' on the figure.

Peak 'b' shows the redissolution of silver which had been previously been deposited, and the anodic run is continued into oxygen evolution 'c'. The cathodic peak 'd' can now safely be identified as arising from the reduction of Au_2O_3.

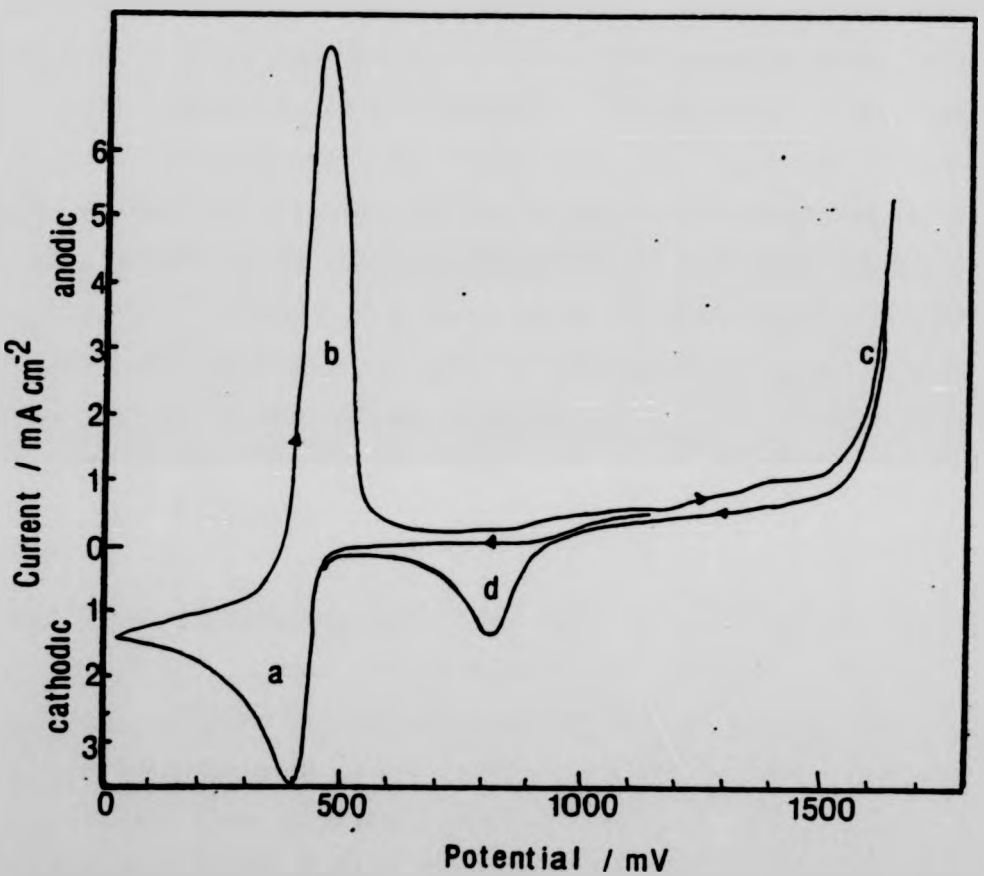

Figure 6.6.4 Cyclic voltammograms for gold in 0.1M HNO_3 with $AgNO_3$. Commencing at 1200mV in the cathodic direction, (a) is due to silver deposition, (b) is the stripping of this silver, (c) is oxygen evolution and (d) arises from the reduction of a gold oxide formed above 1200mV. Ramp rate: 50mV s^{-1}

It is concluded that the large peak produced on cyclic voltammograms of silver-gold alloys demonstrates the prior formation of Au_2O_3 during the anodic potential sweep. A simple comparison of the areas of the the anodic and cathodic peaks, shown in figure 6.6.5, gives an approximate guide as to the relationship between silver dissolution and gold oxidation. The smaller the ratio of the area c of the cathodic peak to the area a of the anodic peak, the smaller is the percentage of the anodic current which has been used for gold oxidation. There is a very close correspondence between the measured ratios and the ratio calculated on the assumption that the ratio of gold atoms oxidised to Au_2O_3 to silver atoms dissolved is the same as the ratio of gold atoms to silver atoms in the specimen.

Whilst this is approximately the case, it has been shown experimentally (the potential/time curve following anodisation, figure 6.6.1) that the maximum thickness of gold oxide is produced with about Au64Ag. Since the area enclosed by the anodic peak is a quantitative measure of gold oxide produced, the final figure in this section, figure 6.6.6, shows similarly that the area enclosed by the cathodic peak (and hence the quantity of gold oxide produced) is at a maximum for a composition of Au60-65Ag. The maximum thickness of oxide, calculated from this figure, is approximately 15Å.

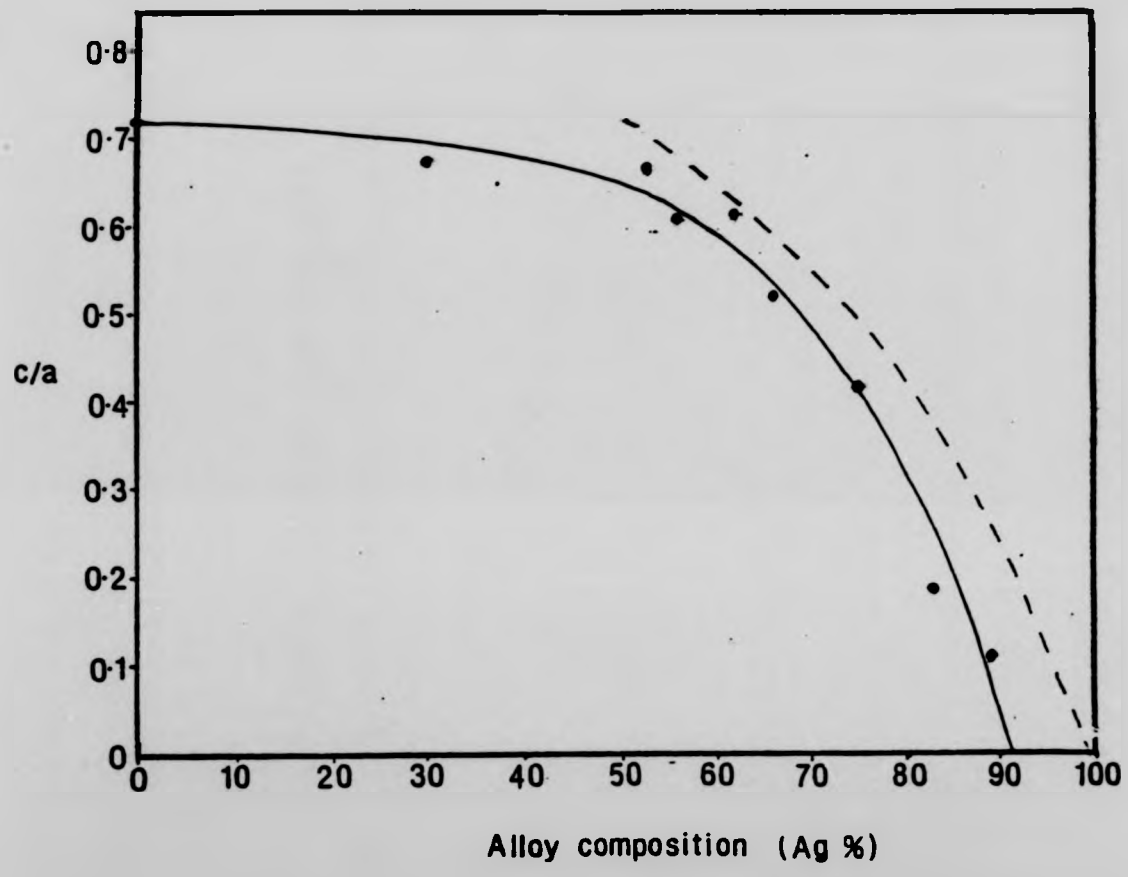

Figure 6.6.5 The ratio of the area of the cathodic reduction peak 'c' to that of the anodic oxidation/dissolution peak 'a', taken from cyclic voltammograms of alloy specimens (solid line). The calculated curve (dashed line) is for the case where the anodic peak is produced from silver dissolution plus gold oxidation to Au_2O_3, the proportions of silver dissolved and gold oxidised being taken as the ratio of silver:gold in the original alloy, whereas the cathodic curve is solely due to the reduction of gold oxide.

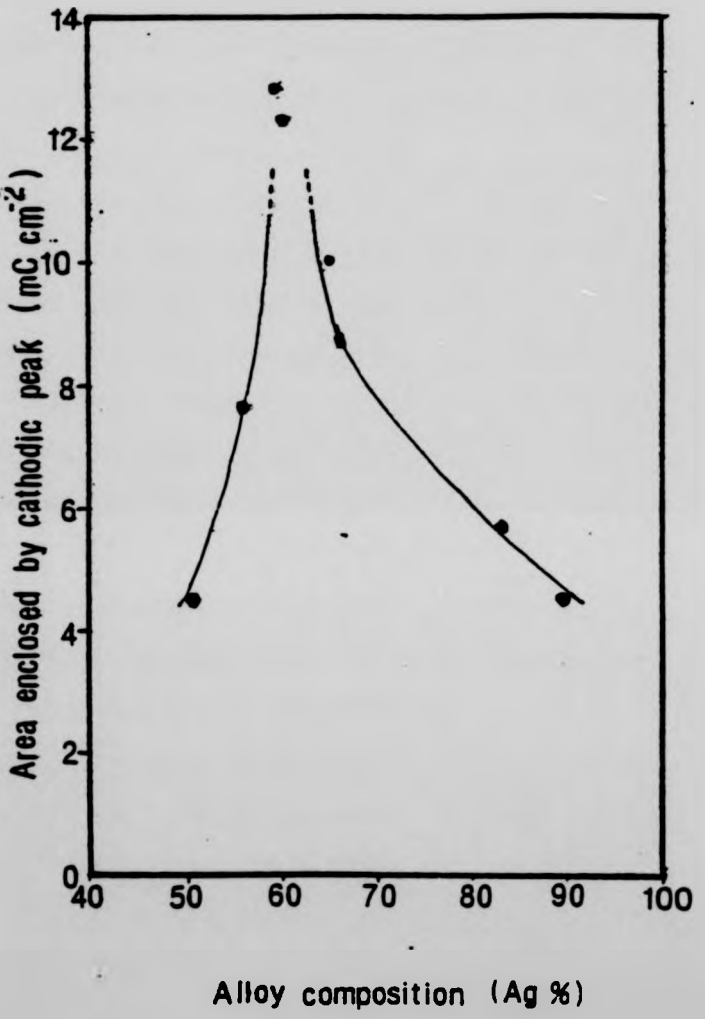

Figure 6.6.6 The variation of the area enclosed by the cathodic peak from cyclic voltammograms) with alloy composition. The area represents the reduction of gold oxide, Au_2O_3.

6.7 Discussion of Anodically Produced Corrosion Micromorphology

The development of the corrosion microstructure in the silver-rich specimens is not significantly affected by alloy composition. In all cases, isolated pits develop over the alloy surface; the diameters of these pits are some 3 to 5nm (in other words, a maximum of about 40 atomic diameters). As more charge is passed, further pits develop and the existing pits extend to form, eventually, a network of surface channels. This is the final stage reached by the less silver-rich specimens, such as Au55Ag, for which the development of corrosion is shown in figure 5.4.1 (a) to (e).

The corrosion microstructure develops beyond this point for the more silver-rich specimens, for example Au65Ag and Au72Ag, shown in the series of photographs 5.5.1 and 5.6.1 respectively. Two main developments can be seen. The first is the development of a penetrating, overlapping structure of tunnels from what was previously a surface structure of channels. The second change is in the shape of the channels and tunnels which, when increasing charge has been passed, become less jagged in appearance indicating that some reordering has taken place to reduce the perimeter lengths of the corrosion structures.

The argument on gold oxide formation and decomposition provided in section 6.6 can now be applied to the corrosion microstructure. The anodic dissolution of silver enhances a

gold oxide formation at the resultant disordered surface; the oxide is, however, only metastable, and is continuously being reduced by water. The mechanism for this is the reduction of the gold oxide whereby gold is transferred from anodic sites within pits to cathodic sites on pit walls.

The most striking feature of the electron micrographs is the small scale of the corrosion microstructure formed on all silver-rich alloys when anodised at 1200mV. It has been argued in the previous section that the chemical dissolution of silver enhances the formation of gold oxide by altering the aqueous environment of the gold in a manner not matched by the anodic dissolution of silver. This implies that gold oxide will play a far more significant part in the development of corrosion structures in chemical corrosion than in electrochemical corrosion, and is borne out when the anodically produced corrosion morphologies discussed in chapter 5 are compared with a typical chemically produced corrosion morphology: figure 6.7.1. The scale of the channels developed chemically is an order of magnitude larger than the scale of anodically produced pits and channels: the former are typically 50nm in diameter, whereas the latter are usually less than 5nm in diameter. The wider channels formed chemically require greater gold mobility, facilitated by the relatively large amounts of gold oxide produced.

The highly oxidising environment of 0.1M HNO_3 and a high potential are the very conditions where an oxide would be expected to form. It is interesting that the pits developed

Figure 6.7.1 A comparison of the size of the corrosion micromorphology developed during corrosion in concentrated nitric acid with that developed under potentiostatic control in 0.1M nitric acid. (a) a 50% silver specimen, corroded for 30s in concentrated HNO_3; (b) a 60% silver specimen, corroded for 30s at 1200mV in 0.1M HNO_3

Photograph (a) has been kindly provided by Professor A. J. Forty, University of Warwick.

Figure 6.7.1 A comparison of the size of the corrosion micromorphology developed during corrosion in concentrated nitric acid with that developed under potentiostatic control in 0.1M nitric acid. (a) a 50% silver specimen, corroded for 30s in concentrated HNO_3; (b) a 60% silver specimen, corroded for 30s at 1200mV in 0.1M HNO_3

Photograph (a) has been kindly provided by Professor A. J. Forty, University of Warwick.

on Au55Ag following anodisation at 1350mV (figure 5.7.2(b) have diameters four or five times larger than the diameters of pits developed at 1200mV on a similar specimen (figure 5.7.2(a). This accords with increased oxide production and subsequent reduction at the higher potential. The size of the corrosion damage suffered by gold after 60s at a high potential (2600mV) is very similar to that produced chemically on alloys, as shown by figure 5.3.2. The formation of gold oxide under these conditions, and the resultant micromorphology, is by analogy corroborating evidence for the role played by gold oxide in the development of an island-channel corrosion structure in silver-gold alloys.

The high-potential anodisation of pure gold has two effects on the diffraction pattern, as shown in figure 5.3.3. Instead of discrete diffraction spots, the diffraction pattern is in the form of rings due to the polycrystallinity of the anodised gold. However, not all of the rings correspond with the diffraction spots of uncorroded gold; additional rings can also be seen. These rings match the additional spots observed with Au55Ag (figure 5.7.2 (b)) which was anodised at 1350mV. Taking the lattice parameter for gold to be $a_o = 4.08\text{Å}$, the lattice parameter for the cubic structure associated with Au55Ag after 1350mV anodisation is $a_o = 5.52\text{Å}$. Similar additional spots in the diffraction pattern have occasionally been observed on other alloys anodised at 1200mV, but they have been of an ephemeral nature, and have disappeared before they could be photographed.

It has not been possible to identify this metastable phase. It is not, however, the phase discussed by Durkin and Forty (1982). They concluded that an overlayer formed by the corrosion of silver-gold alloy in nitric acid is probably gold (I) oxide, the lattice parameter for which is a_o = 4.91Å. The identity of the new phase with a_o = 5.52Å was also not determined from the JCPDS Powder Diffraction File Search Manual (1979). It is not any previously reported oxide or nitrogen-containing compound of gold or silver, nor is it any known salt which could be formed with likely contaminants, notably chlorine and carbon.

CHAPTER 7

SUMMARY AND PROPOSALS FOR FUTURE WORK

7.1 Summary of Major Results and Conclusions

This work has shown that potentiostatic methods can be used to part silver from silver-rich silver-gold. The lowest potential at which silver dissolution commences has been termed the silver dissolution potential, E_{Ag}, and the value of E_{Ag} has been shown to be composition-dependent, being related (in 0.1M nitric acid) to the concentration (C_{Au} atomic percent) of gold by:

$$E_{Ag} = 350 + 18C_{Au} \text{ mV (s.c.e.).}$$

This relationship has been used to provide a quick and easy rapid assay of silver-rich thin films, since it has also been shown that E_{Ag} may be obtained from an anodic voltammogram: it is the lowest potential at which a significant current can be measured. Initial tests have shown that a similar relationship applies to bulk specimens, although, in the case of bulk specimens, the shapes of the voltammograms differ from the shapes of voltammograms obtained with thin films.

The original decision to use thin films for the electrochemical characterisation of silver-gold fortuitously produced the opportunity both to confirm some previously known

aspects of the parting of silver from silver-gold, and to detect hitherto unsuspected phenomena. Since the amount of silver in these thin films is in limited supply, it was possible to use electrochemical means to remove all available silver in a short time. Direct measurements by E.D.A.X. were used to show that silver can be fully parted from alloys with an initial silver atomic concentration of 80% or above; incomplete parting occurs with 55% to 80% silver (greater parting taking place for the more silver-rich alloys in this composition range); silver can not be parted from alloys with initial silver concentrations of 55% and under, although measurements indicate a small quantity of silver can be dissolved, probably from one or two atomic layers on the metal surface.

Another significant conclusion from electrochemical results is that, during the dissolution of silver from silver-gold, a metastable surface gold oxide is formed. This oxide (which is only two or three atomic layers thick) was detected by measuring the charge-transfer efficiency for the dissolution of silver, by determining the potential/time behaviour of the specimens following anodisation, and by producing cyclic voltammograms with thin films: the small charge associated with the formation of the oxide would not have been detected if thicker specimens had been used. Additionally, voltammograms with thin films showed that at a potential of about 1200mV (s.c.e.) gold forms an oxide; a similar oxide is produced on gold-rich silver-gold, though at less noble potentials. The potential for the formation of this oxide and the potential

for the dissolution of silver (E_{Ag}) are shown to be the same, about 960mV, for a composition of about Au65Ag. Furthermore, it has been shown that the thickest films (about 15Å) develop on alloys of this composition.

A major aspect of the transmission microscopy was the design, fabrication and use of a specialised teflon electrochemical cell. It has been possible to use this cell for the electrochemical treatment of specimens as thin as 250Å, the specimens being mounted on 3.05mm diameter grids for electron microscopy. With this cell, electrochemical treatments can be applied to high-quality films, avoiding, for example, unwanted pre-treatment corrosive stripping or post-treatment electrochemical thinning which might themselves have produced corrosion morphologies.

The cell was used under potentiostatic control to cause controlled dealloying of a range of thin, electron-transparent silver-rich silver-gold films. Following partial or complete dealloying, a range of initially silver-rich silver-gold specimens was examined with transmission electron microscopy. The early stages of corrosion, following small charge densities, are shown to consist of the formation of isolated pits with diameters of about 50Å which nucleate over the surface. When more charge is passed, the pits appear to develop into channels some 50Å wide. The channels form networks, initially in the intragranular regions but, when more charge has been passed, the entire surface (including grain boundaries and the regions surrounding holes in the

films) ultimately becomes covered with channel networks. This is the 'final' corrosion morphology developed on alloys with initial silver concentrations of between 55 and 70%. In the case of alloys with initial silver concentrations of over 70%, the 'final' corrosion morphology consists of an overlapping structure of channels and tunnels.

A new phase, thought to be an f.c.c. structure with the lattice parameter a_o = 5.52Å, has been identified from the diffraction pattern of corroded alloy specimens. The diffraction spots produced by this phase appear to correspond with new rings which appear on the diffraction pattern of gold films following anodisation at high potentials (around 2600mV). This new phase is possibly an oxide, which may be solvated; indeed, it is possibly the same metastable species which, as electrochemical measurements have shown, is formed during silver dissolution from silver-gold. It is proposed that the gold is redeposited at the sides of pits and channels when the oxide is reduced by the electrolyte. The formation and reduction of the oxide, therefore, may play a significant part in the development of corrosion micromorphologies.

7.2 Possible Further Studies

An immediate area for further investigation is the kinetics of the silver-gold/nitric acid system. The formation of the surface species, the dissolution of silver and the 'final' composition have all been shown to be potential-dependent, but kinetic influences have not been fully investigated. It is

likely that kinetic effects are very important, particularly in the first few seconds of potentiostatic corrosion; for example, the balance between the rate of formation and the rate of decomposition of the new species will be expected to alter with time. The nature of the kinetics may provide evidence as to the role played by this species, and it might also indicate how it is formed.

An interesting future study would be the determination of the nature of this species. If it is a gold oxide, then the gold:oxygen ratio may be found by carrying out careful coulometric and perhaps gravimetric measurements. This will entail high levels of electrolyte purity, particularly pre-electrolysis to sweep out as many impurity ions as possible, and deoxygenation (in, for example, a catalytically-scrubbed nitrogen-atmosphere) to improve the knowledge of oxygen availability. An extension of this would be to use a non-aqueous electrolyte, such as acetonitrile, in deoxygenated conditions or with known concentrations of dissolved (molecular) oxygen. A further range of experiments which may assist in the characterisation of the new species is to examine the effect of different electrolytes and of pH on the formation and dissolution of the surface phase.

Although it has been suggested in this thesis, it is by no means certain that the formation and decomposition of the new phase provide the means whereby gold is transferred from within developing pits, channels and tunnels to their walls. However, if the experimental conditions can be created and

applied to electron-transparent silver-gold alloy films such that silver may be dissolved from them without the formation of the associated phase, or with the controlled formation of that phase, its influence on the development and nature of corrosion morphologies may be determined. In addition, it would be valuable to use these techniques to examine whether pits initiate at identifiable sites on the electrode surface. Such sites may be structural features, such as the 'supersteps' mentioned in this thesis, or they may be regions of a particular alloy composition. Such information could perhaps be used to create a better model for the atomic processes which occur during the early stages of dealloying.

Finally, the applicability of the specially designed electrochemical cell (the teflon cell) to other alloys should not be ignored. The cell avoids some of the complications which arise when other methods are used to thin specimens for electron-microscopy, may perhaps aid corrosion investigations of metals prepared as thin films by, for example, vapour deposition or sputtering techniques.

REFERENCES

Albery, J. (1975), Electrode Kinetics, Clarendon Press, Oxford

Armstrong, G., Himsworth, F.R. and Butler, J.A.V. (1933), Proc. Roy. Soc. A, 143, 89

Bakish, R. and Robertson, W.D. (1956), Acta. Met. 4, 342

Bard, A.J. and Faulkner, L.R. (1980), Electrochemical Methods, John Wiley and Sons, New York, Chichester

Bassett, G.A. and Pashley, D.W. (1959), J. Inst. Metals, 87, 499

Birke, R.L. and Roe, D.K. (1965), Anal. Chem., 37(4), 450

Brummer, S.B. and Makrides, A.C. (1964), J. Electrochem. Soc., 111, 1122

Burton, W.K., Cabrera, N. and Franck, F.C. (1951), Phil. Trans. of the Royal Society of London A, 248, 299

Cadle, H.S. and Bruckenstein, S. (1974), Anal. Chem., 46, 16

Cahan, B.D., Nagy, Z. and Genshaw, M.A. (1972), J. Electrochem. Soc., 114, 698

Cahan, B.D., Ockerman, J.B., Amlie, R.F. and Ruetschi, P. (1960), J. Electrochem. Soc, 107, 725

Czanderna, A.W. and Summermatter, R. (1976), J. Vac. Sci. Technol., 13, 384

Deborin and Erscher (1940), Acta Physicochim, 13, 347

Durkin, P. (1982), Ph.D. Thesis, University of Warwick, Coventry

Durkin, P. and Forty, A.J. (1982), Phil. Mag. A., 45 no. 1, 95

Edeleanu, C. and Forty, A.J. (1960), Phil. Mag., 5, 1029

Evans, U.R. (1960), The Corrosion and Oxidation of Metals, Redwood Press, Trowbridge and London

Evans, U.R. and Hoar, T.P. (1932), Proc. Roy. Soc. A, 137, 343

Fain, F.C. and Macdonald, J.M. (1974), Phys. Rev. B, 9, 5099

Forty, A.J. (1981), Gold Bull., 14, 1

Forty, A.J. and Durkin, P. (1980), Phil. Mag. A, 43

Forty, A.J. and Durkin, P. (1981), Phil. Mag. A, 42, 295

Forty, A.J. and Rowlands, G. (1981), Phil. Mag. A., 43, 171

Gerisher, H. and Tischer, R.P. (1954), 58, 819

Goodhew, P.J. (1972), Practical Methods in Electron Microscopy, North Holland Publishing Company, Amsterdam/London

Graf, L. (1956), Stress Corrosion Cracking and Embrittlement, ed. Robertson, W.D., John Wiley and Sons, Inc., New York.

Graf, L. and Budke, J. (1955), Z. Metallkunde, 46, 378

Harwood, J.J. (1956), Stress Corrosion Cracking and Embrittlement, ed. Robertson, W.D., John Wiley and Sons Inc., New York

Hickling, A. (1942), Trans. Faraday Soc., 38, 27

Hickling, A. and Taylor, D. (1947), Disc. Faraday Soc., 1, 277

Hubbard, A.T. (1980), J. Vac. Sci. Technol., 17(1), 49

Kirsch, R.G., Poate, J.M. and Eibschutz, M. (1976), App. Phys. Lett., 29 no. 12, 772

Kortum, G. (1965), Treatise on Electrochemistry, Elsevier, Amsterdam, London, New York

Laitinen, H.A. and Chao, M.S. (1961), J. Electrochem. Soc., 111, 832

Latimer, W.M. (1952), The Oxidation States of the Elements and

their Potentials in Aqueous Solutions, edition 2, Prentice-Hall Inc., New Jersey

Luthor and Pokorny (1908), Z. Anorg. Chem., 57, 290

Makrides, A.C. (1962), Corrosion, 18 (9), 338t

Nernst, W. (1904), Z.Physik. Chem., 47, 52

Nguyen Van Huong, G., Hinnen, C. and Lecoeur, J. (1980), J. Electroanal. Chem., 106, 185

Oesch, U. and Janata, J. (1983), Electrochim. Acta, 28 (9), 1237

Ogura, K., Haruyama, S. and Nagasaki, K. (1971), J. Electrochem. Soc., 118, 531

Pashley, D.W. (1959), Phil. Mag., 4, 316

Pashley, D.W. and Stowell, M.J. (1963), Phil. Mag., 8, 1605

Pickering, H.W. (1968), J. Electrochem. Soc., 115, 43

Pickering, H.W. (1970), J. Electrochem. Soc., 117, 8

Pickering, H.W. and Swann, P.R. (1963), Corrosion, 19, 369

Pickering, H.W. and Wagner. C. (1967), J. Electrochem. Soc., 114, 698

Pourbaix, M. (1973), Lectures on Electrochemical Corrosion, Plenum, London, New York

Pourbaix, M. and Vandervelden, F. (1965), Corros. Sci., 5, 81

Powder Diffraction File Search Manual (1979), Joint Committee on Powder Diffraction Standards, Pennsylvania, U.S.A.

Rudd, E.J. (1977), Thin Solid Films, 43, 1

Sawyer, D.T. and Roberts, J.R. (1974), Experimental Electrochemistry for Chemists, John Wiley and Sons, New York, London, Sydney, Toronto

Schmid, G.M. and O'Brien, R.N. (1964), J. Electrochem. Soc., 108, 726

Shewman (1970), Physical Metallurgy, ed. Cahn, R.W., North Holland Publishing Co., Amsterdam and London

Shreir, L.L. (1976), Corrosion, vol. 1 edition 2, Newnes-Butterworths, London, Boston

Swann, P.R. and Duff, W.R. (1970), Met. Trans., 1, 73

Tafel, J. (1905), Z. Physik. Chem., 50, 641

Tammann, Z. and Brauns, E. (1931), Z. Anorg. Chem., 200, 209

Thomas, G. (1962), Transmission Electron Microscopy of Metals, John Wiley, New York

Thompson, A.H. (1979), J. Electrochem. Soc., 126, 4

Tischer, R.P. and Gerischer, H. (1958), Z. fur Elek. U. Phys-Chem., 62, 50

Tokutaka, H., Nishimori, K., Tanako, K., Takashima, K., Hency, J. and Langeron, J.P. (1981), J. Appl. Phys. (U.S.A.), 52 no. 10, 6109

Watanabe, J. and Gerisher, H. (1981), J. Electroanal. Chem., 117, 185

West, J.M. (1970), Br. Corros. J., 5, 65

Whitney. W.R. (1903), J. Am. Chem. Soc., 25, 394

Willens, R.H. (1962), Fifth International Congress of Electron Microscopy, Philadelphia